Czech Technical University in Prague

Faculty of Mechanical Engineering

Dissertation thesis

New possibilities for gearwheels of automotive gearboxes

Ing. Ondřej Miláček

Doktorský studijní program: Strojní inženýrství

Studijní obor: Dopravní stroje a zařízení

Supervisor

doc. Dr. Ing. Gabriela Achtenová

2021 Prague

Acknowledgement

Firstly, I would like to thank to doc. Dr. Ing. Gabriela Achtenová for a professional guidance of this thesis. Secondly, I would like to thank to all colleagues which participated at this project, i.e. Ing. Jiří Borovička and Ing. Jaroslav Prokop, Ph.D. for technical support while providing tests. Thirdly I would like to thank to our colleagues from cooperating industrial companies, namely Michael Andersson, Ph.D from Höganäs AB, Ing. Martin Knobloch and Dipl.Ing. Michael Hirsch from Profiroll Technologies GmbH. In this chapter has to be mentioned also my friend Ing. František Siegl, who helped me enormously with the development of the software for asymmetric gearing design. Last but not least I would like to thank to my wife Zuzana for her support and huge patience during this thesis writing.

Declaration of Authorship

I hereby certify that this thesis has been composed by me and is based on my own work, using only the literature and sources listed in the bibliography.

Prohlášení o autorství

Prohlašuji, že jsem tuto disertační práci vypracoval samostatně, s použitím odborné literatury a pramenů uvedených v seznamu, který je součástí této práce.

In Prague / V Praze dne: …… ……..

Signature / podpis autora

Abstract

This thesis deals with an application of the gearwheels made of PM (Powder Metal) in automotive gearbox and has two main parts. In the first one there were manufactured and tested PM gearsets with an original (symmetric) geometry and special heat treatment (Hot Isostatic Pressing - HIP). In the second part there were designed, manufactured and tested PM gears with an asymmetric profile. These gears had also special surface treatment – rolling. To be able to design an asymmetric gearing profile a specific software had to be developed. Endurance tests of these PM gearwheels were performed in laboratories of CTU in Prague. Their results are described in this thesis.

Anotace

Tato práce se zabývá náhradou sériového soukolí v automobilní převodovce náhradním soukolím vyrobeného ze slinutých práškových kovů (PM – Powder Metal) a má dvě hlavní části. V rámci první části byla vyrobena a zkoušena PM kola s původní (symetrickou) geometrií a speciální tepelnou úpravou – HIP (Hot Isostatic Pressing). V rámci druhé části byla navržena, vyrobena a zkoušena PM kola s asymetrickým profilem. Tato kola měla speciální povrchovou úpravu, a sice válcování. Aby bylo možné navrhnout ozubení s asymetrickým profilem, musel být pro tento účel vyvinut speciální program. Zkoušky těchto PM soukolí byly provedeny v laboratořích ČVUT v Praze. Jejich výsledky jsou také popsány v této práci.

Keywords:

involute gearing, PM (Powder Metal), asymmetric profile, automotive, gearbox, HIP (Hot Isostatic Pressing), rolling

Klíčová slova:

evolventní otzubení, PM (Powder Metal – prášková metalurgie), asymetrický profil, automobilní, převodovka, HIP (Hot Isostatic Pressing), válcování

Content

List of Symbols

Latin alphabet symbols

symbol	meaning	unit
A	asymmetry ratio	[-]
a_n	nominal center distance	[mm]
a_w	working center distance	[mm]
b	facewidth	[mm]
c_a	tip -root clearance	[mm]
c_a	profile crowning magnitude	[μm]
c_b	lead crowning magnitude	[μm]
D	ball diameter used for the measurement over balls	[mm]
d	reference diameter	[mm]
d_a	addendum (tip) diameter	[mm]
d_g	balls centers distance (diameter)	[mm]
d_w	working diameter	[mm]
h_{aP0}	addendum height of the rack (tool)	[mm]
E	Young's modulus of elasticity	[MPa]
F	force	[N]
$f_{H\alpha}$	profile slope deviation	[μm]
$f_{H\beta}$	helix slope deviation	[μm]
i	number of teeth to be measured (spaned)	[-]
j_n	normal backlash	[mm]
j_t	transverse backlash	[mm]
$k_{H\ FEM}$	recalculation coefficient for Hertzian stress	[-]
$k_{F\ FEM}$	recalculation coefficient for bending stress	[-]
M	measurement over balls	[mm]
m_n	normal module	[mm]
m_t	transverse module	[mm]
p_{rP0}	tool's protuberance magnitude	[mm]
p_{t0}	transverse pitch at tool's reference plane	[mm]
p_t	transverse pitch at reference diameter	[mm]
p_{tw}	transverse pitch at working diameter	[mm]

r	reference radius	[mm]
r_w	working pitch radius	[mm]
s_{n0} (s_{P0})	tool thickness at its reference plane	[mm]
s_{na}	normal tooth thickness at its addendum	[mm]
s_{ta}	transverse tooth thickness at its addendum	[mm]
s_{tw}	transverse tooth thickness at working diameter	[mm]
s_{t0}	transverse tooth thickness at tool's reference plane	[mm]
x	profile shift coefficient	[-]
z	number of teeth	[-]

Greek Alphabet Symbols

symbol	**meaning**	**unit**
α_{gc}	touching angle between the ball and coast flank	[°]
α_{gd}	touching angle between the ball and drive flank	[°]
α_{prP0}	protuberance angle	[°]
α_{KP0}	tip chamfer ramp angle	[°]
$\alpha_n(\alpha_{P0})$	normal profile (pressure) angle	[°]
α_t	transverse profile (pressure) angle	[°]
α_{tw}	working transverse pressure angle	[°]
β	helix angle on reference diameter	[°]
β_w	helix angle on working diameter	[°]
ε_{ball}	angle between tooth axis and ball axis	[°]
ε_α	transverse contact ratio	[-]
ε_β	axial contact ratio	[-]
ε_χ	total contact ratio	[-]
η	efficiency	[-]
ν	Poisson's ratio	[-]
$\nu_{c,d}$	involute's roll angle – coast,drive	[°]
π	Ludolph's Constant	[-]
ρ	osculation radius	[mm]
ρ_{aP0}	addendum radius of the rack (tool)	[mm]
σ	stress	[MPa]

σ_F	bending stress	[MPa]
σ_H	Hertzian stress	[MPa]

Subscripts

symbol	**meaning**
a	addendum (tip)
coast	relating to the coast side
drive	relating to the drive side
H	Hertzian
F	bending
n	normal
t	transverse
w	relating to working plane(diameter)
0	relating to the tool
1	relating to gear 1 (power input, pinion)
2	relating to gear 2(power output)
Σ	summative

Abbreviations

symbol	**meaning**
AC	alternating current
CNC	computer numerical control
CTD	constant torque device
CTU	Czech Technical University
CV	constant velocity
DIN	Deutsches Institut für Normung
EDM	electrical discharge machining
EM	electromotor
FEM	finite element method
FFT	fast Fourier transform
FPGA	field programmable gate array

FZG	Forschungsstelle für Zahnräder und Getriebebau
HCR	high contact ratio
HIP	hot isostatic pressing
ICE	internal combustion engine
ISO	International Organization for Standardization
LOM	light optical microscope
MBS	multi body system
PC	personal computer
PGS	planetary gear set
PM	pretensioning mechanism
PM	powder metal
PTU	planetary torque unit
RMS	root mean square

List of Figures

List of Tables

1 Introduction

Involute gearing has been produced for more than hundred years. Therefore, there have been developed many sophisticated methods and pieces of software for its designing and dimensioning including loading conditions within its lifetime. The description of its geometry is quite demanding and the easiest type of it is the symmetrical one, which is also standardized and commonly used. Till now, the technology (geometry, material, heat treatment, etc.) has been very well fine-tuned. The way to the improvement (e.g. durability lengthening) is either in the geometry optimization or in gearwheels material.

In this thesis is described the current state of the art in the field of gears production. Then, testing methods of gears and improvements of the test bench used within this thesis are described. Furthermore, follows the description of the geometry of the involute gearing with an asymmetric profile and the software for its designing. The method of the strength computation of asymmetric gears is described too. Then the production process, testing and test results of produced gears of the gearset for automotive gearbox manufactured by the PM (Powder Metal) technology is described.

2 Current State of the Art

In this chapter is short introduction to the branch of automotive gearboxes. Furthermore, the current state of the art of gearing materials, gearing production technologies and gearing tooth profiles is described.

2.1 Automotive Gearbox Design

Generally, gearboxes are used in many different technical fields to reach desired output parameters with given input (source) parameters of the, e.g. electromotor or Internal Combustion Engine (ICE). This transformation is done with help of the gear ratio. There are many types of gearboxes specially designed for their purposes. An example of two different gearbox designs is depicted in Figure 2-1. On the left side is an example of the industrial winch gearbox, on the right the shafts with gearwheels of typical manual automotive gearbox is depicted. In this figure are clearly visible differences in design between both these gearboxes. In the industrial gearbox, shafts are very short and stiff, the gearbox housing (cast) is very robust because such gearbox is securely bolted to a drivetrain frame. Gearing parameters (tooth profile, module) are very often standardized. Furthermore, the ratio is constant.

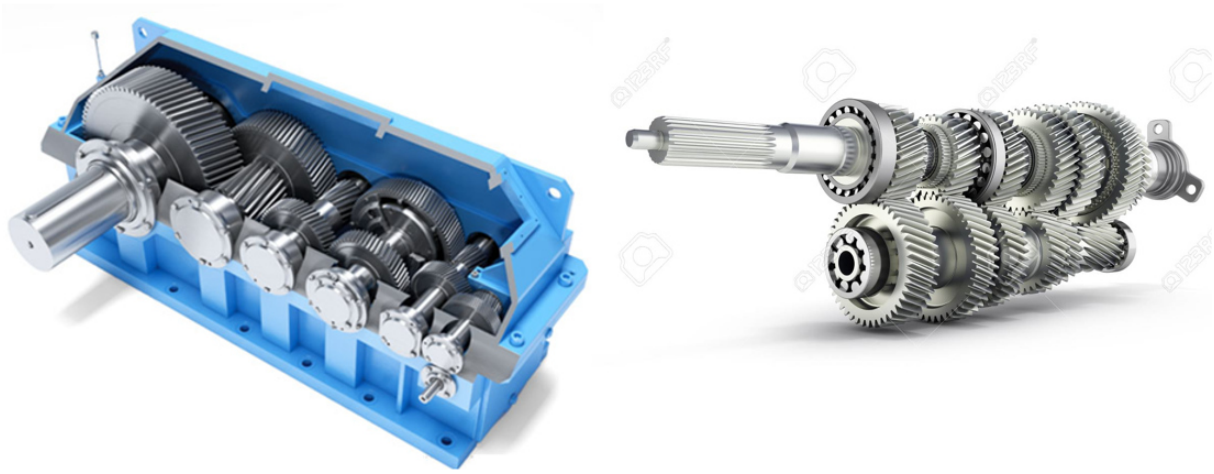

Figure 2-1: Typical appearance of the industrial (left) and automotive (right) gearbox. [1], [2].

The design of automotive gearbox must fulfill many specific requirements. The most important of them is its low weight and for the case of the transversal position also its length. The weight is in automotive industry crucial, because it influences passive resistances of the car and thus also the power demands and final fuel consumption. Furthermore, it must allow shifting. For this reason, the architecture is very specific. There is a requirement to design all parts as light as possible. The shafts are very long and with small diameter, the gearbox casting wall is also very thin, mainly made of aluminum alloy. The consequence of this is that high deformations occur in the mesh and accurate tooth flank modifications are necessary. In addition, very important demands are also the limited build-in space and gearbox noise reduction.

2.2 Gearing Manufacturing Technology

In this chapter is described the most commonly used technologies for the gearing manufacturing.

2.2.1 Traditional Gearing Manufacturing Technologies

The gearing manufacturing process can be provided by more methods. The most commonly used method is the milling. This technology is used as the initial phase to get the rough gearing shape. It is very productive. An example of this operation is depicted in Figure 2-2 (left). There are more types of this technology but for this thesis it is not important. After the milling process the gear is commonly provided the heat treatment - hardening (e.g. case hardening or nitriding) and subsequently the final gear's geometry (including tooth flank modifications) is reached by grinding. An example of this operation is depicted in Figure 2-2 (right). The gearing can be also produced only by grinding technology, without initial milling.

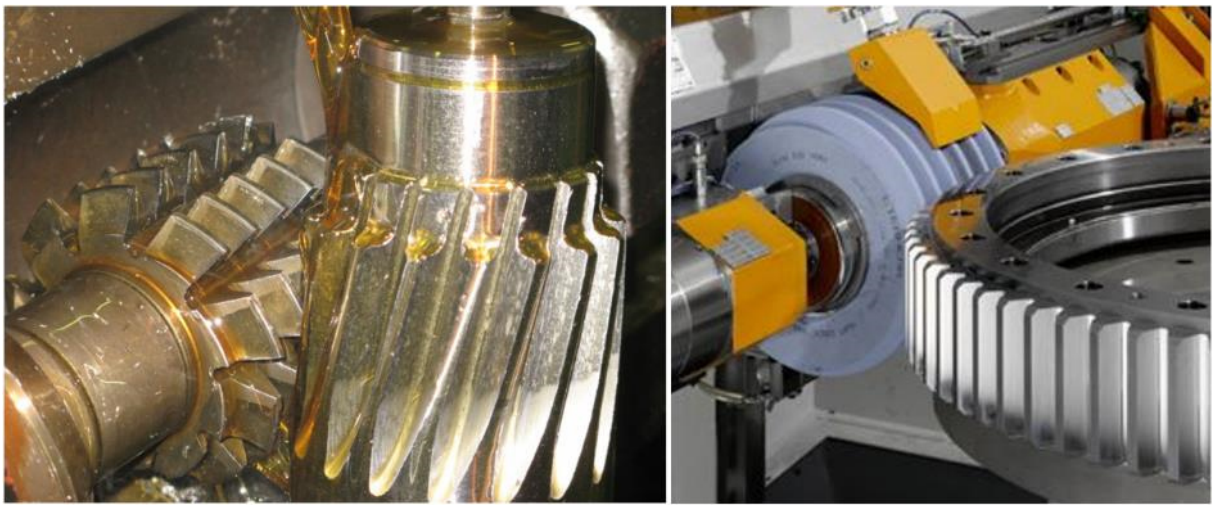

Figure 2-2: Typical gearing manufacturing process – milling (left) and grinding (right) [3], [4].

From the point of view of the kinematic, these two technologies are identical, despite the used tool.

Next possible way how to produce a gear is the **non-chipping** technology. As an example can be mentioned the EDM (Electrical Discharge Machining) technology – wire cutting.

Another possibility for gear production is the rolling technology. This technology description follows in next chapter.

2.2.2 Rolling Technology Description

Rolling technology is widely used e.g. for thread manufacturing. In the branch of drivetrain, it is commonly used for involute splines manufacturing on the shafts in the gearbox or on half axles and flanges. The advantage of this technology compared to standard chipping production methods (milling, turning, grinding, etc.) is in:

- short production time
- better (compact, smooth) surface quality
- improved mechanical properties (tensile strength) thanks to cold forming
- no waste material

In the Figure 2-3 there is depicted the basic principle of rolling technology for the case of the thread rolling. The dies are pushed by needed force to form (reshape) the workpiece.

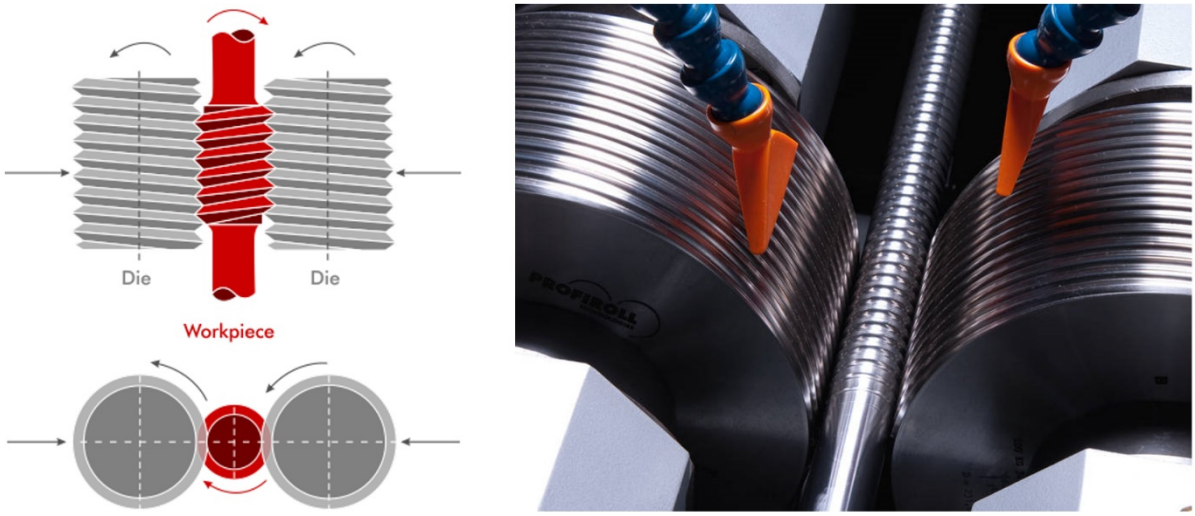

Figure 2-3: Principle (left) and real appearance (right) of the thread rolling [5], [6].

Similar situation arises while rolling of involute splines and gearings. Only the dies profiles are changed accordingly to the desired final shape. An example of the helical gearing rolling is depicted in Figure 2-4.

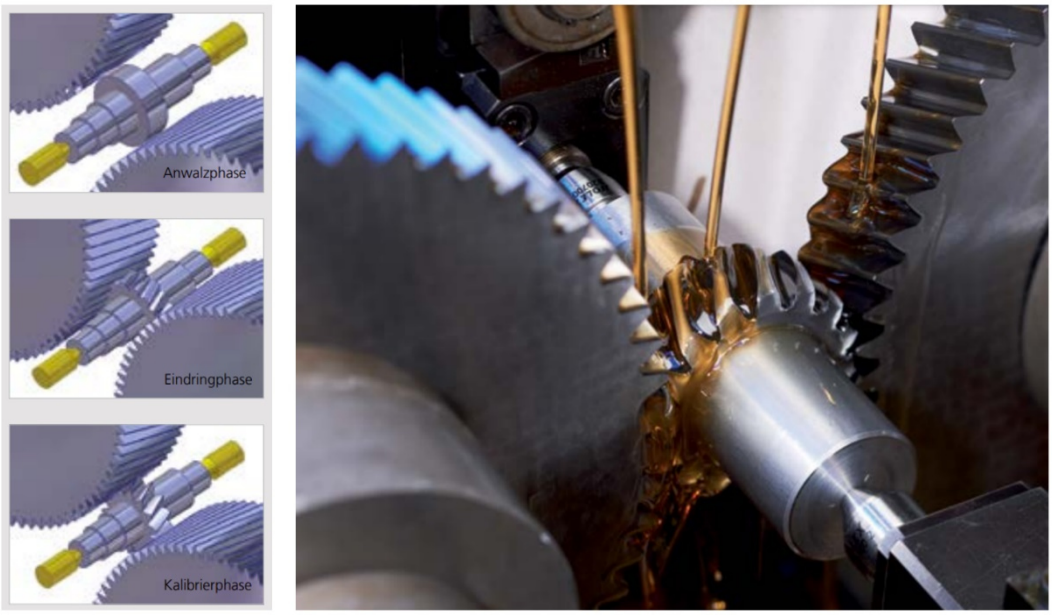

Figure 2-4: Model (left) and real appearance (right) of the helical gearing rolling [7].

2.2.3 Gearing Manufacturing Technology Research Conclusion

In the previous chapters were briefly described possible production technologies used in the gearing field. In automotive (mass production) is standardly used milling and after heat treatment grinding or honing as final operation. The rolling technology is commonly used for involute splines (with small modules) on shafts. It would be interesting to apply this technology also for automotive gearset, especially from the point of view of the base material properties improvement thanks to cold forming. Furthermore, within this thesis there was found a partner, who is worldwide known in the field of the rolling technology. For this reason, the **rolling technology** was chosen as the production technology of investigated gears within this thesis.

2.3 Gears Materials

2.3.1 Standardly Used Materials of Gears

Gears have been produced for many years and thus also many types of materials have been used. The material is always depending on gearset loading conditions. The most common materials in automotive are forged or alloyed steels with a final heat treatment – e.g. carburizing or nitriding – as a hardening treatment. To improve basic material's properties, special coatings can be used, e.g. PVD (Physical Vapor Deposition) technology.

Very interesting technology seems to be the PM (Powder Metal) technology. Its positives are very remarkable in the mass production. Furthermore, next advantage of this technology is especially in the product's homogeneity and isotropy. The detailed description of this technology branch follows.

2.3.2 Powder Metal (PM) Materials Description

"While a crude form of iron powder metallurgy existed in Egypt as early as 3000 B.C., and the ancient Incas made jewelry and other artifacts from precious metal powders, mass manufacturing of P/M products did not begin until the mid- or late-nineteenth century. At this time, powder metallurgy was used to produce copper coins and medallions, platinum ingots, lead printing type, and tungsten wires, the primary material for light bulb filaments. By the 1920s the tips of tungsten carbide cutting tools and nonferrous bushings were being produced. Self-lubricating bearings and metallic filters were other early products." [8].

Generally, the powder metal technology is processed in three basic steps: powder preparation (mixing), die compaction and sintering. In following chapters all these operations will be briefly described.

The process starts with the used powder mixing, when a base powder is mixed with alloying elements to reach desired material properties. Next step is the kneading together with the polymers and a wax to assure the shape stability after the pressing or molding. The main pressing operation "die compaction" follows. To be able to provide correctly this operation, some geometrical conditions must be maintained to assure sufficient densifying in the total die volume. After the compaction the shape of the pressed part is fixed only by additional material and is in so called "green state" and the pressing product is usually called "**green part**". The strength of this product is very low and is used only for the manipulation. It can be broken only by hand! This compaction process is schematically depicted in Figure 2-5.

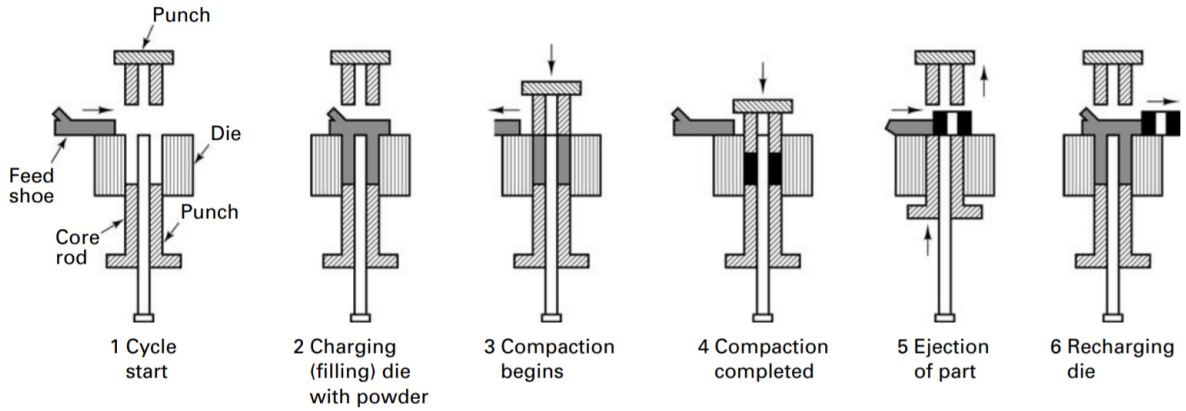

Figure 2-5: Typical compaction sequence for a single-level part, showing the functions of the feed shoe, die, core rod, and upper and lower punches. Loose powder is shaded; compacted powder is solid black [9].

Next operations are provided in a sintering furnace with controlled atmosphere, to remove the oxygen and prevent the oxidation of the metal parts in the green part. Very often some inert gasses are used, e.g. argon. The other possibility is to use vacuum in the furnace. At the beginning in the low temperature phase the green part is slightly preheated to allow the debinding operation, when almost all additional binding material is removed (melted). Subsequently the high temperature sintering follows. In this phase the powder particles, which are still only touching each other, are sintered. This means that these powder particles are firmly connected and the product gains ultimate strength. During this operation the volume of the sintered part is reduced. This fact must be taken into account while the designing of the pressing die geometry. The schematic structure of the PM material in certain stages of the sintering process in the furnace is depicted in Figure 2-6.

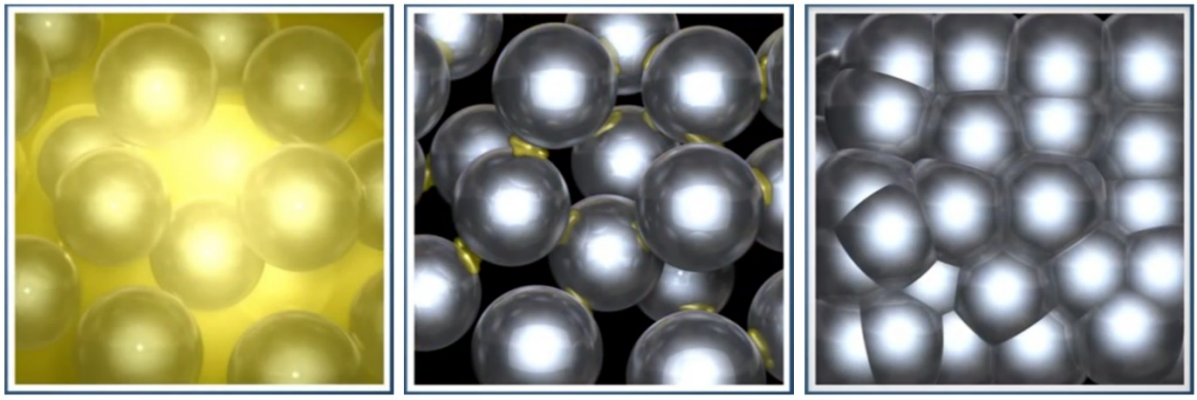

Figure 2-6: Schematic structure of the PM material in certain stages of the sintering process in the sintering furnace [10].

The PM technology can be very productive, especially in the mass production of parts with more complicated design, which could be standardly produced only by CNC milling from a full material. Next very important advantage of this technology in comparison to wrought steel is the green part's homogeneity and isotropy.

On the other hand, there are some geometry limitations of the PM green parts, e.g. the height of these parts cannot exceed some limits to assure "same" material properties (density) in the whole part's volume. From the physical principle, the density in the part manufactured by die

compaction process according to the Figure 2-5, it is clear, that the highest density will be reached on the green part's touching surface to the upper and lower punch. The lowest density is than always in the middle of the compacted part's height due to internal friction between PM grains. Gearwheels can be standardly produced by this technology including the gearing in one pressing operation.

On the other hand, one very important disadvantage is unfortunately a natural property of all PM products. It is the porosity. A typical example of the material structure is depicted in Figure 2-7.

If the part made by PM technology is loaded by tensile stress (e.g. while bending), the surface porosity can help to a crack initiation. This issue can be eliminated by additional technology treatment (densification), which will be described in following chapters.

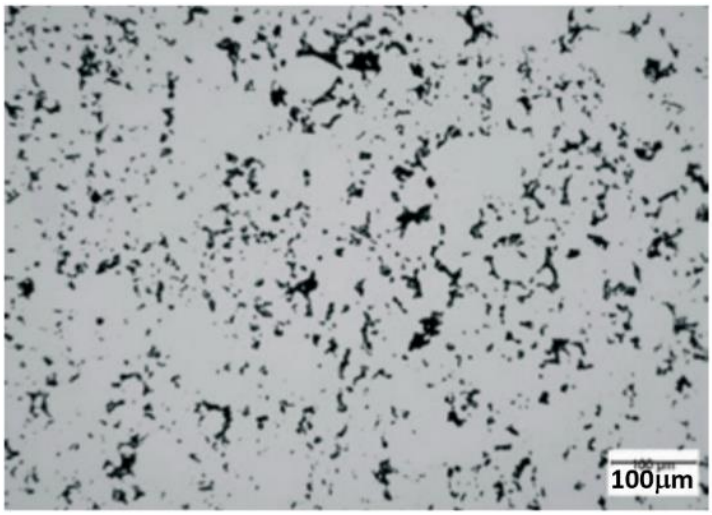

Figure 2-7: An example of a typical structure in a metallographic cut of a PM part prepared by polishing [11].

2.3.3 Hot Isostatic Pressing (HIP) Technology Description

In general, the PM technology has already been introduced in previous chapter including its most important positive and negative specialties. The biggest problem is the natural porosity of the material, Figure 2-7. One of possible ways to this issue elimination, is the usage of the HIP technology.

HIP technology is an additional process which improves product's mechanical properties. It reduces the porosity and simultaneously increases the part density. It is a combination of application of high temperature and pressure. This is standardly done in high pressure containment vessel. The gas inside the vessel is an inert one, to avoid chemical interaction with densified parts. For this purpose, argon is commonly used. After closing and filling the vessel with the gas it is heated. This causes also increasing of the gas pressure, which is applied to parts from all directions. For this reason, this procedure is called "**Hot Isostatic Pressing**". According to the densified material, determined time period must be spent in this state.

Besides density increase HIP process also increases material homogeneity, reduces internal voids and additional internal stresses caused by technology, e.g. casting, forging, welding, machining etc.. One of many descriptions of this process is described in [12].

In PM technology branch the standard process is the PM part compaction and afterwards its sintering in the furnace. The HIP process is only an additional option to improve its mechanical properties. An example of this technology application is depicted in Figure 2-8.

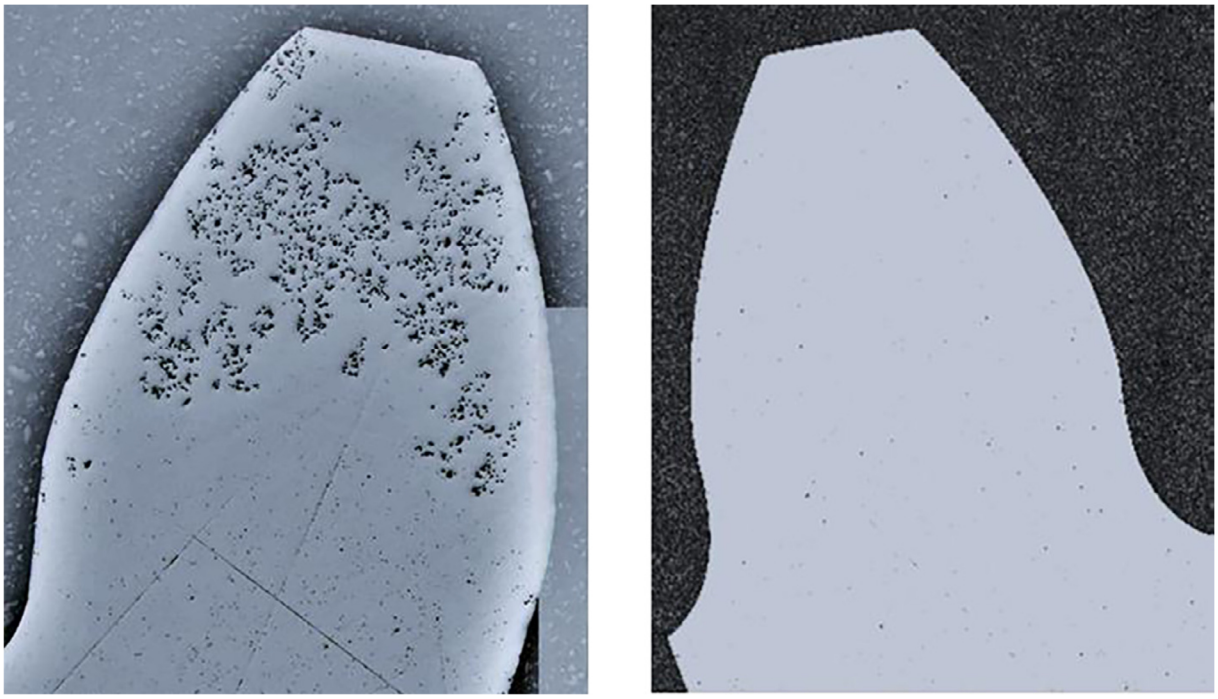

Figure 2-8: Illustration of HIP:ing with still open porosity (left) and closed porosity (right) [12].

2.3.4 Application of PM gears in automotive gearbox

The PM technology has already been applicated in automotive gearbox. The paper [34] describes the application of PM gears made by pressing, sintering and surface densification using transverse rolling from the point of view of the geometry quality. “It is shown that PM gears can be manufactured well within the DIN “quality 8” tolerance fields” [34].

Next application of PM gears in automotive gearbox is described in [35]. In this case a gearset of a passenger car **Smart Fortwo** was by the company Höganäs AB redesigned to the PM variant to maintain the original reliability, tested and evaluated after 200 000 km of real driving. In this case the HIP technology wasn`t applied.

2.3.5 Gearing Material Research Conclusion

In the previous paragraphs were very briefly described common materials used in the gearing production. Very innovative and interesting seem to be especially the PM material. For this reason, the **PM material** was chosen as an investigated gears material within this thesis.

2.4 Gearing Geometry

2.4.1 Gearing with an Involute Profile

The vast majority of produced gears has an involute profile. In the course of time some of these profiles were standardized. The most commonly used profile for general purposes is the profile "1,25/0,38/1,0 ISO 53:1998 Profil A" with a normal pressure angle of 20°. This kind of gearing is called "normal-contact-ratio" (NCR) gears. The values used in the profile description determine the relative height coefficients "dedendum/root radius/addendum". By using of this profile there are alternating one and two teeth pairs in the mesh, which causes the abrupt stiffness change along the line of action. This situation, where the transverse contact ratio $\varepsilon_\alpha \in (1,2)$ is for the spur gearing depicted in Figure 2-9 (left). To eliminate this issue, the gearing with **HCR (High Contact Ratio)** profile can be used. The aim of this profile is to reach the integer value of $\varepsilon_\alpha \in N$ (2, 3, 4 …). To preserve the original transverse pitch, the value of normal pressure angle α_n must be reduced. An example of such gearing is depicted in Figure 2-9 (right).

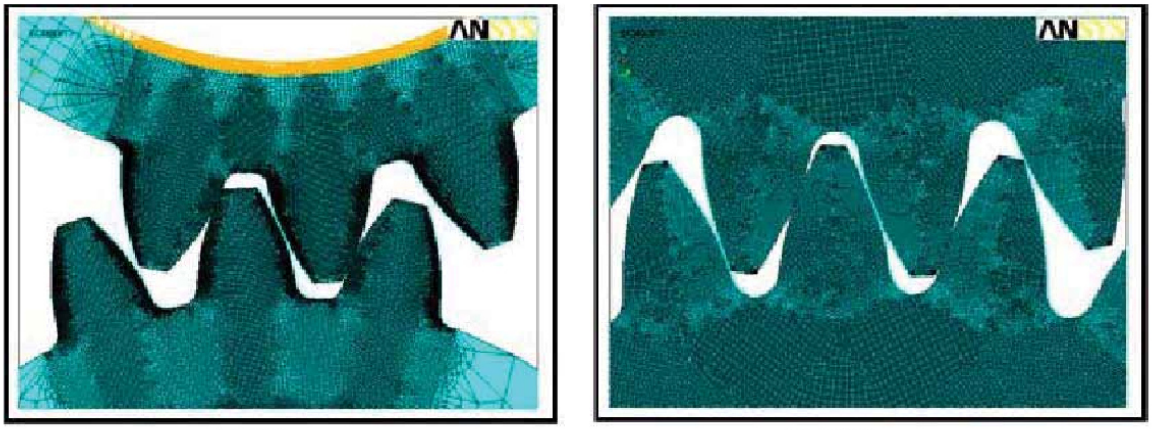

a) NCR gear b) HCR gear

Figure 2-9: Typical appearance of standard NCR (left) and HCR (right) gearing [33].

The stiffness along the line of action is then much smoother, and thus the load capacity is increased and in addition the vibration and noise excitation is lowered. For helical gearing this "integer" condition holds true for the total mesh ratio ε_χ which is influenced by the axial contact ratio ε_β.

In automotive industry (mass production) this profile is commonly used, because it is worth to buy a very expensive manufacturing tool with this special profile despite its high price.

The most important source of emitted noise from the gearing is mainly the non-constant mesh stiffness between mating gearwheels in the gearset. The noise reduction criterion is important for hybrid and especially and electric vehicles, where the typical ICE noise is no more present.

Except involute gearing with symmetric non-standard profile, the next possibility is a usage of the involute gearing with an **asymmetric profile**. This means, that there are different pressure angles on both sides, Figure 2-10. This profile can be used for contact pressure reduction if loading conditions are significantly different on both tooth sides, e.g. in helicopter rotors drivetrains.

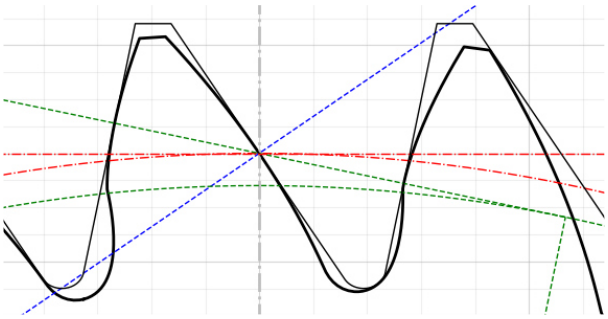

Figure 2-10: Appearance of the involute gearing with an asymmetric profile.

The geometry of the involute gearing with an asymmetric profile has been very well described.

The result of the scientific contribution describing the asymmetric gearing is commonly a created software, which considers the geometry of the rack tool. The gearing profile is created as the result of the mating with a rack cutter (trochoidal movement), which simulates the situation while manufacturing. This approach was used in [27] and [28], Figure 2-11.

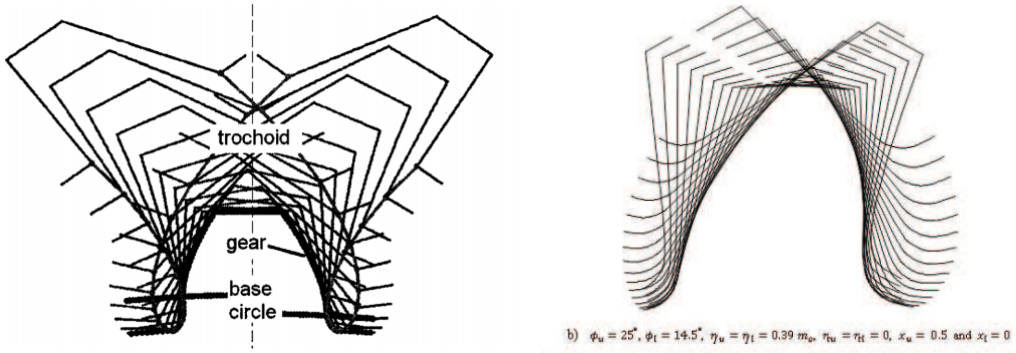

Figure 2-11: Generation simulation showing trochoidal movement of rack cutter tooth [27] (left), [28] (right).

The geometry of the internal asymmetric gear is described in [29]. The basic profile and meshing principles of an internal involute asymmetric gear is computed using a double envelope concept. In this paper is also presented an influence of the gears misalignment on the mesh parameters (quality), Figure 2-12.

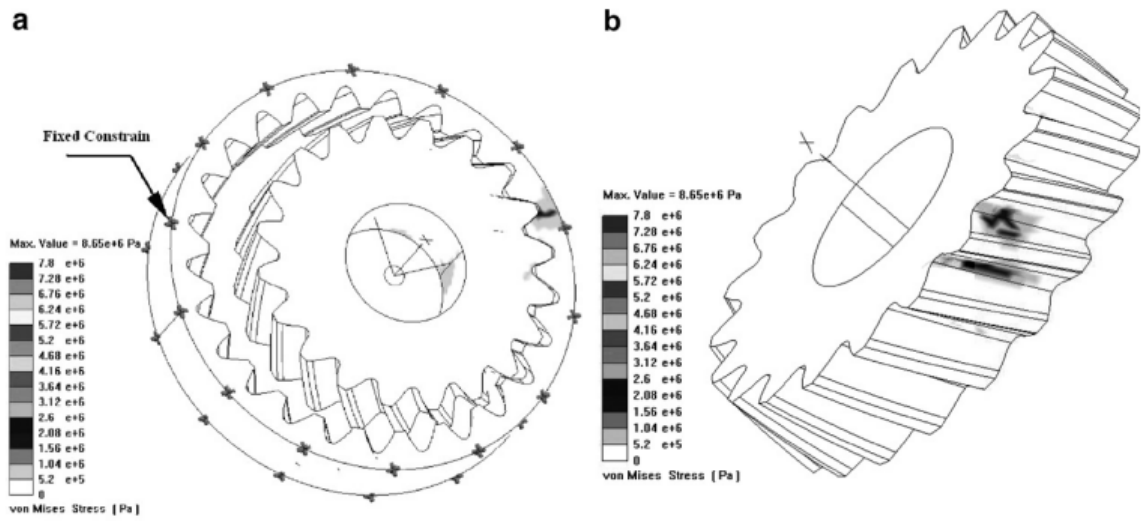

Figure 2-12: Internal gearset with asymmetric involute gearing of a pump [29].

The application of the spur gearing with an asymmetric profile in the gear pump from the point of view of the hydraulics is introduced in [30]. Thanks to asymmetric profile can be reached an improvement in the flow (lower non-uniformity) and the overall size of the pump, Figure 2-13.

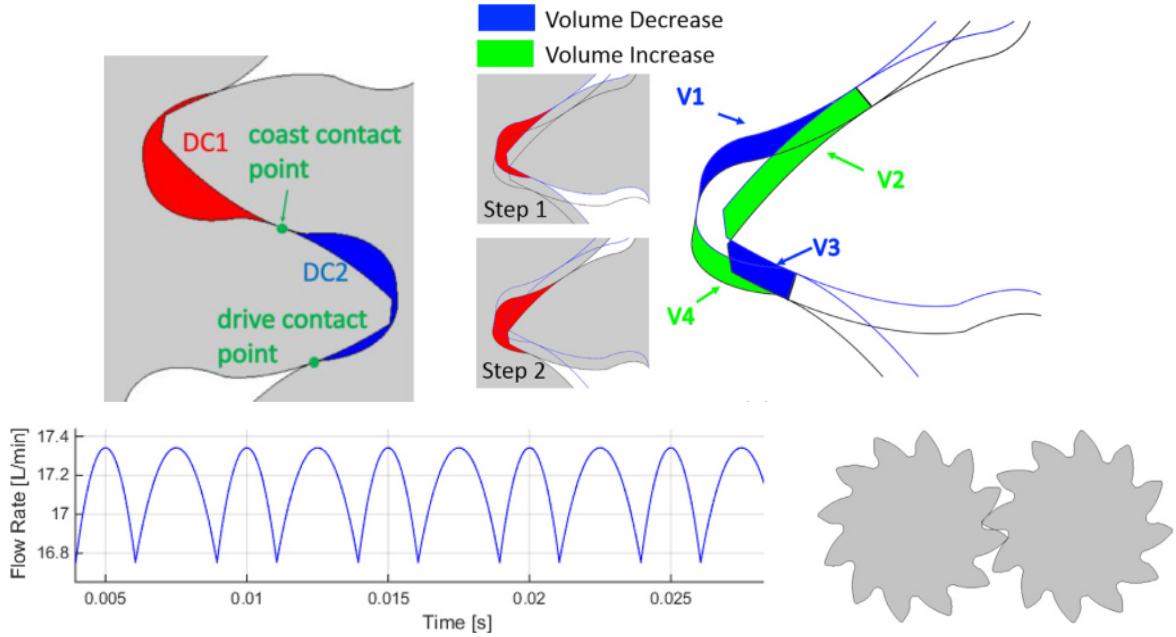

Figure 2-13: External spur gearset with asymmetric involute gearing of a pump [30].

The method for the determination of the bending stress in the tooth root on the drive side is described in [31]. This computation was done using a modification of the computation method from the standard DIN 3990/Method C and ISO/TC 60. The influencing stress concentration factors were defined for all important gearing parameters.

The influence of the asymmetric gear profile on the impact strength was investigated in [32], it was shown that the asymmetric profile is better from this point of view, Figure 2-14.

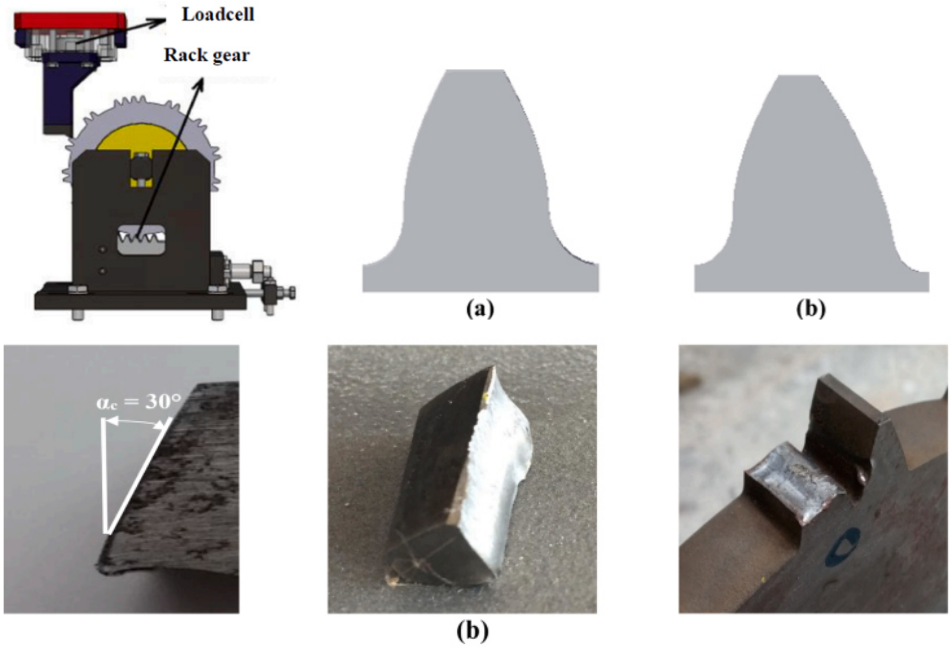

Figure 2-14: Result of the impact strength test of an asymmetric gear [32].

Next very important source regarding the geometry and stress analysis of asymmetric involute gearing was the book by A. Kapelevich [25] and a dissertation of A. Langheinrich [26].

2.4.2 Gearing with Non-Involute Profiles

2.4.2.1 Cycloidal Gearing

Next type of used gearing can be marked as gears with non-involute profiles. The first type is the **cycloidal gearing**. Its characteristic S-shaped teeth are created by rolling the roll circle along the pitch line, Figure 2-15. There are more possible geometries, so called **epicycloidal** and **hypocycloidal** gearing, when the roll circle is not being rolled along a pitch line but along the pitch circle.

Positive property of the cycloid gearing is that thanks to the S-shaped tooth flank the surface stress is significantly reduced compared to involute gearing. The negative property is very expensive and time demanding manufacturing process. Furthermore, this gearing generates high transmission error and vibrations if working center distance varies from its theoretical value.

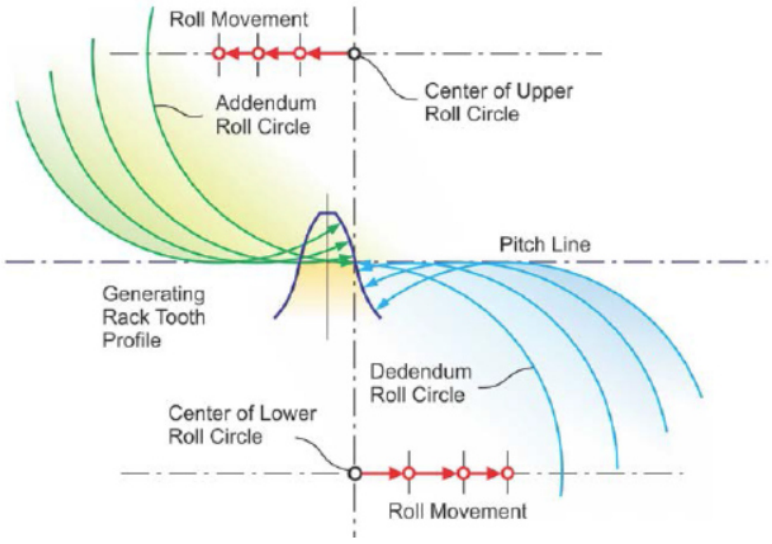

Figure 2-15: Cycloidal generating rack profile development [13].

2.4.2.2 Wildhaber-Novikov Gearing

Next type of gearing with non-involute profile is the Wildhaber - Novikov gearing. It was invented by Ernest Wildhaber in 1926. The gearing with similar function was also invented by Michail Novikov 30 years later. For this reason, final name of this gearing was the combination of these two names. The characteristic property of this gearing is the **circular profile** in the transverse plane.

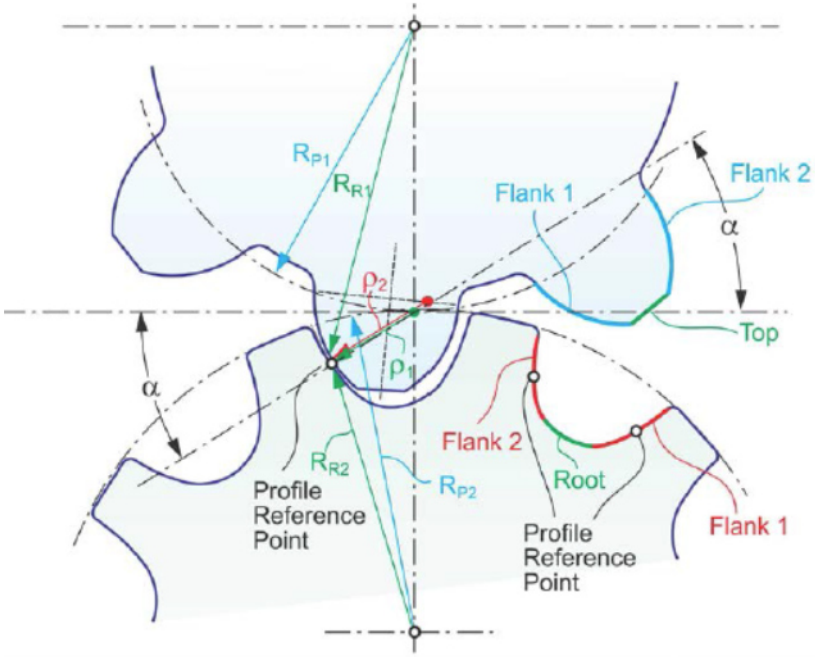

Figure 2-16: Wildhaber-Novikov gearing design - circular profile in transverse plane [13].

Unfortunately, the circular profile doesn't fulfill the condition of the gearset's constant ratio. This issue is depicted in Figure 2-17 (left). For this reason, the mesh point must be moved back to the gearset axis thanks to precise value of the helix angle. This means that the mesh (contact) point must be moved along the facewidth, Figure 2-17 (right).

The positive property of Wildhaber-Novikov gearing lays in the large contact area, and thus very low contact pressure. The geometry is also very positive from the point of view of lubricant film

thickness. For both these reasons the load -carrying capacity is several times higher in comparison to involute gearing.

The disadvantage of this type of gearing lays in a complicated rack tool geometry and furthermore in the strictly given value of the helix angle to assure constant ratio. Its value is also dependent on the facewidth. This condition evokes high sensitivity of the transmission error (working smoothness) on real tooth flank precision and real working axes distance.

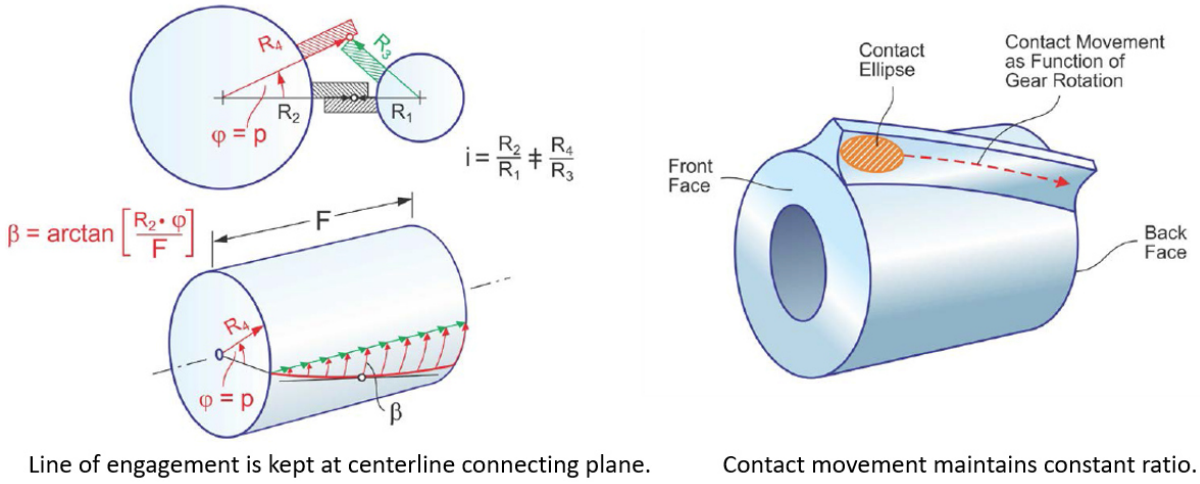

Figure 2-17: Wildhaber-Novikov gearing function – needed helix angle [13].

There are still several gearing types, e.g. "Extended version of Wildhaber-Novikov gearing", where the tooth height is increased and the tooth flank consists of a convex circle at the addendum and a concave circle at the dedendum, Figure 2-18. This allows to finetune the gearing properties.

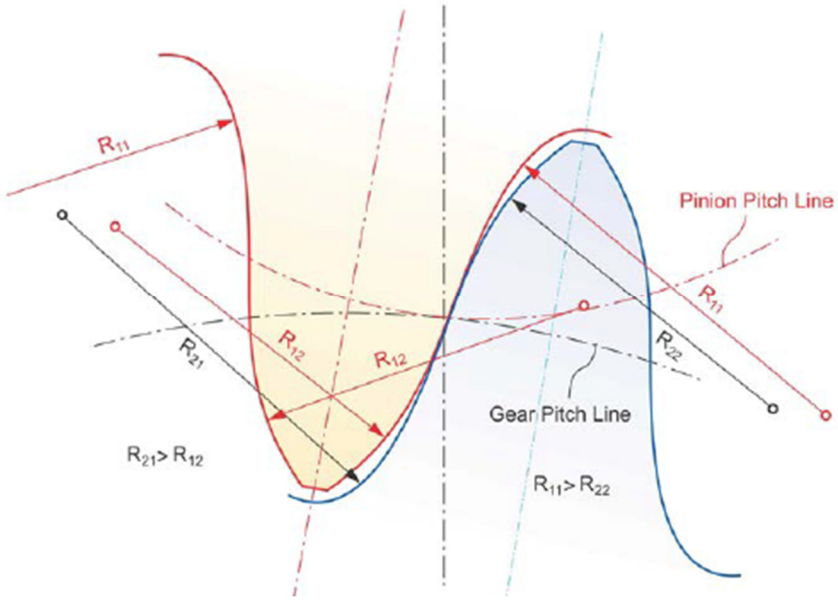

Figure 2-18: Wildhaber-Novikov gearing – extended version [13].

Next improvement to this gearing was done by prof. Nagata in 1981, who improved the gearing geometry definition directly on the manufacturing tool. The new profile has a circular addendum and a dedendum that consists of two involutes that blend at mid-dedendum, Figure 2-19.

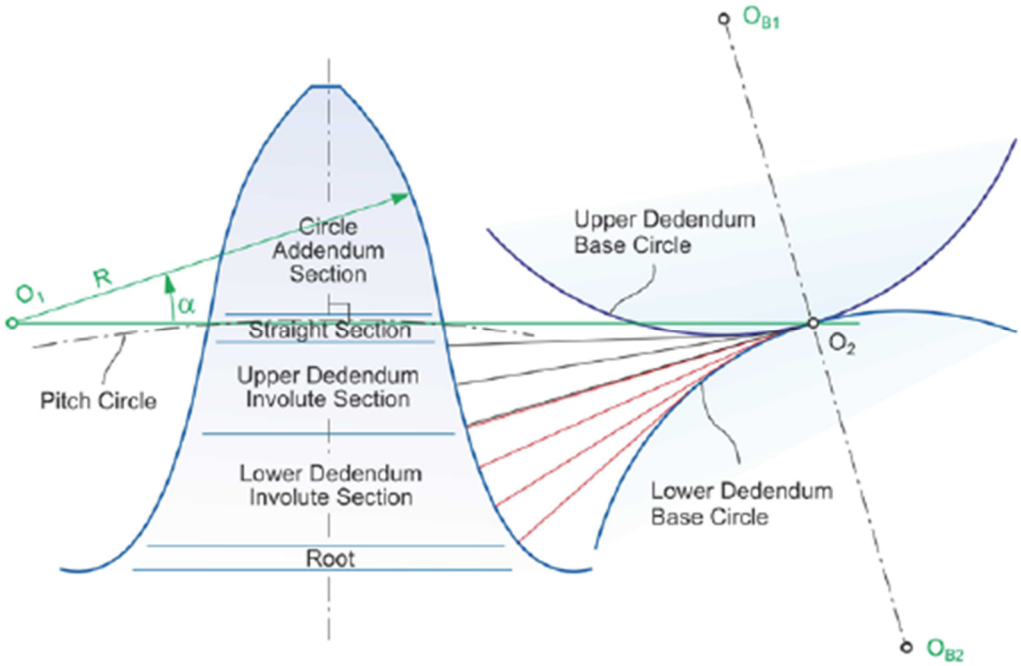

Figure 2-19: Design of Wildhaber-Novikov-Nagata gearing – circular addendum and involute dedendum profile [13].

2.4.2.3 Convoloid Gearing

Convoloid gearing has very similar design as Wildhaber-Novikov-Nagata gearing. It was introduced in 2011 by Bernard Berlinger and John Colbourne. This type of gears is commonly used in wind turbines transmissions for its advantage in lowering contact stresses.

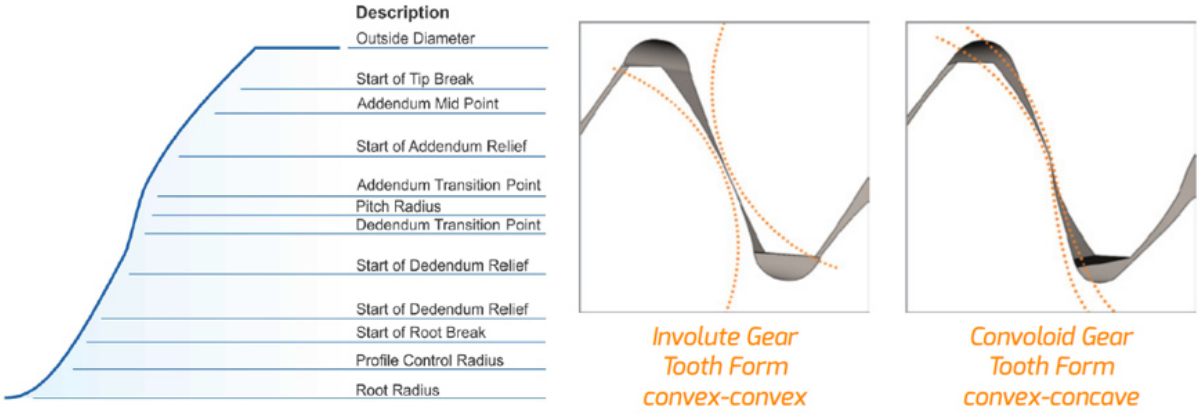

Figure 2-20: Design of convoloid gearing – convex-concave contact [13], [14].

"The addendum has a convex shape, while the dedendum is concave. The transition zone at the pitch point seems to be "S-shaped" rather than the straight section of Nagata's development. The authors report that the tooth profiles are computer calculated as a point cloud for each application case individually.

One interesting conclusion of Berlinger's and Colbourne's findings is the fact that while involute gearing fit well with traditional, mechanical gear manufacturing machines, it is outdated for today's engineering and manufacturing environment. Test rig investigations of Convoloid gears resulted in 20%-35% increased torque levels vs. involute gearing. The center distance insensitivity of involute gears seems not to be given, but the inventors state that the Convoloid gears can withstand the customary deflections given in modern gearboxes.

An interesting aspect of Convoloid gears is that the tooth contact can move from root to top while maintaining the correct ratio. This makes Convoloid gears independent from the helix angle and allows a choice of suitable helix angles, depending on gearbox application requirements. The Convoloid profile of Figure 2-20 (left) refers to the final teeth, not to the rack profile. In order to establish the rack cutter profile, the kinematic relationships, e.g., of a hobbing process, have to be employed to calculate a point-based cutting edge definition." [13]

2.4.3 Gearing Geometry Research Conclusion

In the previous chapters there were described the most important types of used gearing geometry. For this thesis it is very important to reach real data from the measurement. Therefore, the finally chosen geometry variant had to fulfill two requirements; it must be non-standard and furthermore manufacturable, to be able to produce it and test it in the laboratory. The compromise of these two conditions was the **helical involute gearing with an asymmetric profile**.

2.5 Demands on New Gear Design

In previous chapters were described geometrical, material and technological aspects of the current gears production. From these descriptions arose demands on new gear solution. The designed gearset should have the potential of:

- endurance strength increase
- production costs reduction
- maintaining original gearset size (original gearbox housing)
- weight reduction

To enable the fulfilment of these above stated demands following methods (ways) can be used:

- new material
- new technology
- new geometry
- combination of above-mentioned ways

3 Thesis Targets

In previous chapter there was described the current state of the art in the field of gears from the point of view of the manufacturing technology, material and geometry.

The intention of this thesis is to apply new technologies on PM material in the field of gears dedicated for **automotive transmissions** and to determine their influence on gearset's endurance. It has two main parts.

In the first part the topic is the application of the HIP technology on gearing with standard symmetric geometry and chip manufacturing. The innovative is in this case not the HIP technology itself, but the field of usage of these HIP:ed PM gears.

The second part deals with the design of asymmetric gear profile to reduce contact stresses between tooth flanks. Furthermore, the gearwheels were manufactured with help of the rolling technology.

In order to be able to design gears with an asymmetric profile, it was necessary to create the appropriate software, because at the time we started this work, no commercial software was available. For the strength analysis of the gearing with an asymmetric profile FEM method was used.

Precise targets definition of this thesis was influenced also by real production possibilities, which were performed by cooperating companies, namely the **Höganäs AB** from Sweden as a specialist in PM (Powder Metal) branch and German **Profiroll Technologies GmbH**, a specialist in branch of the rolling technology. Next very important role played a car producer, who provided us all necessary support during the gears manufacturing, measuring and testing.

Almost all endurance test results of gears made of new materials (or using new technologies) were performed on test rigs very similar to Figure 4-7. In this case the target is to shorten the test, thus the torque is increased appropriately. This means, that gearboxes, shafts and bearings are very robust, to have the gearing as the weakest part in the whole testing circuit. Tested gearing is commonly a spur gearing, the lubrication is realized using pipes, which deliver the oil directly in the gear mesh, or at least the oil circulation is used not to exceed allowed temperature.

In the automotive gearbox the situation is very different from above mentioned loading conditions. The weight is very important, therefore the gearbox cast is made of the aluminum alloy with thin walls, long thin shafts lead to high displacements due to bending and the oil can be cooled only using fans. Local loading conditions are unique for each speed stage in the gearbox.

From all these limiting conditions emerged targets of this thesis to be fulfilled. These targets are stated in following points:

1. **Determine endurance potential (strength) of gears with original design made from PM material with special technology (HIP) based on test results performed directly in automotive gearbox**

2. **Determine endurance potential (strength) based on test results of gears with asymmetric profile made from PM material with special surface treatment (rolling) based on test results performed directly in automotive gearbox**

To be able to accomplish the above stated targets, these special gears must be designed, produced and tested. For this reason, this thesis continues with the detailed description of gears testing methods in the Chapter 4.

Afterwards, the test bench, which was used for the testing and its improvements, are described in Chapter 5.

4 Automotive Gearbox Testing

In general, the newly designed part (gearset) must be always tested before it is put into operation. More types of tests of automotive gearboxes are described in following chapters.

4.1 Functional Tests

Nowadays, there are many sophisticated pieces of software for the strength analysis of designed parts. These programs apply commonly the FEM analysis directly in a MBS (Multi Body System), where the whole assembly of all important mating parts can be designed as a complex unit. An example of such software in the branch of the gearing can be the KissSoft (KissSys). In this software can be designed whole gearbox including shafts, bearing and of course a gearbox housing. Interacting conditions between all these separate parts must be precisely defined. After applying certain load (torque) on given shaft, all reacting forces between parts are computed. In the next step, if material parameters of the parts are known, needed stresses and deformations can be computed. These data serve subsequently for a final microgeometry tuning. In case of the gearing these parameters are the tooth flank modifications (helix and profile angle, crowning).

Despite all these sophisticated methods, real tests directly on the gearing must be performed to verify preliminary calculations. The description of such type of the tests follows.

4.1.1 Shaft Deformation Measurement

Each real part with defined material properties deforms under any loading conditions. This deformation magnitude is significant especially in case of long thin parts, which are typically in case of automotive gearboxes, the shafts. To be able to verify their spatial deformation (shape of their deformation curve) under certain loading (applied torque), these deformations must be measured. An example of such deformation measurement is depicted in Figure 4-1.

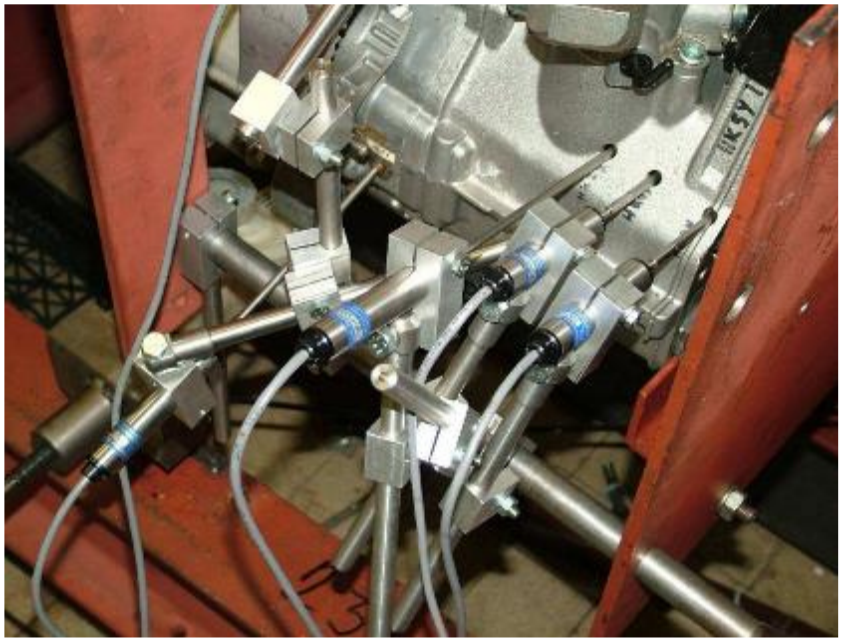

Figure 4-1: Example of the shaft deformation measurement under certain loading conditions in the laboratory of the TU of Ostrava

There must be drilled some holes in the gearbox cast to enable to touch directly the shaft inside by precise length sensors. The principle of this measurement is to measure linear shaft displacement in certain direction in more places and ideally also in more directions (planes). From these values can be subsequently computed real shaft deformation. It should be reminded that this test is the static one, shafts with gearwheels don't rotate, only the torque is applied.

4.1.2 Contact Pattern Test

Contact pattern test must be done before the endurance testing. The aim of this test is to describe real load distribution on the loaded tooth flank. The basic principle of this test lays in painting of one chosen tooth flank at each gearwheel by a special color. Afterwards a certain torque is applied, and the painted tooth of each gearwheel must pass through the mesh only once. During this passing through the mesh the color paint is pushed out of the tooth flank and thus the loaded area (mesh pattern), which was used while gear meshing is then visibly marked (area without a paint).

Standardly, this test has two types of results, so called "single" and "summative" one. The "single" result of the contact pattern test is reached after passing the painted tooth through the mesh only once. So, the mesh happens only between one single tooth of each gearwheel. More interesting from the point of view of the gearset meshing quality, is the summative result of the contact pattern test. In this case this painted tooth passes through the mesh with all teeth of the mating gearwheel. This means, that the number of rotations of the gearwheel with a painted tooth must be same as the teeth number of the second gear. An example of such test result is depicted in Figure 4-2.

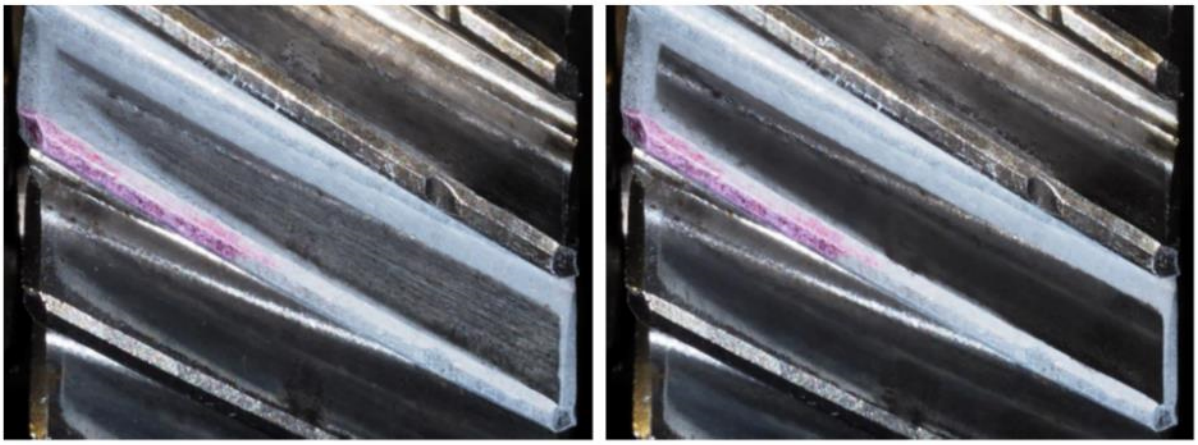

Figure 4-2: Example of the contact pattern test results appearance – single mesh pattern (left) and summative mesh pattern (right).

In the appearance of the summative mesh pattern there is included the influence of inaccuracies of all teeth mating in the gearset. If the total mesh pattern is similar to the single mesh pattern, it means, that the mesh quality (gearing precision) is uniform among the whole circumference.

4.2 Endurance Testing

In the previous Chapter 4.1 there are described ”static” test methods for determination of shaft deformation and load distribution (mesh quality) on tooth flanks by certain load (torque) level. These parameters are very important from the point of view of the gearset endurance. The resistance against all possible gearing failures is the most important parameter, and thus must be tested. The purpose of these endurance tests is to determine fatigue parameters of tested gearset material for more load (stress) levels. It means to find out for certain load (stress) level the number of cycles until some failure appears (S-N curve). If these material curves are known, then it is possible to design a gearset with respect to its desired number of lifetime cycles. These material curves data (S-N curves), acquired while testing, are then used in appropriate standards. Testing methods, described for example in the standard **ISO 6336-5:2003** in a Chapter 4, will be shortly described in following chapters.

4.2.1 Allowable stress numbers determination - Method A

“The allowable stress numbers for contact and bending are derived from endurance tests of gears having dimensions closely similar to those of the gears to be rated, under test conditions which are closely similar to the intended operating conditions.” [15] Using this method is the best way how to determine the gearing endurance, because here the loading conditions are very close to the real operating regime, i.e. the combination of bending and Hertzian stresses with slipping velocities. For testing of the gearing in this way two basic principles can be used, see following chapters.

4.2.1.1 Open Test Bench

The so called “Opened test bench” is commonly used for the gearing testing and its principle is depicted in Figure 4-3. The power is created in the driving dynamometer, then it flows through the gearbox and finally it is wasted in the braking dynamometer. This wasted energy it either transformed into the heat or can be recuperated back to the electricity network.

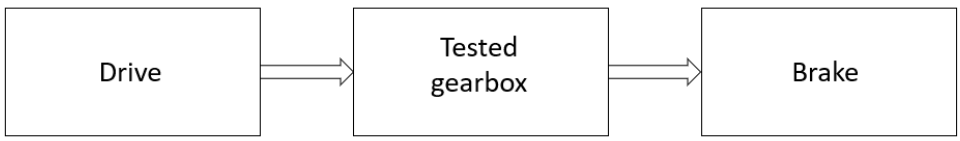

Figure 4-3: Scheme of the opened test bench principle

In case of standard automotive drivetrain, the power is created in the ICE and subsequently it flows through the gearbox and half-axles to driven wheels. To emulate this power flow scheme, special test bench, designated for automotive gearbox testing, is placed in laboratories of the CTU in Prague. The advantage of this test bench lays in the ability of applying the loading spectrum of all speed stages to the gearbox in the same manner, as it was measured while real driving tests at the polygon. Its appearance is depicted in

Figure 4-4 and the power flow diagram is depicted in Figure 4-5. It consists of three dynamometers, one of them is working in the motor mode (emulate the ICE), other two in the generator mode (emulate passive resistances). Power is transmitted from the driving dynamometer through the belt drive, supported in two bearing houses, to the input shaft of

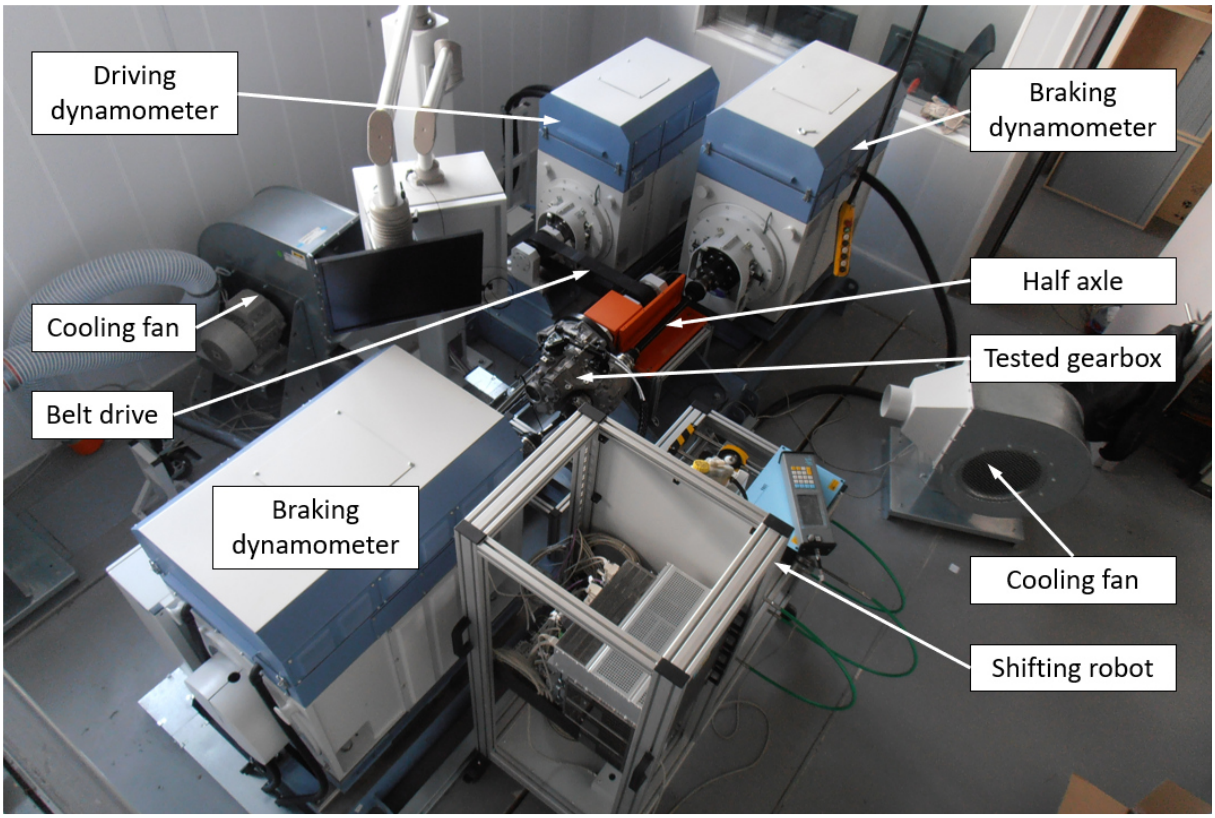

Figure 4-4: Appearance of the opened test bench for automotive gearbox testing in laboratories of CTU in Prague

the tested gearbox. Its both outputs are then connected to braking dynamometers by two standard automotive half axles. To enable the shifting, standard friction clutch including the flywheel is used at the gearbox input. To eliminate dynamic overloading (torque peaks) while shifting during the test,

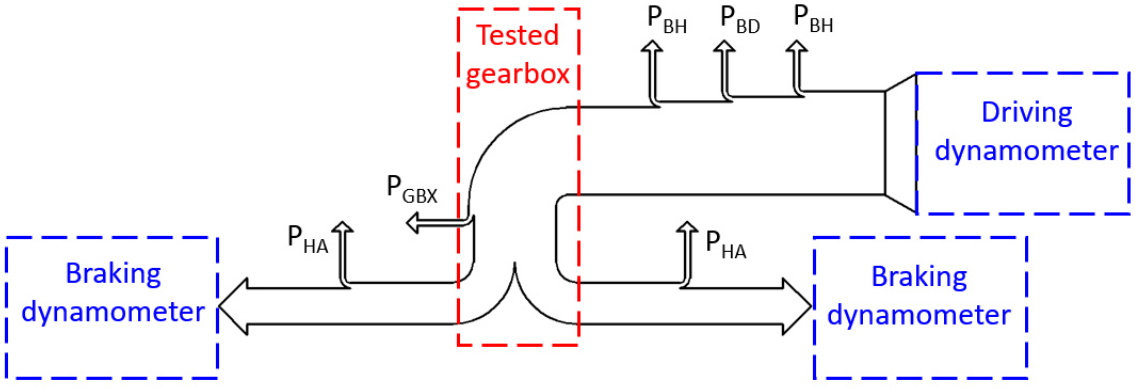

Figure 4-5: Power flow diagram of the opened test bench for automotive gearbox testing in laboratories of CTU in Prague

special protective coupling is placed between the belt drive and the flywheel. An integral part of this test bench is the shifting robot. It is connected to the gearbox using standard bowdens completed with a gear lever. This gear lever base is fixed to the shifting robot frame and is manipulated in two directions (axes x and y) by two servomotors. Third servomotor controls the clutch pedal. Thanks to

this test bench, it is possible to test the gearbox as a complex unit, including bearings, synchro rings, final drive and the differential.

Two more remarks should be mentioned to this test bench. The first one relates to the way of usage of the dynamometers. It is clear, that all of them can work either in motor- or generator mode. Furthermore, regarding to this test bench design, it should be mentioned that all these three dynamometers are mounted to a common cast iron plate, which is supported to the ground (floor) by eight air springs, because of vibrations damping. The position of these dynamometers can be adjusted arbitrarily, according to the tested drivetrain, e.g. for a gearbox for longitudinal drivetrain conception (tractor) or hybrid vehicle with a planetary power split device.

Second remark to this test bench focuses on its electric equipment, which consists of three frequency convertors for the dynamometers. Generally, the frequency convertor principle lays in rectifying of input 50 Hz AC voltage to DC voltage, which is consequently changed back to AC voltage, but with another frequency according to desired dynamometer speed. At the input to the main electric switchboard, the rectifier for supplying the common DC circuit, is used. From this DC circuit is consequently powered the driving dynamometer. On stators of braking dynamometers, AC voltage of different frequencies, depending on their rotor speed, is generated. This power is again rectified and connected to the common DC circuit in the main switchboard and can be repeatedly used for further test bench driving. Finally, it is necessary to take from the electricity network only the power corresponding to the sum of all mechanical and electrical losses. It can be said, that this test bench is “open” in mechanical part and “closed” in electrical part, which enables the power circulation and energy savings.

4.2.1.2 Closed (Back-to-Back) Test Bench

Gearing endurance tests, according to the method “A” (Chapter 4.2.1), can be also performed using another type of the test bench, which is so called “closed” or “back-to-back” test bench. In comparison to opened test bench, this type of test bench has big advantage in its power demands, because of usage the power circulation. This circulation has been already mentioned in previous chapter, but there it was “closed” only in the electrical way. In this case, the power circulation is achieved in the mechanical way due to its special design. Its basic principle and power flow diagram are depicted in Figure 4-6.

The closed test bench consists of two gearboxes (gearsets), one of them is so called “tested” one. The second is the “technological” one and serves only for the closing of the circuit. The essential condition for correct function is that both these gearsets must have same gear ratio.

The input shaft is divided into two parts (shafts) by a friction clutch. After locking of one input shaft, usually by a locking pin to the frame, the second one can be subsequently loaded by the desired torque M_2. This torque evokes, depending of the circuit’s stiffness, some angular displacement between both clutch functional surfaces. In this position is then the clutch fixed and the torque (pretension) in the circuit remains. Subsequently, the locking pin can be removed, and the already pretensioned circuit can be driven (rotated) by a torque M_1. For this driving serves the connected electromotor, which must overrule only the passive resistances in the circuit.

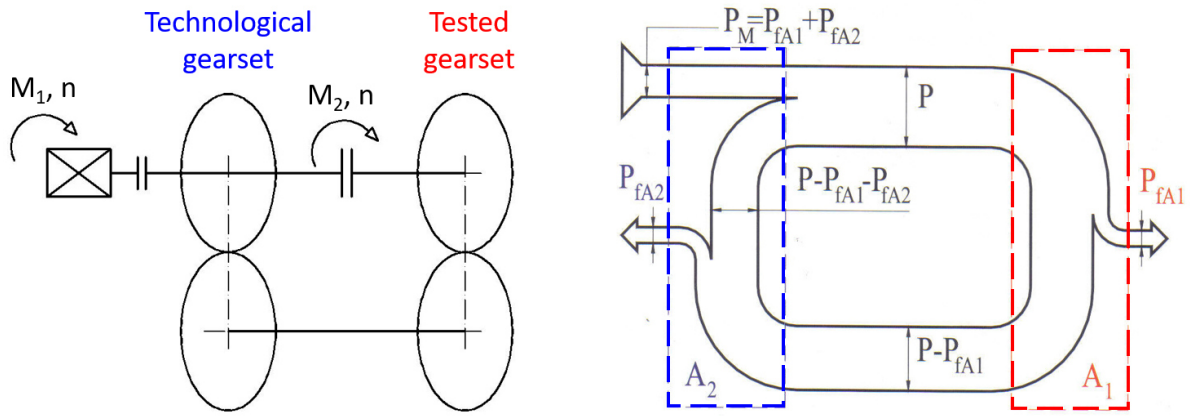

Figure 4-6: Scheme (left) and the power flow diagram (right) of the closed (back-to-back) test bench for gearset testing [16].

In the Figure 4-6 is in the power flow diagram visible the amount of power, which can be reused in the circuit due to the circulation. The gearbox role (tested/technological) is determined by the power flow direction in the circuit. In general, the power vector is given as the vector product of the loading torque vector and the vector (direction) of rotation. In the Figure 4-6 is the tested gearbox marked as A_1, the technological one as A_2.

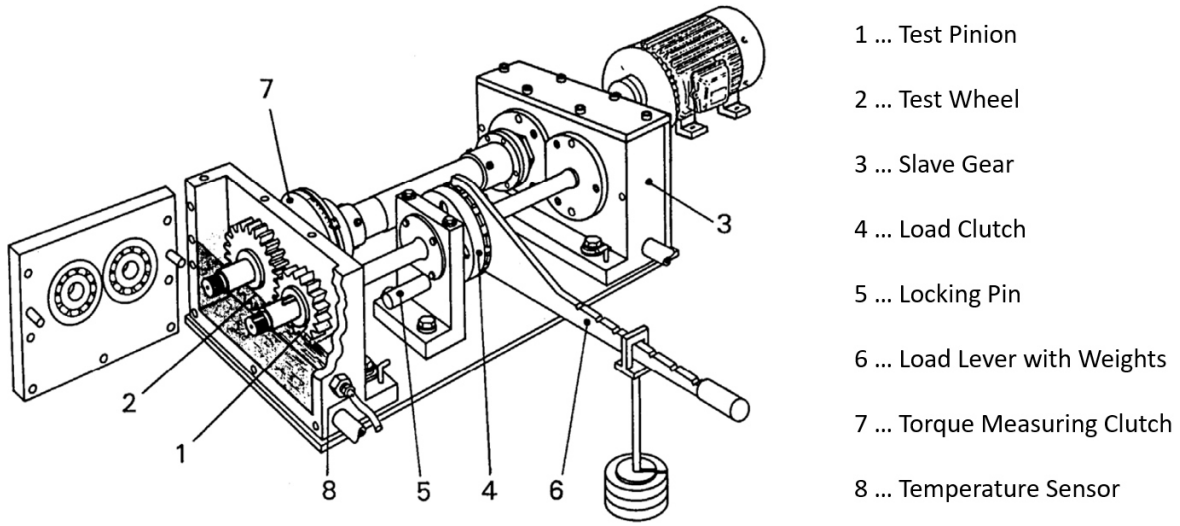

Figure 4-7: Appearance of the original back-to-back test rig designed by Prof. Gustav Niemann [17].

One of the world's leading gearing research institutes, the FZG (Forschungsstelle für Zahnräder und Getriebebau), is situated in Germany in Munich. This institute is the part of the Faculty of Machine Engineering at the TU Munich and was founded by Prof. Dr.-Ing. Gustav Niemann in 1951. In the Figure 4-7 is depicted a closed (back-to-back) test rig designed by Prof. Niemann.

Loading torque is here evoked by weights hung on the lever, the friction (load) clutch is here realized by two flanges screwed together using the bolts around the circumference. An example of the back-to-back test rig in FZG in Munich is depicted in Figure 4-8, in this case for testing of hypoid gearing. This figure was taken by me during a lab tour within the International Conference on Gears 2013.

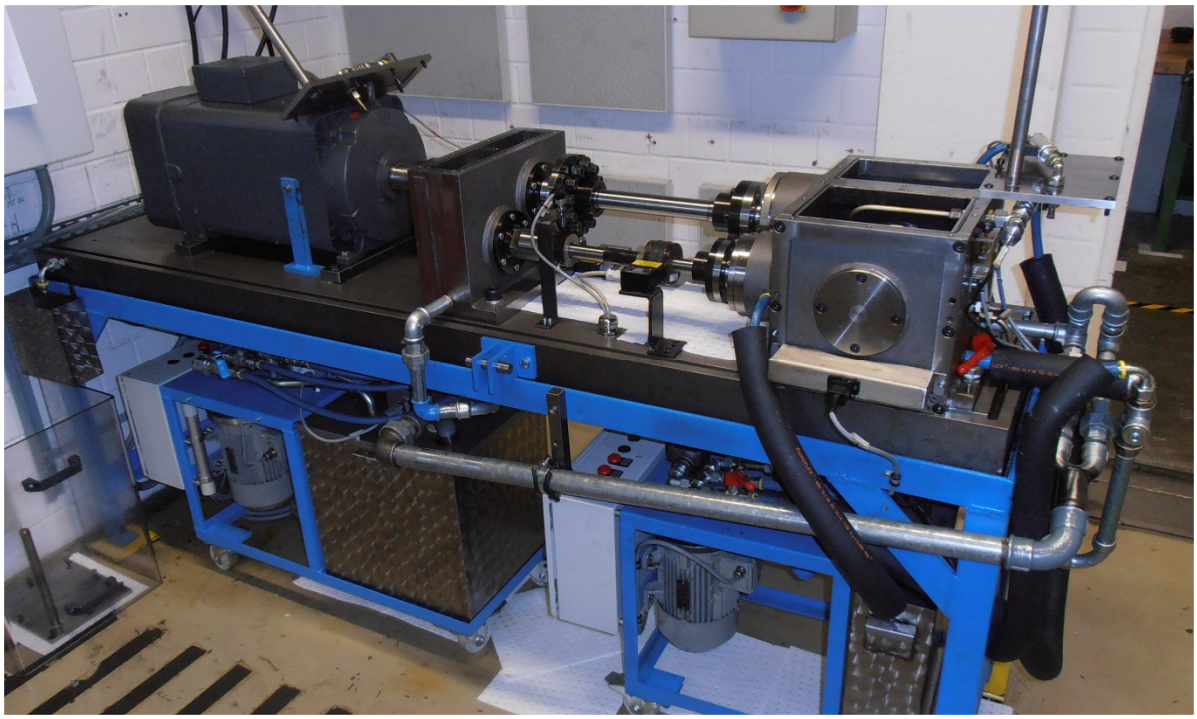

Figure 4-8: An example of the back-to-back test rig for hypoid gearing testing in FZG in Munich.

4.2.1 Allowable stress numbers determination - Method B

"The allowable stress numbers for contact and bending were derived from endurance tests of reference test gears under reference test conditions. Tooth-root allowable stress numbers were also derived from pulsator tests. Practical experience should be taken into account" [15]. From this citation it is clear, that tests performed by this method are using a type of loading, which does not exactly correspond to real gearing loading in a gearset. The pulsator testing, already mentioned in the citation, is a typical example of such type of test. The principle and real appearance of a pulsator testing is depicted in Figure 4-9. The advantage of this type of endurance testing lays in its quickness

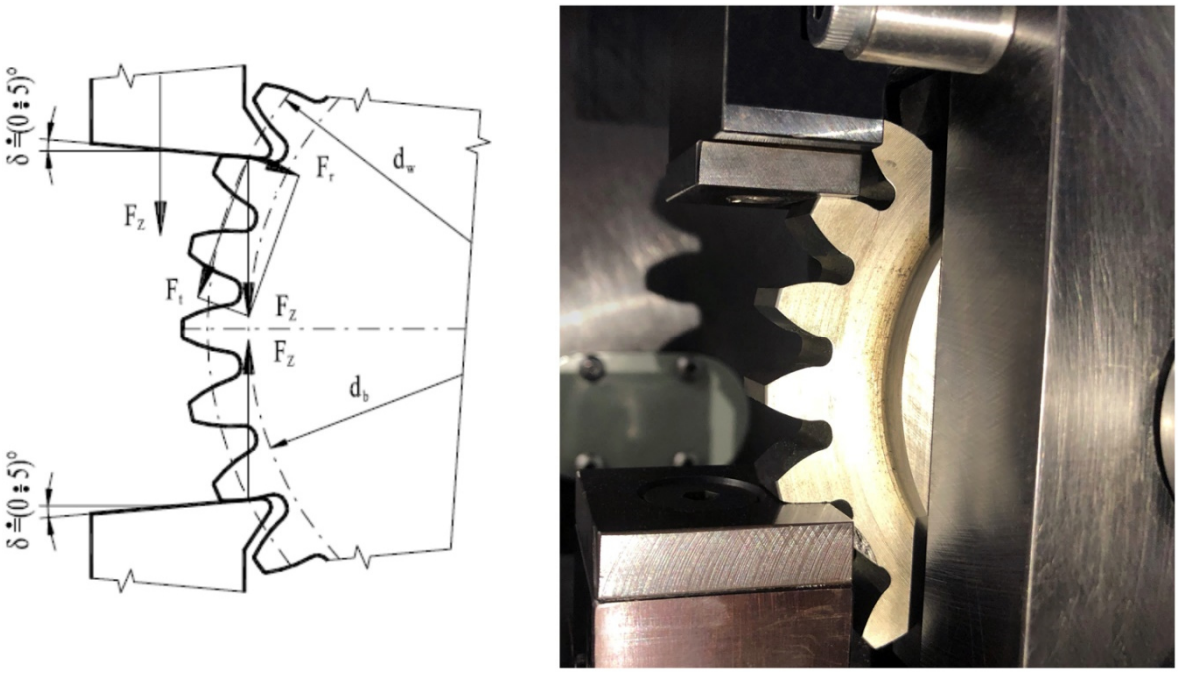

Figure 4-9: Principle (left) [18] and real appearance (right) of pulsator testing [19].

in comparison to standard tests according to the method A (4.2.1). The second advantage of this testing lays in the fact, that only one gearwheel can be used for more tests. This can be seen also in the lower right part of the Figure 4-9. One tooth has already been broken off.

At the opposite side, first disadvantage of pulsator testing lays in the way of loading. The tooth is purely loaded by forces between pulsator jaws without any movement. In a gearbox, while shafts rotating, sliding velocity occurs between mating tooth flanks. This fact influences test results and must be considered while test evaluating. For this reason, can be pulsator testing used only for the observing of tooth root resistance against the breakage.

Second disadvantage lays in a geometrical restriction, because pulsator testing can be performed only on spur gearing, which is used in automotive gearboxes very rarely, e.g. reverse gear.

Third disadvantage is in the course of loading cycle. The comparison of bending stresses in the tooth root for standard and pulsator test is depicted in Figure 4-10. In case of standard testing, the tooth is loaded only while passing through the mesh. This bending stress depends on number of teeth in the mesh, so it is not constant. The rest of the revolution is the tooth not loaded, so the bending stress equals to zero. In case of pulsator tests the force applied to the tooth has purely sinusoidal character and cannot decrease to zero because of assuring the correct gearwheel position between pulsator jaws. From all these reasons, pulsator test results must be recalculated to equivalent values corresponding to standard endurance tests according to the method A (4.2.1).

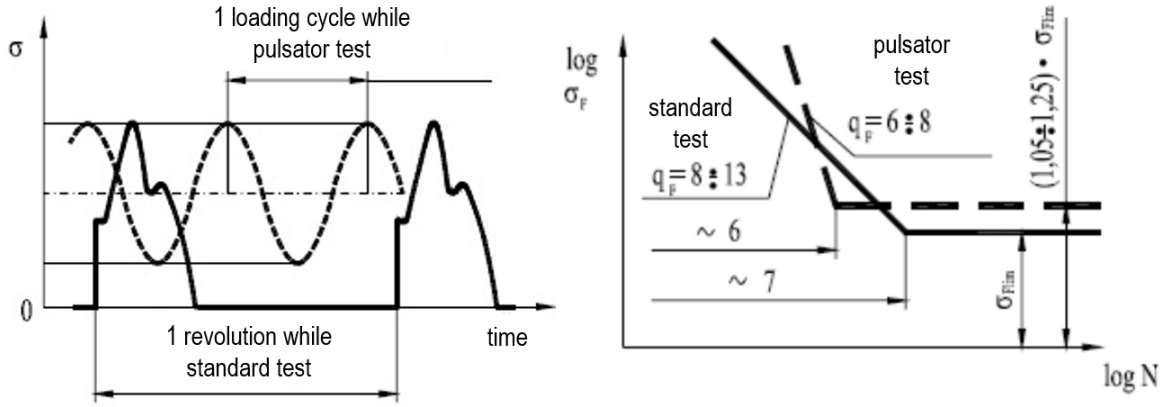

Figure 4-10: Comparison of loading cycle course (left) and resulting S-N curves (right) while standard and pulsator testing [20].

4.2.1 Allowable stress numbers determination - Method B_k

"Allowable stress numbers for bending are derived from the results of testing notched test pieces. Preferably, the ratio of the test piece notch radius to thickness should be similar to that of the fillet radius to the tooth-root chord in the critical section and the surface condition should be similar to that of the tooth root. When evaluating test data, it should be understood that test pieces are usually subjected to pure, alternating bending stress, whereas in the case of a gear tooth the fillets of the teeth are subjected to combined bending, shear and compressive stresses. Data on the various materials can be obtained from in-house testing, experience or from the literature." [15] This type of test can be used in field of automotive transmissions only as the comparative or preliminary one. Scheme of this test is depicted in Figure 4-11. Tested notched piece is clamped in the jaws and loaded by the force F in precise position to simulate root bending stress as at the gearwheel.

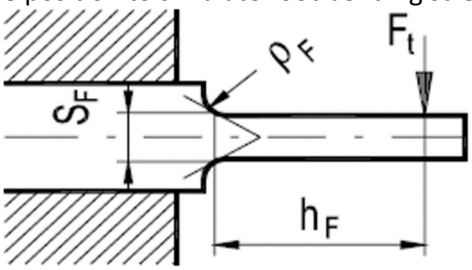

Figure 4-11: Scheme of endurance test according to method B_k performed at the notched test piece [20].

4.2.1 Allowable stress numbers determination - Method B_p

"Allowable stress numbers for bending are derived from the results of testing un-notched test pieces. See 4.4 for comments on evaluation of test results. In order to take into account the effect of notch sensitivity, it is necessary that actual notch form and notch factors be included in calculations; thus their results will be influenced by the extreme unreliability of these factors. Data on the various materials can be obtained from known test facilities or from the literature (see Bibliography)." [15]

4.3 Test Method Choosing within this Thesis

In previous chapters were described methods, which can be used for gearing testing. From their description it is clear, that the way how to get best results, is within usage of the method A (4.2.1), which enables to apply testing conditions very close to the real ones. Next argument for choosing this type of testing is, that in case of automotive gearboxes both types of the failure (pitting and tooth breakage) can occur. To get the most representative test and to cover all possible gearing failures, **testing according to the method A (4.2.1) was chosen within this thesis**.

5 Used Test Bench Description

5.1 Test Bench Appearance and Improvements

The test bench used for providing endurance tests within this thesis was originally designed and produced at the Technical University of Ostrava in 2002. It is a back-to-back test stand designed directly for testing of the automotive gearboxes MQ200. The specialty of this stand is the way of mounting of gearboxes on the test rig. Both gearboxes (tested and technological) are installed in the same manner as they are functioning in the car. The gearbox is standardly screwed together with engine cast. This assembly is then hung up to the test-stand frame on two silent-blocks, firstly on the engine side and secondly on the gearbox side. Finally, a reaction strut is mounted to the lower part of the gearbox. This strut transfers reactional force, which arises as the reaction to the sum of applied input and output torques.

Because the gearsets are tested directly in the original gearbox housing, same conditions in the gear mesh are ensured, e.g. shaft and bearing deformations, lubrication, etc. This fact is very positive from the point of view of test results credibility.

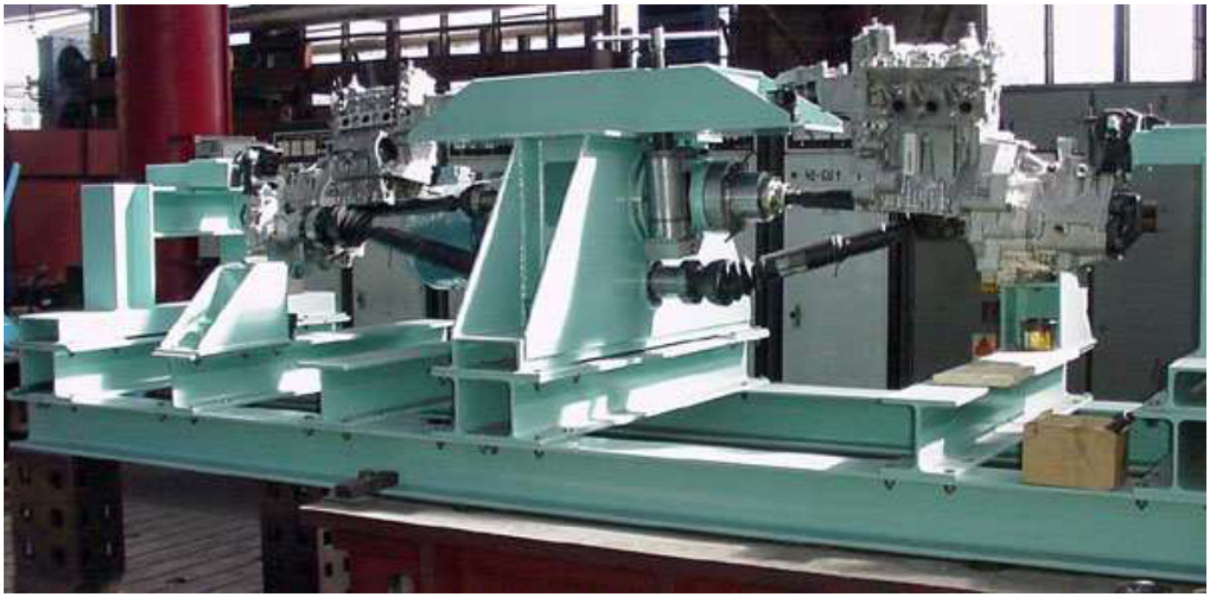

Figure 5-1: Back-to-back test rig for endurance tests of the gearbox MQ200 designed at TU of Ostrava – original appearance [21].

The closed circuit is realized by joint shafts, connecting both standard automotive gearboxes. This means, that each gearbox has two output flanges for driving both wheels at the axle. But in this test stand the power must be transmitted only through one of them. For this reason, differentials in both gearboxes must be disabled. This can be done either by mounting of a special part, which connects the differential pin directly with one output flange, or the bevel gearset must be welded.

Since this test bench was constructed, several fundamental changes (improvements) have been made to it. Its initial appearance is depicted in Figure 5-1. There is visible a striking console in the middle part, to which silent blocks on the engine side were attached. In this state was this test bench transported to heavy laboratories of CTU in Prague at Juliska. During its operation, it was found, that joints at lower (output) shafts are getting overheated by higher loads due to quite big

value of the angle in these joints. It is clearly visible in Figure 5-1. To overcome this issue, the test bench was extended approximately by 67 cm at each side, to current length of 5 meters. This lead to reducing the angle in these joints and hence their overheating was prevented. Due to this lengthening, the middle common console was replaced by two separate vertical consoles for engine silent blocks mounting. All four lengthening parts (HEB profiles) were simply screwed to the original base profiles using a steel plates, each by eight screws. Because the test bench was placed directly on the floor, this type of connection was sufficient. Its lengthened version in CTU laboratories at Juliska is depicted in Figure 5-2. The reduction of joint shafts angles in comparison to Figure 5-1 is obvious.

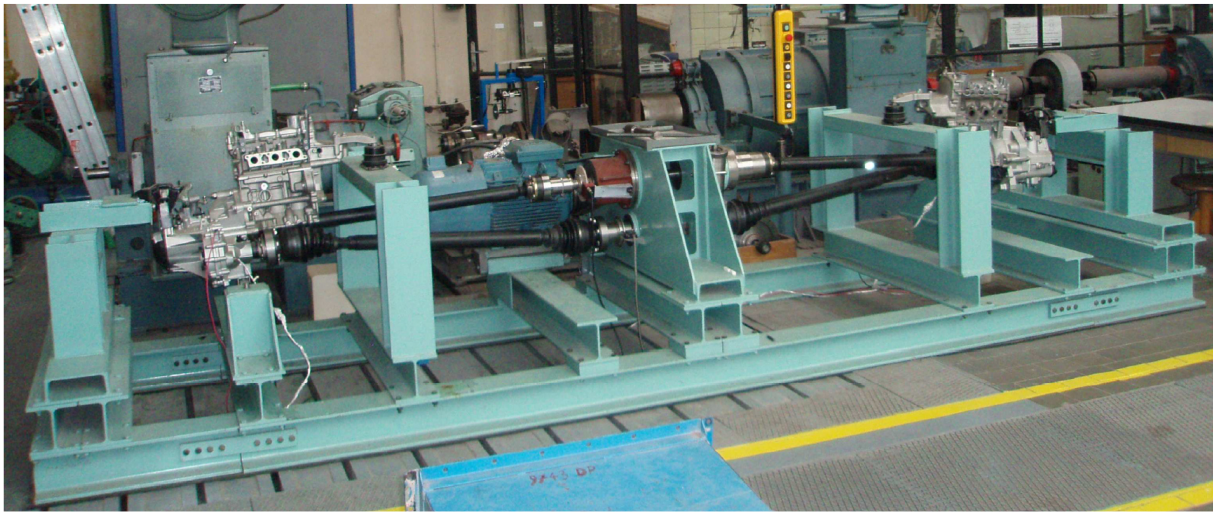

Figure 5-2: Appearance of the lengthened test bench in the labs of CTU in Prague at Juliska

The load limits of the stand are resulting mainly from the torque and rotation limits of the joint shafts. The limits given by joint shafts are relevant for lower gears (1st and 2nd). For the load of upper gears (5th and 6th) can be limiting the losses in the circuit, i.e. the maximal power of the electromotor. Basic parameters of the test stand are stated in Table 5-1.

Maximal electromotor power	22 kW
Maximal rotations on the input shaft of the tested gearbox	4200 rpm
Estimated maximal circulating power in the stand	90 kW
Torque limit for the maximal rotations on the input shaft of the gearbox	220 Nm
Torque limit on the input shaft for the 1st speed	100 Nm

Table 5-1: Basic parameters of the back-to-back test stand for automotive gearbox MQ200.

The lengthening of the test bench was the last improvement done by TU of Ostrava. Further described changes and improvements have already been realized at CTU in Prague.

The appearance of this test bench was presented in [36].

5.1.1 Input Shaft Supporting Bearing

The joints overheating issue was solved by lengthening of the test bench, but on the other hand, the mass of the shafts has increased. This issue was significant mainly on input shafts, because of their higher rotational speed. This “upper” joint shaft was connected to the gearbox input shaft

using a flange with involute splines. It can be said, that the heavy joint shaft was hung up at the gearbox input shaft. To allow the gearbox change, small clearance in the connection was needed. From the point of view of torque transmission, the clearance was no problem. On contrary, due to gravity force, the clearance allowed small angular displacement between the input shaft and the flange, and thus eccentricity and shaft gyratory vibrations increased, despite joint shafts were dynamically balanced during their production.

To eliminate this issue, supporting bearing for angular displacement restraining, was used. Its appearance in the cross section is depicted in Figure 5-3. The outer bearing ring was placed to the engine block instead of the crankshaft. In this version of the engine cast, its lower part was used also for the crankshaft placing. Until this moment, there was no need of the lower engine block part and the engine block served only for holding the gearbox in the test bench frame. Since this moment its function has changed, which lead to the necessity of precise (coaxial) position of the engine- and gearbox cast. For this reason, standardly used centering pins had to be used while assembling these two casts.

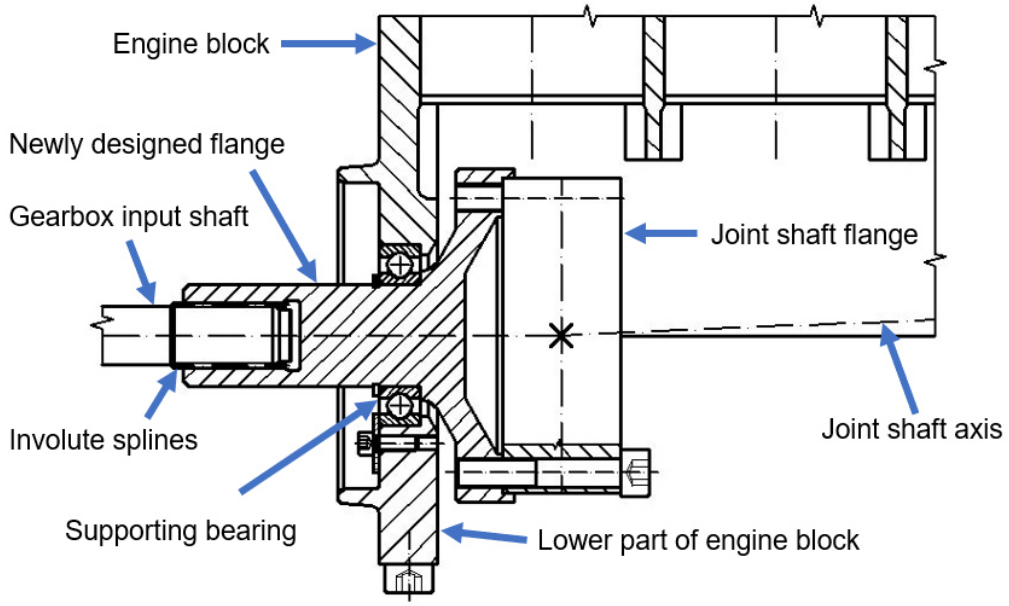

Figure 5-3: Cross section view of the new input flange and supporting bearing of the input shaft

This design improvement helped to solve the issue of gyratory shaft vibrations, because the heavy long shaft is now fixed to the engine block using supporting bearing and doesn't "hang" at the gearbox input shaft. This bearing absorbs disturbing radial forces and thus the gearbox input shaft is loaded only by a torque.

5.1.2 Horizontal Gearbox Positioning

Thanks to the supporting bearing, vibration issues on both input shafts were solved. In this state the test stand was able to run standardly by 3000 rpm on the input shaft. But during the testing it was found, that lower (output) shaft joints are damaged much often, than on the upper (input) one. The way how to solve this issue, was in next decreasing of the joint shaft angle. Originally, the assembly of the gearbox and the engine block was in the stand placed in the position, when the gearbox axis was inclined by 3°. This assembly position is standardly used in the vehicle. In this

position, the angle of the upper shaft was almost zero. So, the way how to solve above mentioned issue, was to lift the whole assembly at the gearbox side to the position, when the gearbox axis becomes horizontal. Both these assembly positions in the test rig are depicted in Figure 5-4. It was reached by the underlaying of the gearbox mounting part about 45 mm with nylon plates. Consequently, to assure correct placement in the test bench, the reactional strut mounting part had to be also lifted about 37 mm. These nylon plates are highlighted by a red color.

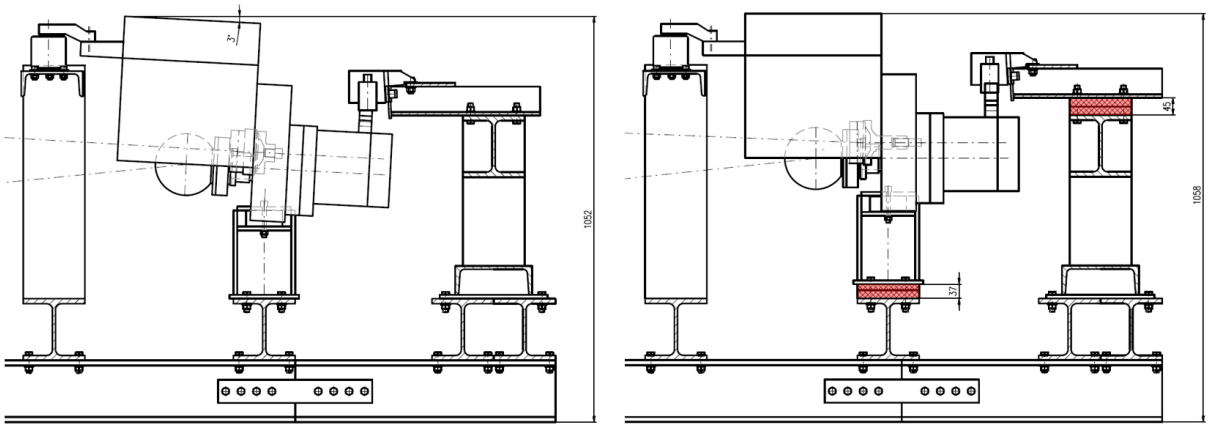

Figure 5-4: Original (left, 3° inclination) and new (right, horizontal) gearbox position in the test bench to decrease the joint angle at output shafts

This change lead to increasing of the joint angle on the input shaft. Simultaneously, the joint angle on the output shaft has decreased, and therefore also its loading. Since this time, the endurance of all joints is approximately comparative.

5.1.3 Air Spring Suspension

In 2012 this test bench has been transported to newly built laboratories in ***Roztoky Science and Technology Park (VTP Roztoky)***. In this building, described test bench has been placed in a laboratory in the 2nd floor. Because of vibrations excited by this test bench, special damping rubber plate was placed under final concrete layer with the thickness of 15 cm. This final concrete layer was cut off from surrounding concrete around the test bench, and thus vibration damping gap was created. This gap was subsequently filled with a silicon sealant. After very short time it was clear, that this preventive damping measure is not sufficient. The vibrations excited while running the test bench were, despite the isolating rubber plate, still very dangerous for the concrete building structure. For this reason, the test bench has been placed at 12 air springs “Faebi 100”. To enable the usage of these air springs, all four lengthening HEB profiles, originally screwed, had to be welded to base HEB profiles. Present appearance of this test bench is depicted in Figure 5-5.

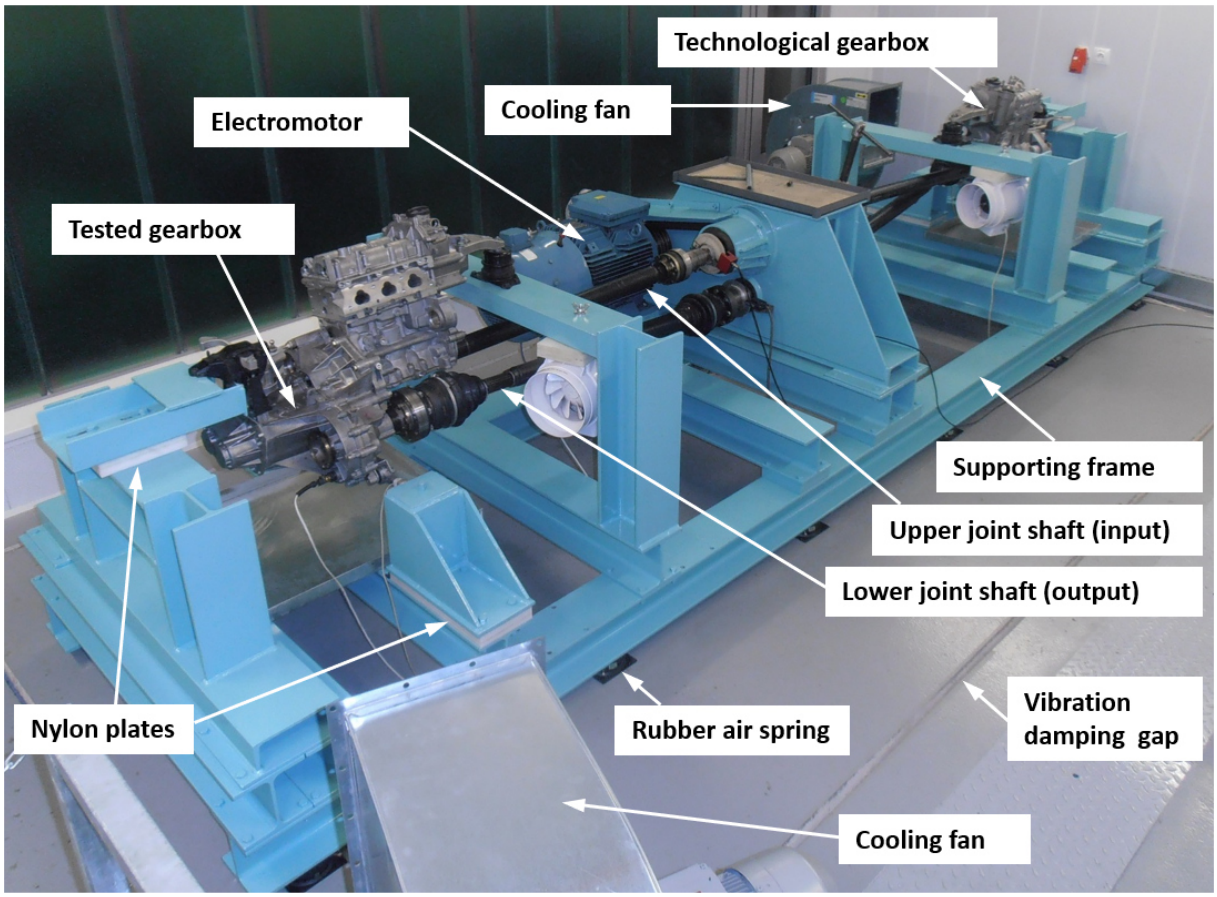

Figure 5-5: Back-to-back test rig in the CTU laboratory in Roztoky Science and Technology Park

5.1.4 Shifting Robots

With a special equipment of this test bench – planetary torque unit – the torque can be changed during the test. This also enables to change the speed stage during the test. Firstly, before shifting the torque must decrease to zero and input shaft speed must decrease to approximately to 200 - 500 rpm. In this state it can be shifted, and the test can continue with another speed stage.

To obtain the fully automatic functioning of this test stand for life cycle tests, the shift robots for gearboxes were conceived. The idea, design and control of the shift robots were prepared within the master thesis of **Ing. Jan Ruprich** – student of the Czech Technical University in Prague.

The original cables and lever arm connecting the cables with internal shift shaft of the gearbox were used. Instead of the mechanism enclosed in the shift lever housing, which normally transmits the movement of the shift lever to the movement of the cables (one cable for selection, one cable for shift), are used two electric servomotors. As stated already in previous chapter describing the manipulation of the test stand, the gearshift can occur in steady state only. Therefor powerful and relatively slowly actuators MecVel AL1 were chosen. The actuator consists of permanent magnet electric motor and worm wheel drive. The actuators are equipped with encoders and 3 limit switches. After the speed is engaged the actuator is slightly moved back to avoid the permanent contact between the shift fork and shift sleeve of the synchronizer. The actuators with maximal length of 300 mm were chosen to have large reserve for any tested gearbox. The cables are guided with help of the SKF profile rail guide LLT. The rail is screwed to the frame of the shift robot. The carriage carries the ends of the cables, which are in the vehicle mounted on the shift lever

mechanism. The detail of the shift robot servomotors is depicted in the Figure 5-6.

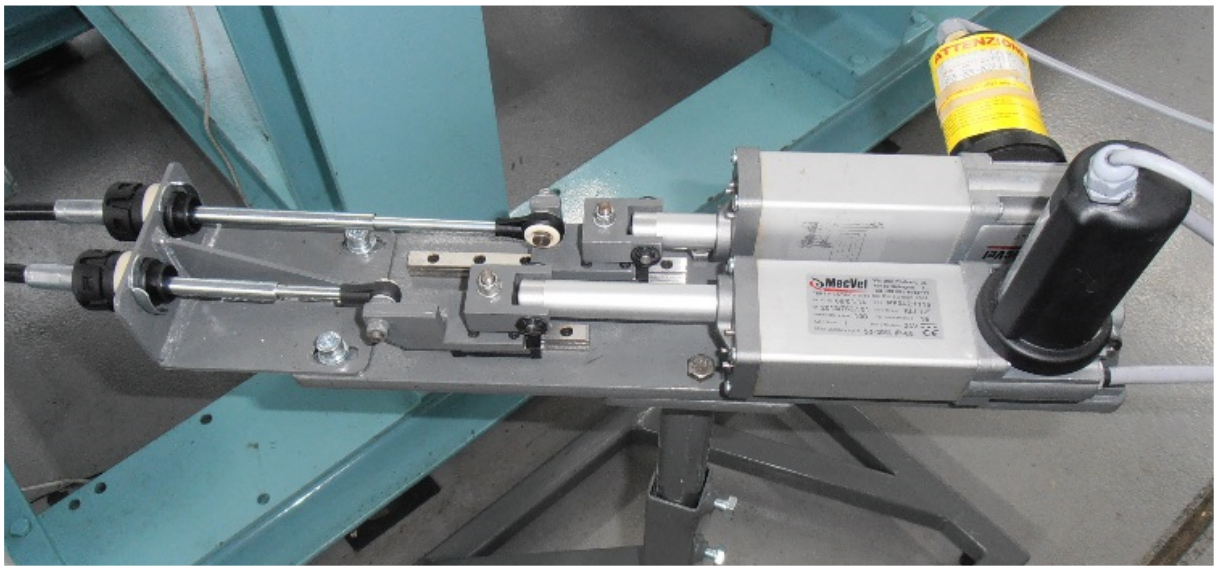

Figure 5-6: Detail of the shift robot servomotors MecVel AL1.

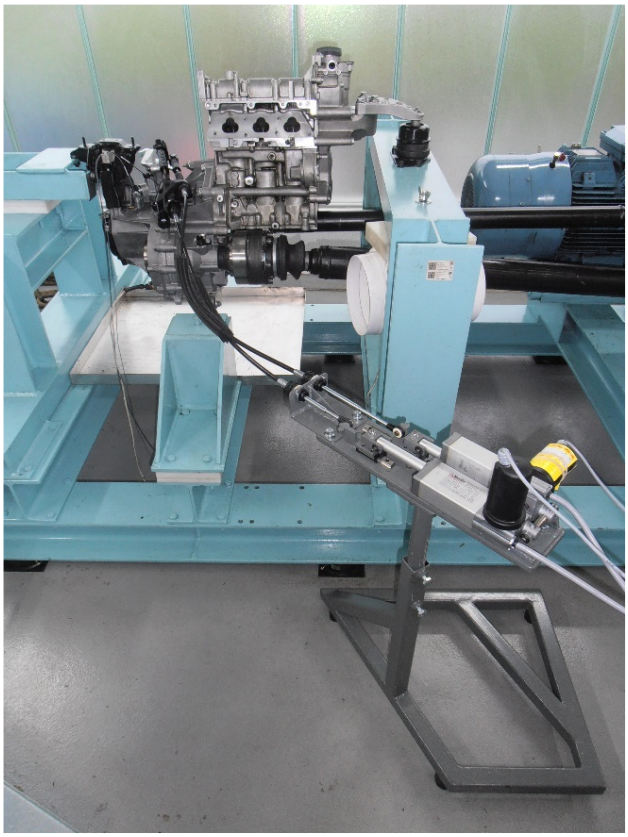

Figure 5-7: Shift robot connected to the gearbox at the test bench using original bowden cables.

From the principle of the test bench conception one very important condition follows, namely that the shifting process must be correctly performed simultaneously at both gearboxes. The observance of this condition is quite demanding. Firstly, maximum shifting force is determined to avoid shifting mechanism damaging. Sometimes it can occur, that the gear shift sleeve doesn't successfully engage to the gearwheel's toothing. And secondly, it must be checked, that same speed stage is shifted at both gearboxes. Due to clearances in the shifting mechanism it can happen, that the selection of the desired speed stage is not correct. This would lead to the situation, when on the tested gearbox is shifted another speed stage than on the technological one. This would cause immediate stopping of the circuit's rotation. If the shifting process is successful, the torque in the circuit must stay on zero while running unchanged shifting input rpm. After this "shift checking period" can be the torque increased thanks to planetary torque unit.

The shifting process correctness can be checked by the controlling software, programmed in LabView, using the signals of loading torques and the signals describing positions and forces of both shifting robots (4 servomotors).

5.2 Measurement Devices and Equipment

To be able to correctly provide the endurance test, some important values must be measured, namely the torques at the input and output shaft, oil temperatures and reactional forces in the struts are measured. Their description follows.

5.2.1 Torque Measurement

The input and output torque is measured using strain gauges, glued on the shafts at an angle of 45°, connected in the full bridge configuration. The output signal of the bridge leads through the amplifier to the antenna rotating together with the shaft. By telemetry transmission, the signal from the rotating antenna is transmitted to a receiver, firmly attached to the test bench frame. The signal then leads by coaxial cable to the ESA Messtechnik device. This device must be calibrated before each measurement. Its analog output signal leads to the measuring card NI PXI 6229, inserted in the NI PXIe-1073 chassis.

5.2.2 Speed Measurement

The rotational speed is measured only at the output shaft. Input speed can be then computed using a total gear ratio. For this measurement an optical sensor Banner SLE10 is used. The optical barrier is realized by a disk with 60 holes evenly distributed around the perimeter. The output signal of this sensor - TTL pulses – is then transferred to a counter. Because the output speed signal was disturbed by the frequency converter, galvanic isolation was inserted between the sensor and the counter NI PCI-6602, inserted in the NI PXIe-1073 chassis.

The second speed source is the electromotor’s frequency convertor.

5.2.3 Temperature Measurement

Temperature in both gearboxes is measured by a Pt100 resistance sensors, type 902040/10. The sensor is screwed into a specially adapted drain plug of the gearbox, close to the differential. The sensor’s signal leads to the measuring module NI 9217, inserted in the integrated NI cRIO-9024 real-time system.

5.2.4 Reaction Force Measurement

The force in the reactional strut is measured using strain gauges connected to a full bridge at an angle of 90°. Used type of the strain gauges is 1-XY13-3/120 with a temperature compensation. Measured signal leads to the NI 9237 module, inserted in the integrated NI cRIO-9024 real-time system.

5.2.5 Vibrations Measurement

Vibration measurement is performed using B&K accelerometers, type 4524-B-001 and 4507-B-004, glued on the gearbox cast surface. Standardly, two accelerometers are applied to one gearbox. Their cables are connected to the NI PXIe-4492 measuring card, inserted in the NI PXIe-1073 chassis. Thanks to these sensors, faults in the gearbox can be detected. These accelerometers on the gearbox housing are depicted in Figure 5-8.

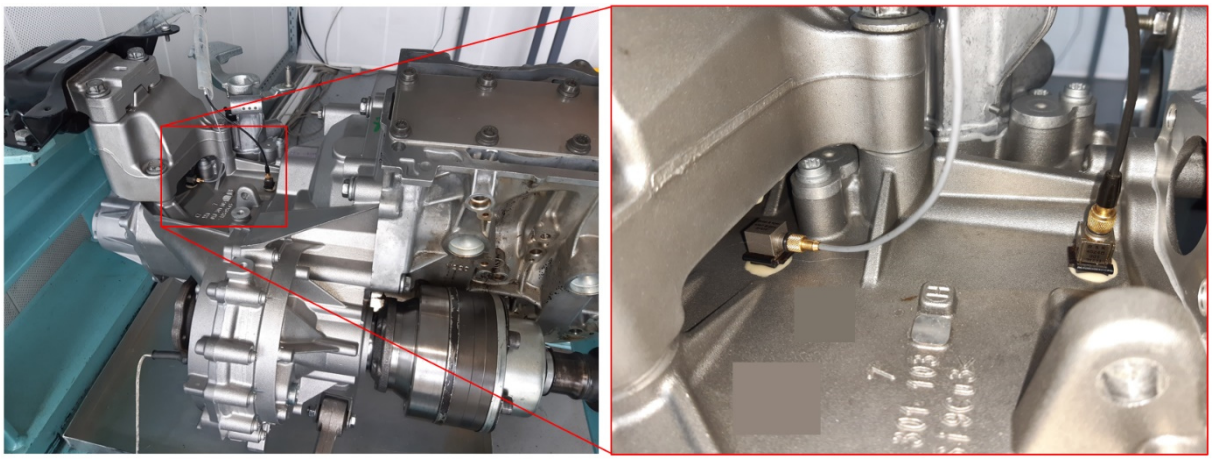

Figure 5-8: Accelerometers placement on the gearbox cast while testing.

Gearbox cast vibrating behavior while testing and best accelerometers position choosing was presented in [37].

5.2.6 Driving Electromotor

Next very important test bench equipment is the electromotor ABB M3BP 180 M2 with the output power of 22 kW and synchronous speed of 3000 1/min. This electromotor is controlled by the ACS800 frequency converter. The communication between the frequency converter and the computer takes place via the OPC protocol. The original software "DriveWindow" is installed in the computer. It is used to operate the electric motor - testing operating states etc. But during standard measurement, the control of the electromotor is fully taken over by the control application of the entire test device programmed in LabView. The communication between the frequency convertor and the PC is both-sided, which means that electric motor is not only controlled by the PC, but many important electromotor (EM) parameters can be also read by the PC, e.g.:

- EM speed
- EM torque
- EM power

5.2.7 Cooling Ventilators

Cooling ventilators are another necessary feature of this test bench. There are used two types of them. Firstly, these are two radial ventilators for cooling the oil in the gearboxes, placed next to the test bench. These ventilators are independently controlled by two small frequency convertors "Emerson, Commander SK". The desired frequency (ventilator speed) is simply controlled by the PC through the analog voltage, depending on the gearbox temperature. The purpose of these fans is that the oil temperature inside the gearboxes does not exceed 90 °C.

Second type of used ventilators is the axial one for cooling the joints of the connecting shafts in the middle part of the test bench. These ventilators are attached to the test bench frame. They are running with constant rpm and are simply controlled (switched on/off) by a relay of the main frequency convertor ACS800. When the main ABB electromotor is running, both these ventilators are running too. Their purpose is that the temperature of the CV joints of the joint shafts doesn't exceed 100 °C.

5.3 Pretensioning Devices

As it was already mentioned in the Chapter 4.2.1.2, when using the back-to-back test rig, some pretensioning mechanisms. It is necessary to twist the two shafts relative to each other and fix them in this position. This angular displacement introduces into the circuit required torque, which loads the gears. Two types of pretensioning devices can be used at this test bench. Both of these were described during the Powder Science Symposium in Sweden [40] and in [36].

5.3.1 Constant Torque Device

The first pretensioning device is used for "one load level" tests, which means, that the load (torque) in the circuit remains constant during the test – **constant torque device (CTD)**. In this case this unit consists of a worm gearset and a friction clutch. The cross section of this device is depicted in Figure 5-9, the clutch principle and real appearance are depicted in Figure 5-10.The basic principle remains same as in case of Niemann's test bench. One shaft is fixed to the frame using a locking pin. On the second shaft is permanently attached a worm wheel. After engaging the worm by its inclining to the mesh with the

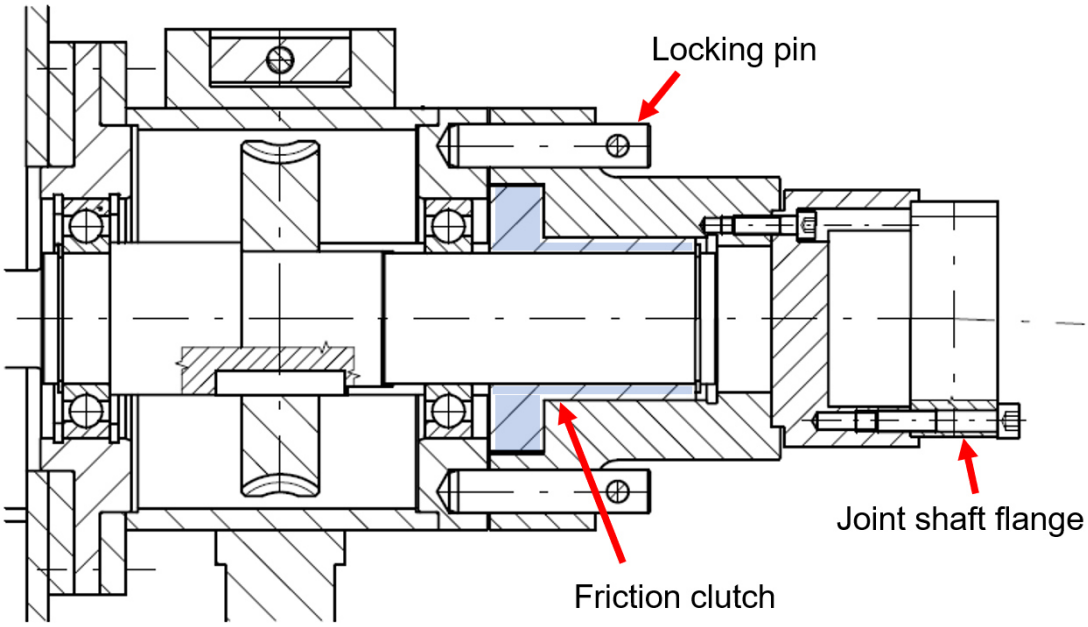

Figure 5-9: Cross section of the pretensioning mechanism for one load-level tests (friction clutch)

worm wheel, it is possible to rotate manually this shaft and evoke desired angular displacement and adequate loading torque. In this relative position both these shafts can be connected thanks to

special friction clutch ETP Techno. The connection is done by a locking screw which pushes on the

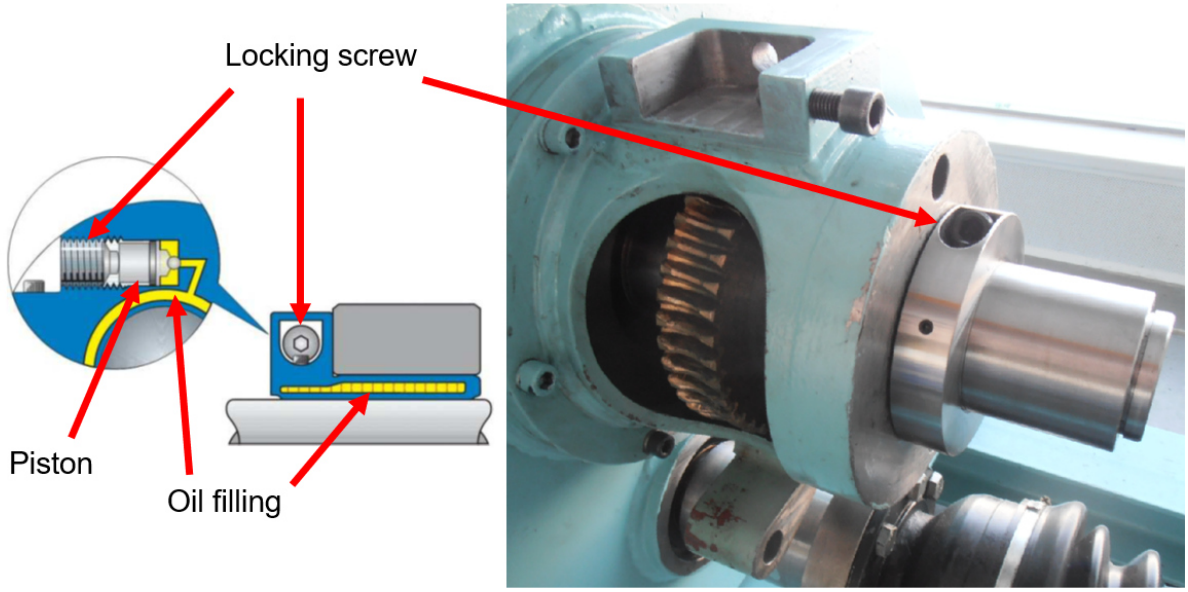

Figure 5-10: Principle and the appearance of the friction clutch ETP Techno on the CTU test stand [22].

piston and increases the pressure of the oil filling and the clutch is consequently deformed. Thanks to this deformation both these shafts are finally connected. After this operation the worm must be disengaged from the worm wheel to enable the shaft rotation.

5.3.2 Variable Torque Device

At this test bench can be also performed tests with variable loading torque (more load-level tests). In case of opened test stand it can be simply done by the power change of driving and braking dynamometers. But for changing the torque in a closed circuit it is necessary to change the relative angle between input shafts while their rotation. For this purpose, special device was designed at the TU of Ostrava, the **planetary torque unit (PTU)**. Its functional scheme is depicted in the Figure 5-11, its cross section is depicted in Figure 5-12.

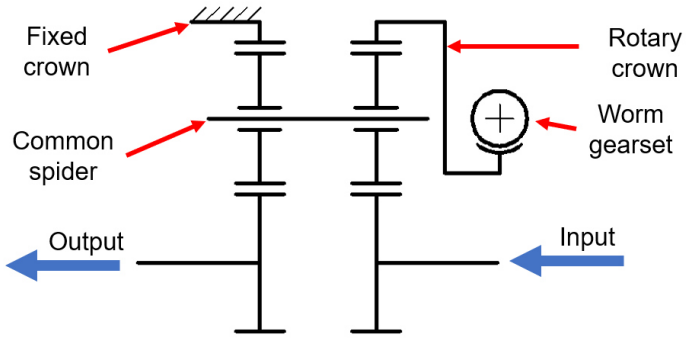

Figure 5-11: Functional scheme of the planetary torque unit for variable torque during the test.

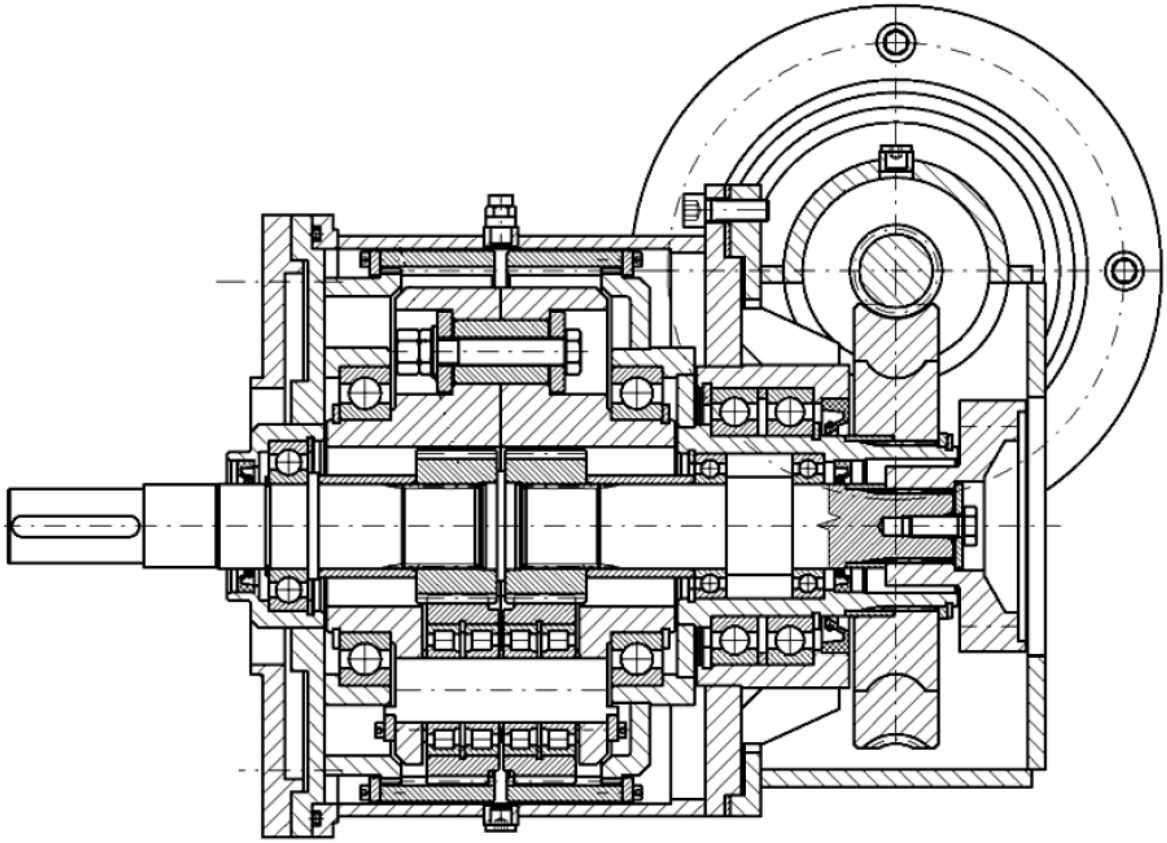

Figure 5-12: Cross section of the planetary torque unit for variable torque during the test.

It consists of two identical single planetary gearsets with spur gearing. One sun gear is connected to the input shaft of the tested gearbox, the second sun is connected to the input shaft of the technological gearbox. Both planetary sets are connected via common spider. The ring gear of one planetary set is blocked and the ring gear of the second planetary set is connected to the worm gear, actuated by an electromotor Siemens 1LA7 113-8AB11 with frequency converter Micromaster 420. When the ring gear is rotated, it leads to the relative movement of the two sun gears, which changes the pretension in the closed-loop. This can happen also during the rotation of both input shafts. But the shifting of the speeds in the gearbox still has to happen in steady state; when zero pretensioning torque is settled, naturally. The number of teeth of these two identical planetary sets are stated in Table 5-2.

Sun gear	Planet	Ring wheel
34	43	119

Table 5-2: Teeth number of gears used in the PTU.

This planetary torque unit is designated for endurance full spectra tests. The maximal power of electromotor equals 1,5 kW, its nominal speed is 705 rpm. The worm gearset ratio is 1:100.

The function of this planetary torque unit was tested for the first time under standard loading conditions in new labs in Roztoky. During this testing some important issues were found.

5.3.2.1 Additional Reduction in PTU

The PTU enables to change the torque in the circuit thanks to the rotation of one of its ring wheels. The torque magnitude, by given relative angular displacement, depends on the circuit's

stiffness, which depends on the shifted speed in both gearboxes. With shifted higher speed (6th) is the circuit much stiffer than with shifted 1st speed. It means that for setting of given torque with shifted 1st speed it is needed much more rounds of the PTU driving electromotor, than with shifted 6th speed.

During endurance tests it is very important to be able to set precisely the loading torque. With PTU usage it was no problem for lower torques and speed stages. But with higher loads, two main problems arose. Firstly, the PTU's electromotor wasn't able to generate sufficient torque to reach desired torque in the circuit. And secondly, it was not possible to precisely set the torque, because the electromotor controlling, despite usage of frequency converter, was too rough. Both these issues were solved by usage of an additional planetary reducing gearbox Apex Dynamics PE120 with ratio 1:10. The PTU's controlling torque has increased and simultaneously also the precision of torque setting has increased thanks to lowering the PTU's ring wheel's rotational speed. The cross section of the PTU in transverse plane including this additional gearbox is depicted in Figure 5-13.

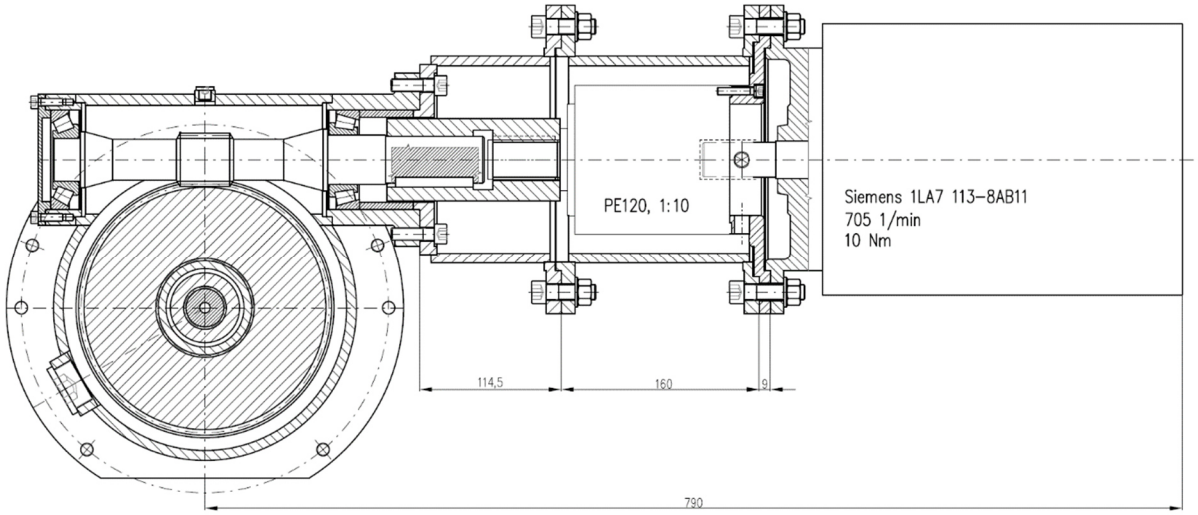

Figure 5-13: Cross section of the planetary torque unit with additional planetary reduction

On the other hand, time ramps for reaching desired torques in the circuit has lengthened. Further negative impact was in weight and length increasing. During endurance tests this whole assembly (test bench) vibrates and because the PTU is screwed to the main test bench frame only by 6 screws around its circumference, additional supporting rod, connected to the electromotor flange, was added to prevent the fastening screws overloading and subsequent PTU's collapse. It is depicted in Figure 5-16.

The problematics of the PTU vibrations was one of the diploma thesis topics of **Ing. Jakub Mansfeld**. Within this thesis, also the time ramps for reaching of the desired torque were measured. The values of these time ramps depend on the torsional stiffness of the whole testing circuit. This means that with another type of the gearbox these values can differ. An example of such measurement for the 2nd speed is depicted in Figure 5-14. It was done in standstill, which means, that the back-to-back test rig wasn't rotating while this measurement. These values are stated in the Table 5-3.

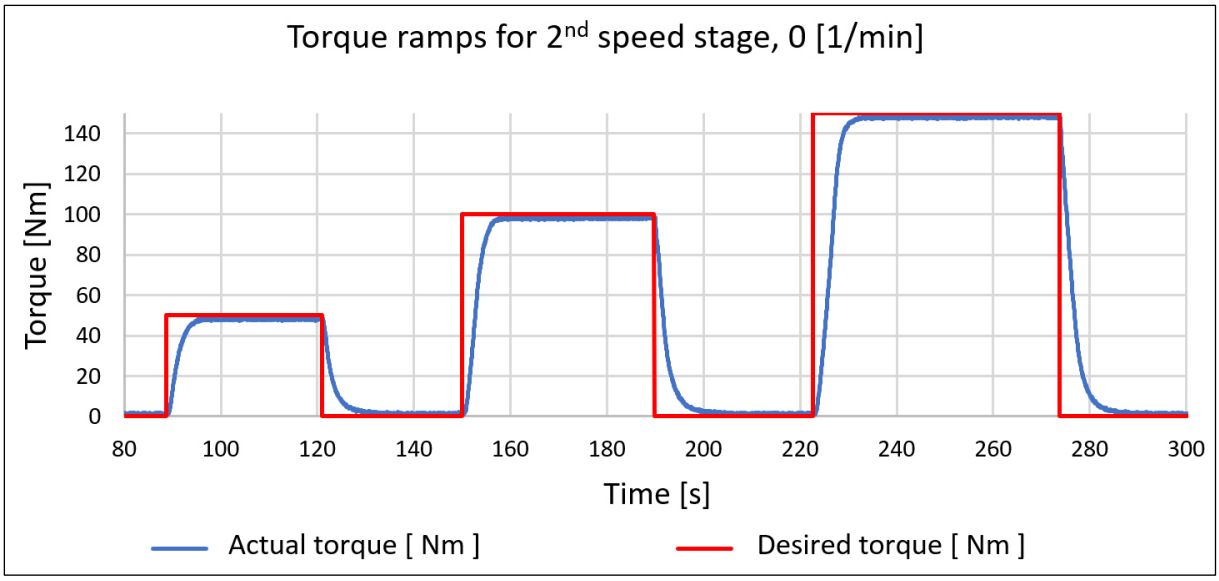

Figure 5-14: Time ramps of the back-to-back test rig equipped with the PTU with additional planetary reduction 1:10, example of the 2nd speed [23].

Speed stage	Total ratio	Time [s]			
		0 – 50 Nm	0 – 100 Nm	0 – 150 Nm	0 – 200 Nm
1	15,738	16,4	20,7	×	×
2	8,477	8,2	9,0	10,0	×
3	5,577	4,1	4,2	4,3	4,5
4	4,235	2,5	2,6	2,9	3,2
5	3,386	1,9	2,0	2,3	2,9
6	2,811	1,7	1,8	2,2	2,6

Table 5-3: Time ramps of the back-to-back test rig equipped with the PTU with additional planetary reduction 1:10 [23].

5.3.2.2 Oil Cooling System of the PTU

Further issue, discovered during the testing, was the overheating of the oil inside the PTU. The box of the PTU is designed with very tight dimensions and originally there was approximately 1 liter of oil only. Firstly, cooling by ventilator was performed, but the heat exchange wasn't sufficient. For this reason, a system for the oil cooling had to be designed.

The cooling system consists of the pump based on the principle of "gerotor" with maximal flow rate 8 l/min and maximal working temperature of 60°C, than of the oil filter and a heat exchanger. Oil flow rate in the circuit is regulated by two valves, which together work as the three-way valve. Originally this planetary unit was not designed for oil circulation, so its design had to be adapted. There were drilled holes for oil input (3/4") and output (6/4"). To assure symmetrical flow

through the PTU these holes must be in the middle position – between both ring gears. The oil must flow through the gap between them, which is only 6 mm wide. This unit can't be pressurized because of radial shafts seals. To minimize the pressure drop at the output from the PTU, so big output (6/4") and nonstandard heat exchanger were used. Standard heat exchangers have too high pressure losses, which is a problem in this case. For this reason, the heat exchanger is designed as a box filled with oil in which is plunged a bended pipe for cooling water with temperature of 6°C. It serves also as an oil stilling tank for air bubbles removing. The scheme and real appearance of this whole cooling system is depicted in Figure 5-15.

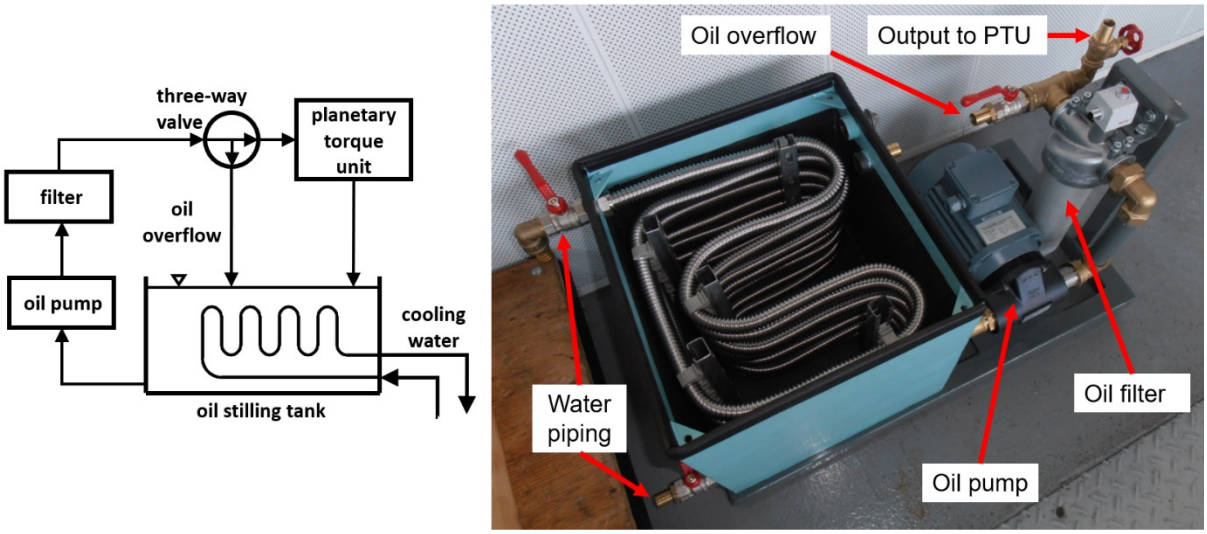

Figure 5-15: Scheme and real appearance of the oil system for PTU cooling

The heated oil flows from the PTU to the stilling tank through a hole in its lid. The overall appearance of the PTU including the oil cooling system, placed in the main test bench frame is depicted in Figure 5-16.

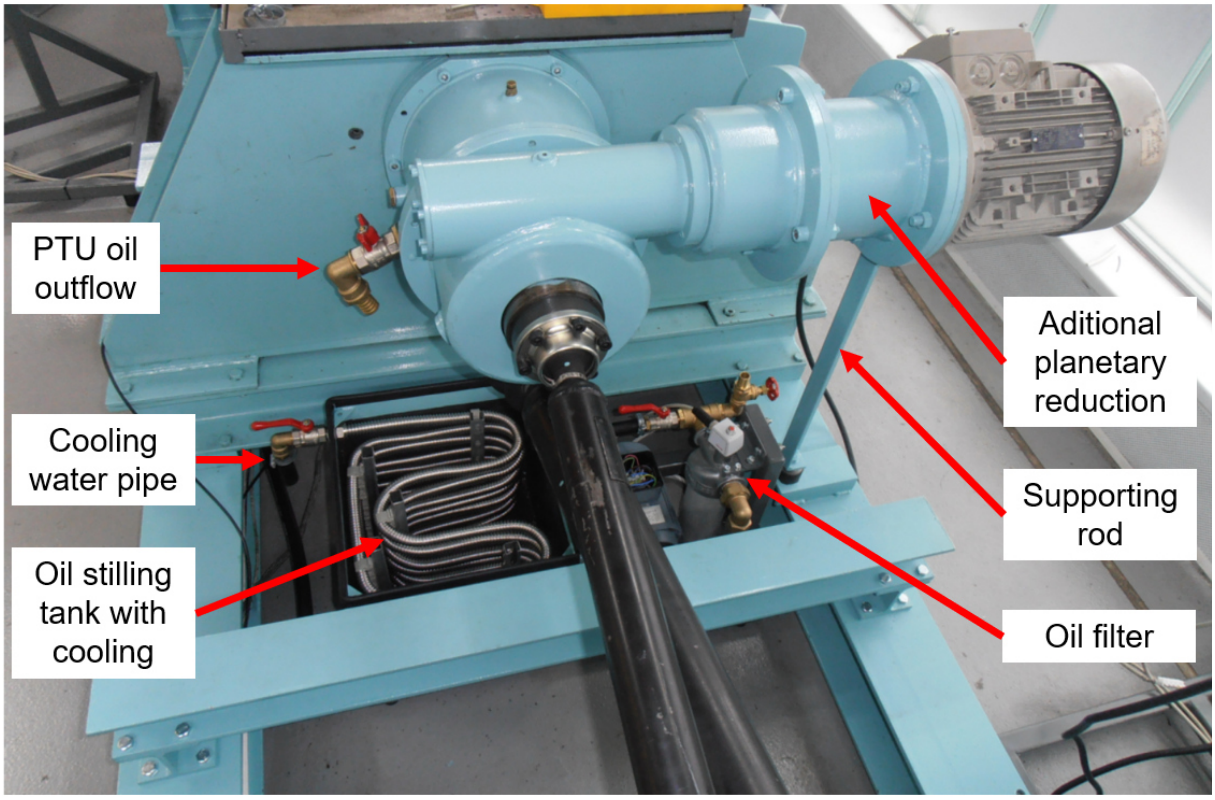

Figure 5-16: Overall appearance of the PTU including the oil cooling system

5.3.2.3 Bearing Change in the PTU

After solving the oil temperature issue thanks to the cooling system, the PTU was able to run much longer than before. But after very short time (few days) next issue arose, namely one of the ball bearings was damaged. The way, how to solve this issue lays in increasing load capacity of the damaged bearing. Because the design of the PTU is very complex, both bearing diameters had to be preserved. The cross section of the original version is depicted in Figure 5-12. This crucial condition lead to the only possible solution, namely usage of the roller bearing "SKF NCF 3008 CV" instead of original ball bearing "SKF 6008". The new bearing has more than three times higher basic dynamic load rating than the original one. The cross section of actual version of PTU is depicted in Figure 5-17. Only small adjustment had to be performed because of the larger width of the new bearing. The shaft had to be adequately machined (turned).

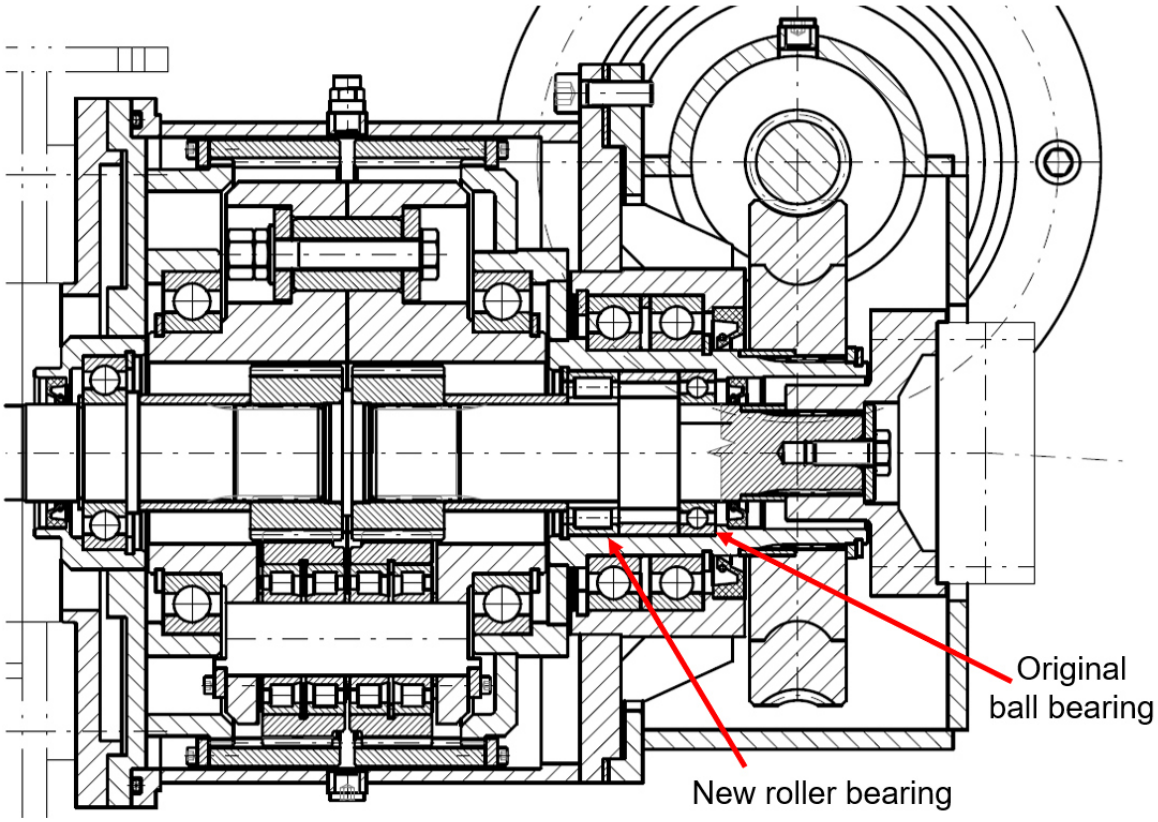

Figure 5-17: Cross section of the PTU with strengthened roller bearing.

Despite the increase of the bearing's basic dynamic load rating, this adjustment is still not enough. For this reason, next step will be a usage of another supporting bearing at the PTU's input shaft flange, which would capture the radial force from the oscillating joint shaft.

5.4 Power Losses

Since this test bench was produced, only the pretensioning device for constant torque was used for testing. The PTU was tested for the first time at CTU in Prague. The biggest advantage of the back-to-back test rig lays mainly in its low power demands while testing. But with the PTU there is in fact used in the circuit another gearbox. For this reason, it was necessary to describe the power demands of the test bench also with this device.

In the Figure 5-18 is depicted a functional scheme of used back-to-back test rig, including all necessary parts, which influence the power losses in the circuit. Used direction of torque and rotation determines the left gearbox as the tested one and the right gearbox as technological. The sum of all power losses is equal to the power of the driving electromotor. The greatest losses are in gearboxes, joint shafts and in pretensioning mechanism.

The torque is measured at two points (1 and 2) marked with crosses. Only in these two points is exactly known the power magnitude and can be calculated the efficiency of the circuit's part between them. At the side of the tested gearbox is the total efficiency determined as a multiplication of efficiencies of input and output shaft and of a tested gearbox. At the technological side is furthermore a pretensioning mechanism. This can be described by the Formula (5-1).

$$\begin{aligned} \eta_{TEST\_part} &= \eta_{JS1} \cdot \eta_{TEST} \cdot \eta_{JS2} \\ \eta_{TECH\_part} &= \eta_{JS2} \cdot \eta_{TECH} \cdot \eta_{JS1} \cdot \eta_{PM} \end{aligned} \tag{5-1}$$

Further there is a strain gauge measurement of the force on the reactional strut of the gearbox mounting. The reactional strut is mounted on the gearbox in a distance l, which is the perpendicular distance from the line connecting both main gearbox assembly mounting points. The distance l = 0,382 m. Using this distance l and measured force F_R on the strut, the value of the reactional torque can be computed as

$$M_R = M_{OUT} - M_{IN} = F_R \cdot l \tag{5-2}$$

The sum of all losses in the circuit is equal to the power delivered from the electromotor reduced due to the efficiency of the belt drive. The subtraction of the power in the point 1 and the power from the electromotor determines the circulating power in the circuit – Figure 5-19.

5.4.1 Power Losses with the Constant Torque Device

In Figure 5-18, depicted losses are simplified, while all bearing losses are neglected. Even with this simplification there are following losses to be determined:

- joint shaft,
- tested gearbox,
- technological gearbox,
- torque unit,
- belt drive.

During the testing, the torque is measured in two points only, and the reactional force can be used for the non-direct check of reactional torque of the gearboxes. Therefore, we need to make the qualified guess of chosen elements. For the joint shafts, the efficiency depends on the bending angle,

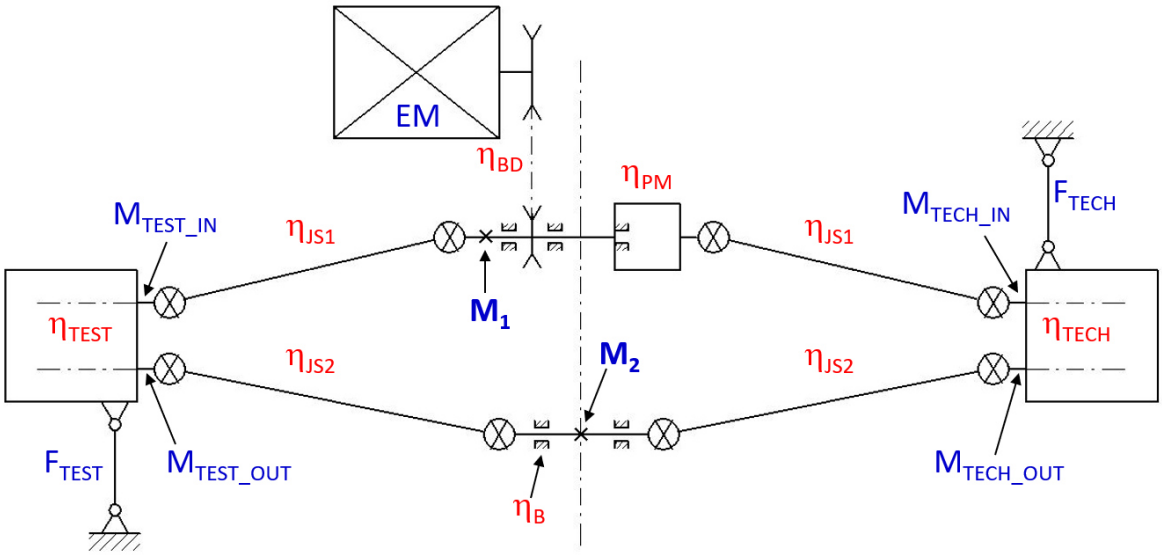

TEST – tested gbx., TECH – technological gbx., EM – electromotor, JS – joint shaft,
B – bearing, BD – belt drive, PM – pretensioning mechanism

Figure 5-18: CTU back-to-back test rig functional scheme

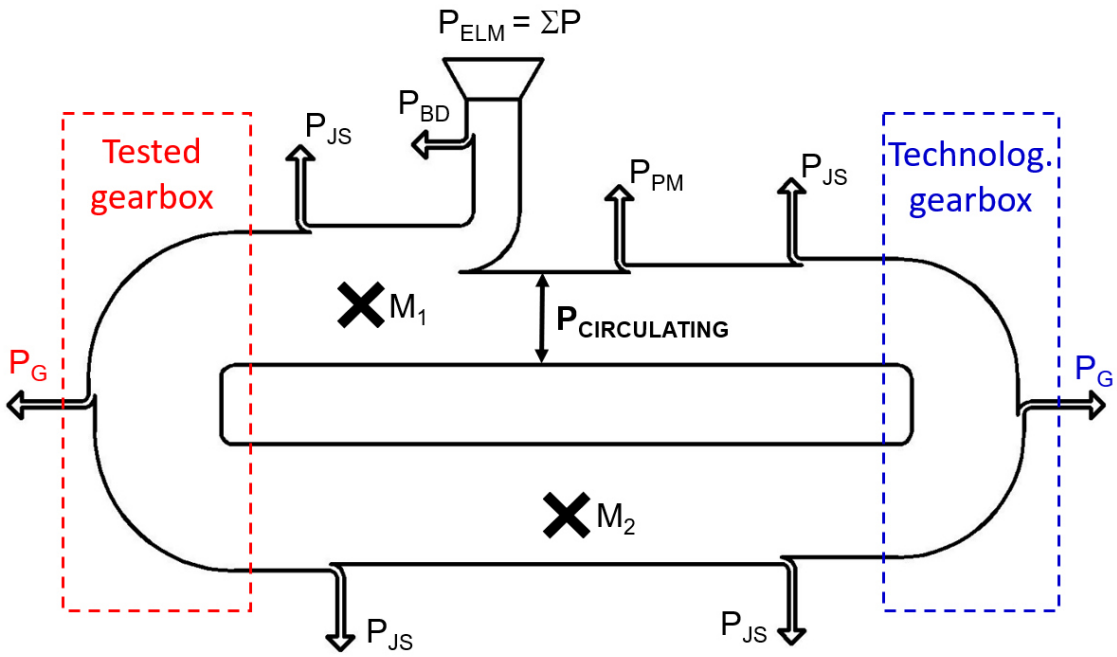

G – gearbox, ELM – electromotor, JS – joint shaft,
BD – belt drive, PM – pretension mechanism

Figure 5-19: CTU back-to-back test rig power flow diagram

and is given by the manufacturer. In our case there are used the joint shafts GKN with the joint type "VL". In the Table 5-4 there are given power losses for the upper and lower joint shafts.

	Joint angle [°]	Power losses [%]	Efficiency [-]
Input (upper) shaft	3.6	0.32	0,9968
Output (lower) shaft	8	0.75	0,9925

Table 5-4: Power losses of joint shafts used at the test bench and their efficiency.

The losses of experimental gearbox will result from the calculation based on measured powers in the point 1 and 2. Because shafts and gears in the technological gearbox rotates in different sense, its efficiency will be guessed. When the stand is equipped with mechanical torque unit no additional losses are added. The efficiency of the belt drive can be obtained by the division of the sum of the lost powers in the whole stand by the power of the electromotor.

Loading torque at gearset in tested and technological gearset can be calculated from measured torque M_1 according to Figure 5-18 and Figure 5-19 using the Formula (5-3). In tested gearbox both – tested (shifted) and final drive gearset must be considered. Both used joint shaft efficiencies are stated in Table 5-4.

$$\begin{aligned} M_{TEST\_gearset} &= M_1 \cdot \eta_{JS1} \\ M_{TECH\_gearset} &= M_1 \cdot \eta_{JS1} \cdot \eta_{Gearset}{}^2 \cdot \eta_{JS2}{}^2 \cdot \eta_{Gearset} \end{aligned} \tag{5-3}$$

The function and power losses diagrams of this special back-to-back test rig were presented in [38].

5.4.2 Power Losses with the PTU

When the test stand is equipped with the planetary torque unit, its efficiency must be guessed. As mentioned, the PTU works as two serially linked planetary gear sets (PGS). The first set has the power flow from sun to spider, when ring wheel is fixed, the second PGS has the power flow from spider to sun (ring wheel is fixed). Generally, the reference value for tooth-friction losses of spur or helical external gear set is in range from 0,015 till 0,025, and for internal gear set is in range of 0,005 till 0,015. The PTU is equipped with spur gearing. For this calculation, the value of **0,015** for external mesh and **0,008** for internal mesh is used. The formula for calculation of efficiency of the planetary gear set (PGS) can be found in [24]. For the first PGS the efficiency can be determined using the Formula (5-4).

$$\eta_{PGS1} = 1 - \frac{i^r \cdot \zeta^r}{(i^r - 1)} \tag{5-4}$$

For the second PGS the efficiency can be determined using the Formula (5-5).

$$\eta_{PGS2} = 1 - \frac{i^r \cdot \zeta^r}{(i^r - 1 + \zeta^r)} \tag{5-5}$$

The multiplication of both PGS efficiencies indicates the overall efficiency of the PTU, which was calculated as 0,965.

$$\eta_{PTU} = \eta_{PGS1} \cdot \eta_{PGS2} = 0{,}965 \tag{5-6}$$

5.4.3 Losses Comparison of both Torque Devices

To be able to compare the power demands of the test bench with the usage of both pretensioning devices, a measurement with both of them was performed. The needed power from electric motor was measured for different values of circulating power, defined by torque and speed of rotation of the gearbox input shaft. The power increase, when the PTU is used instead of the manually operated device for constant torque, was measured for all speed stages. As an example, resulting difference between both powers when 3rd speed was shifted is depicted in the Figure 5-20.

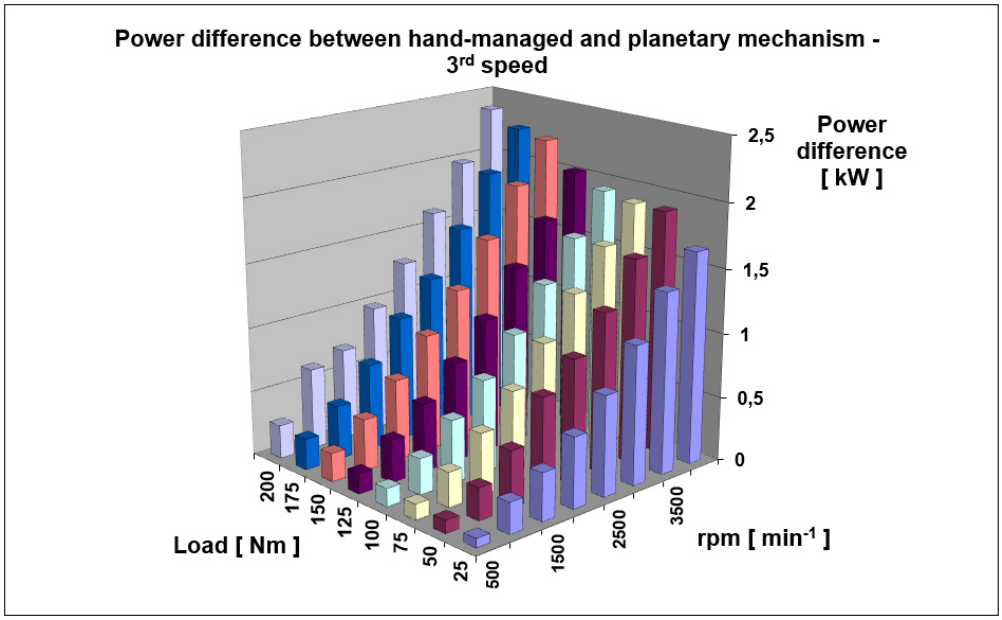

Figure 5-20: Power difference between constant torque device and the PTU at the 3rd speed.

When constant torque device is used, power losses of the PM consist only of two ball-bearings, so its losses can be neglected. This fact means, that the values of measured power difference between both PMs, depicted in Figure 5-20, are directly power demands of the PTU. In the Figure 5-21 are depicted these power losses of PTU related to loading power.

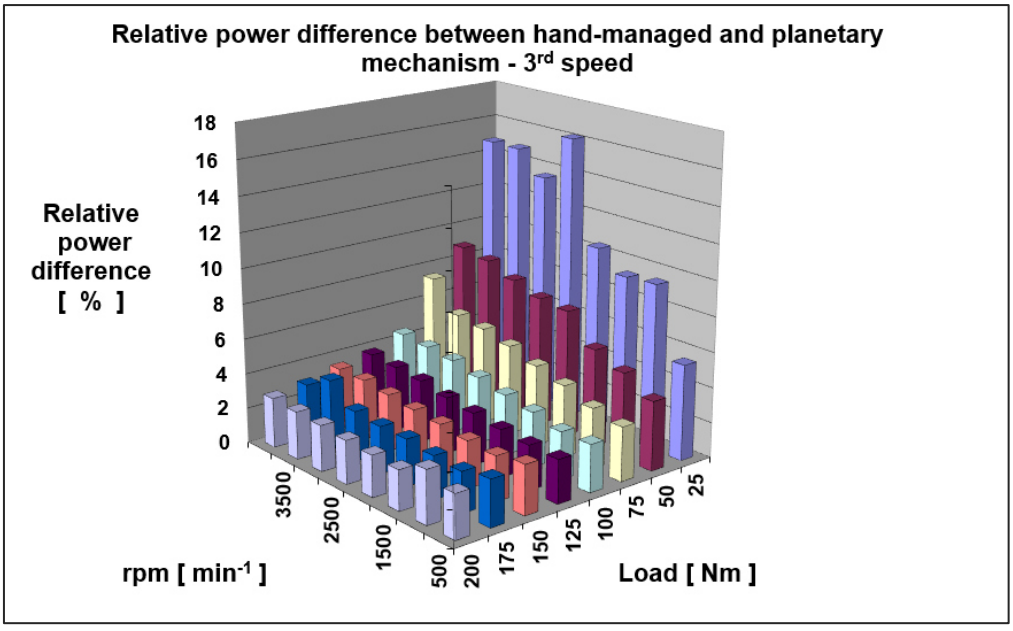

Figure 5-21: Relative power losses of the PTU at 3rd speed related to the loading power.

The values depicted in Figure 5-21 were obtained from data of Figure 5-20 using next Formula (5-7).

$$P_{PTU} = \frac{\Delta P}{M_1 \cdot \omega_1} \cdot 100\% = \frac{P_{elm\_PTU} - P_{elm\_CTD}}{M_1 \cdot \omega_1} \cdot 100\% \quad (5\text{-}7)$$

If there are known relative power losses and loading power, the efficiency of the PTU can be simply calculated using Formula (5-8)

$$\eta_{PTU} = 1 - \frac{P_{elm\_PTU} - P_{elm\_CTD}}{M_1 \cdot \omega_1} \quad (5\text{-}8)$$

In Figure 5-22 are depicted measured efficiencies of the PTU; as an example was taken the case when the 4th speed is shifted. In this figure can be seen the difference between measured efficiencies and the calculated one (0,965). For other speeds are the measured values of course very similar. The shifted speed changes speed of rotation and torque at the output (lower) shafts of the test bench, not the input parameters where PTU is placed.

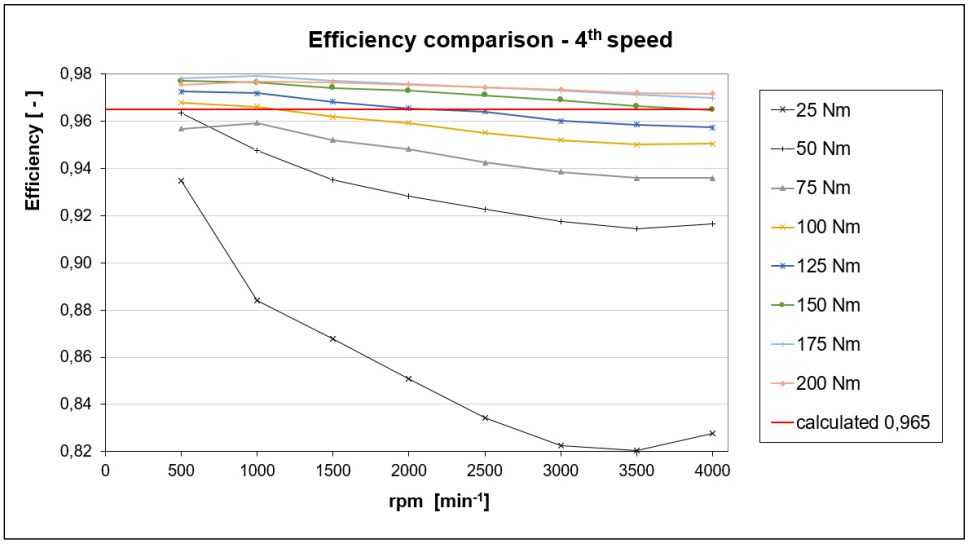

Figure 5-22: Comparison of measured and calculated efficiency of the PTU at 4th speed.

In Figure 5-22 can be seen that analytically calculated efficiency of the PTU and its efficiency calculated from measured values matches only for higher torques. The difference between the theoretical value and measured one equals +/- 1,5 %. The measured efficiency decreases with increase of speed of rotation, due to higher fluid friction losses. Important difference between theoretical and real value of the efficiency is for partial loads (25 Nm - 75 Nm). In theoretical calculation only the tooth-friction loss is included. The load dependent friction losses of bearings, losses due to centrifugal forces, etc. are excluded – this can explain the large difference between calculation and reality for partial load.

In Figure 5-23 and Figure 5-24 are as an example depicted comparisons of absolute and relative values of power demands of the test bench for shifted 3rd speed at the highest possible torque, which is 200 Nm. In case of relative power demands, values are related to loading power ($M_1 \cdot \omega_1$) according to the Formula (5-7). For all speeds was defined the same torque at the gearbox input shaft (200 Nm), only for the 1st speed was the input torque limited to 125 Nm due to the output shaft capacity. The power was measured by different speed of rotation of the gearbox input shaft.

Generally, the power demand is increased with the higher shifted speed. The explanation can be in increased losses of the gearboxes due to the higher speed of rotation of the output shaft, and therefore for higher churning losses.

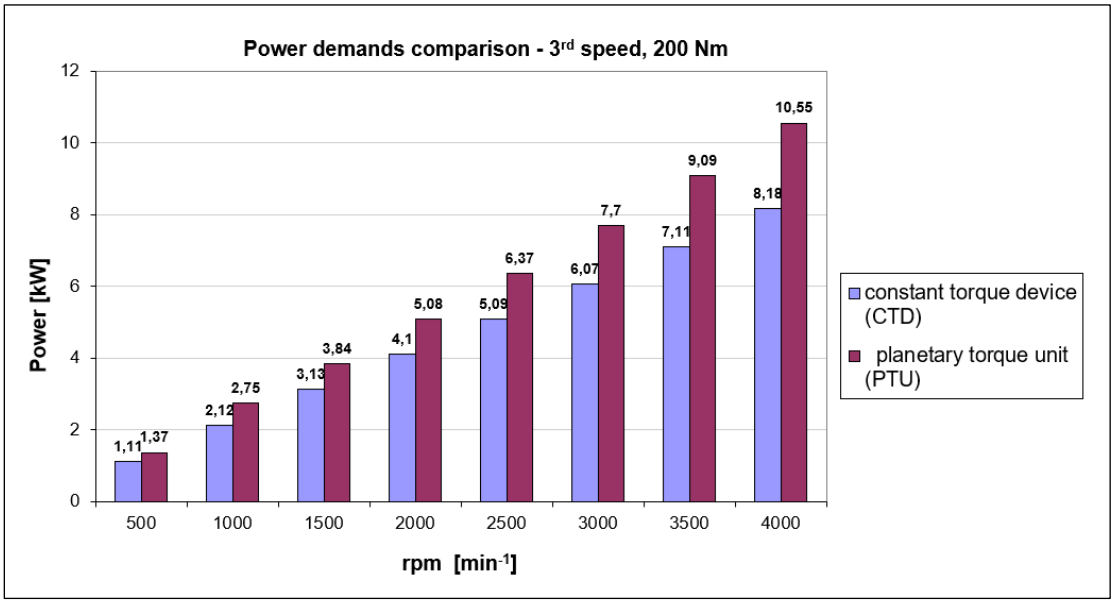

Figure 5-23: Comparison of absolute power demands at 3rd speed.

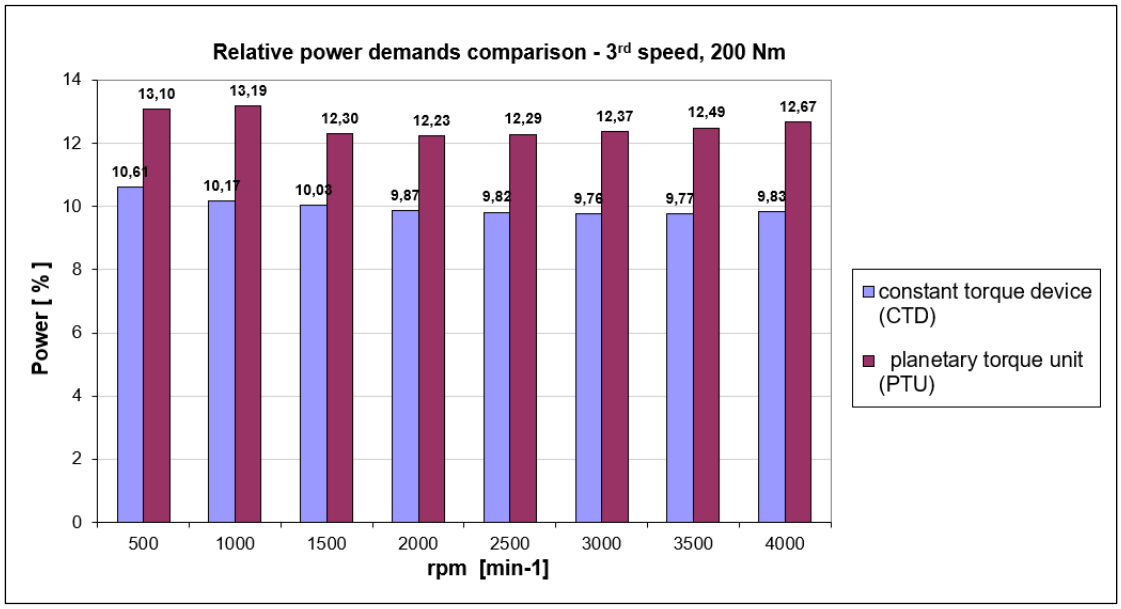

Figure 5-24: Comparison of relative power demands at 3rd speed.

From the torque and speed of rotation it is possible to calculate the magnitude of loading power inside the closed-loop. Let us take as example the highest speed of rotation. Maximal input shaft speed of rotation is 4000 rpm. For the 1st speed the loading power inside the closed loop is 52,3 kW (125 Nm), for all other speeds the circulating power equals 83,7 kW (200 Nm).

From the magnitude of the loading power and measured value of the electric motor power can be calculated the percentage of the needed power related to loading (test) power. These relative power losses are stated for all speed stages in Table 5-5.

Shifted speed	Torque [Nm]	Spread of power losses in the test bench [%]	
		Constant torque device (CTD)	Planetary torque unit (PTU)
1	125	12,65 – 13,74	16,79 – 17,44
2	200	10,71 – 12,48	13,41 – 14,88
3		9,77 – 10,61	12,23 – 13,19
4		10,20 – 10,94	12,72 – 13,39
5		10,15 – 10,72	12,44 – 13,70

Table 5-5: Spread of total power losses in the test bench [%] related to loading power.

5.4.4 Determination of Power Losses in Tested Gearbox

In previous chapter is described how the losses of the different parts of the closed-loop can be determined. In this chapter will be stated the losses of the tested gearbox and the belt drive. The main results are summarized in the Table 5-6. The gearbox efficiency was determined for both torque devices (CTD and PTU). The highlighted values (yellow) were measured. The values in bold are results from measurement and calculation. All other values were calculated or estimated.

Results for 3rd speed	Constant torque device (CTD)	Planetary torque unit (PTU)
M_1 [Nm]	198,5	196,7
n_1 [min^{-1}]	4000	4000
P_1 [kW]	83,15	82,40
M_2 [Nm]	878,9	871,55
n_2 [min^{-1}]	861,3	861,3
P_2 [kW]	79,27	78,61
t_{TESTED} [°C]	55,9	73,4
$t_{TECHNOL}$ [°C]	53,6	64,8
η_{TESTED}	**0,9636**	**0,964**
$\eta_{TECHNOL}$	0,959	0,960
$\eta_{BELT\ DRIVE}$	**0,971**	**0,981**
$\eta_{PLANETARY\ PTU}$	-	0,965

Table 5-6: Conditions under which were performed tests for evaluating efficiencies in the testing circuit and their values for both pretensioning devices for 3rd speed.

This whole power analysis in the closed circuit was presented in Detroit in [39].

5.5 Controlling Test Rig Program

To assure correct test rig controlling during the test, special program in the software **Labview** was created. In this chapter it is briefly described. The development of this program has started in 2007 and has been continuously improved.

In the initial version, the biggest task was to develop a communication between the frequency convertor and the controlling PC. This was done by an OPC server using a data socket, physical connection is assured using an optical cable. Next step was to complete all necessary signals acquisition, i.e. torques, rotational speed and temperatures. In the initial phase, the testing was performed only with the human service. The saved file name, starting a stopping of the test bench had to be done manually by the operator. Used pretensioning device was only the worm gear with the friction clutch – for constant torque.

Because endurance tests are very time demanding, it was very desirable to use also the time during the night. Each morning the gearboxes had to be warmed up before the testing, which took approximately a half an hour. For this reason, the upgrade to an unattended operation was done. To enable it, the controlling automat had to be developed. In this automat it is possible to set the number of last tested cycle and the number of cycles (hours) to be tested. To enable to run the test bench in the unattended regime, the automatic filename system was created. The overall appearance of current version of this program with the description is depicted in Figure 5-25.

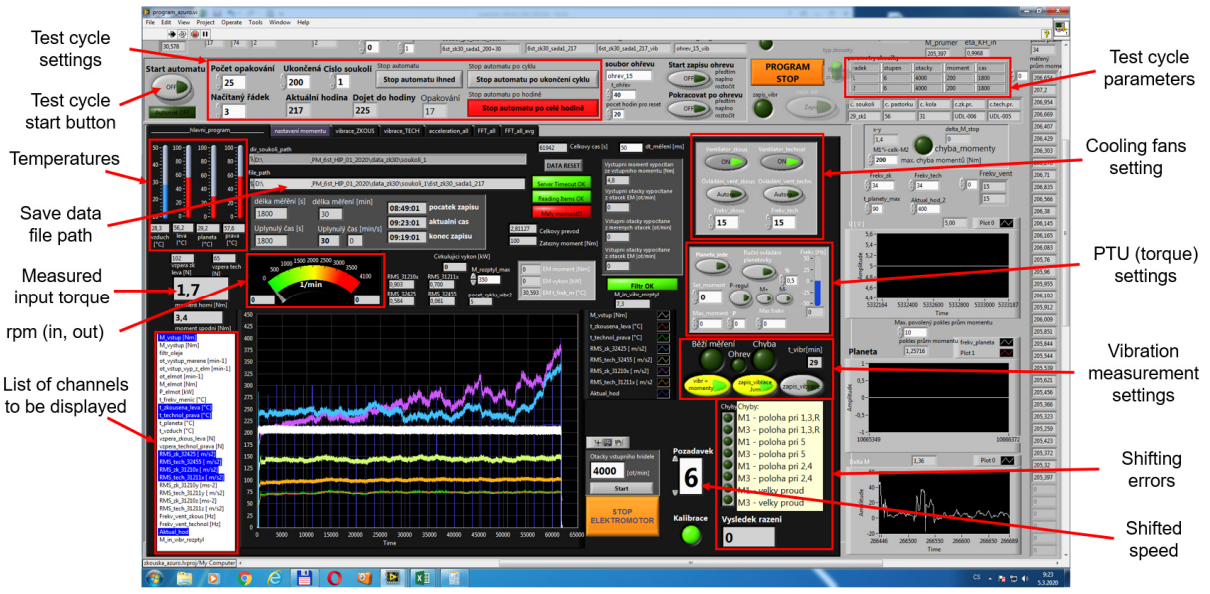

Figure 5-25: Appearance of the controlling program for the test bench – created in LabView

Next very important improvement, which was crucial for the unattended operation, was the vibration measurement for the fault detection. If the vibrations level exceeds the determined value, the test cycle can be stopped. This situation can happen e.g. for a tooth breakage or a bearing failure. A detailed view at the signals depicting area can be seen in a Figure 5-26. At the left side channels to be displayed can be chosen. Here is depicted an example when a bearing failure in the tested gearbox occurred.

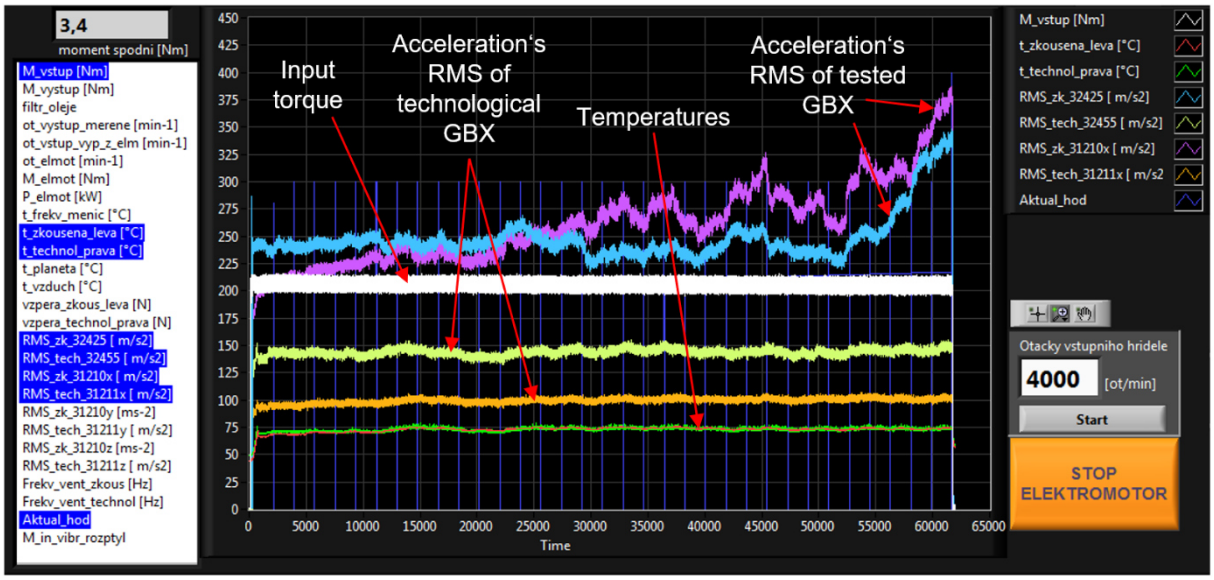

Figure 5-26: Detailed view at the chosen signals depicting area.

This whole program was created standardly in a block diagram. It is meaningless to describe this whole program in detail. For this reason, only main structures of this whole block diagram will be described and depicted. In Figure 5-27 can be seen the initial step which takes place immediately after the program starting. In the lower block are set basic initial parameters of the test, e.g. number of teeth, main directory for files saving etc. The function "Stacked sequence" is used for this purpose.

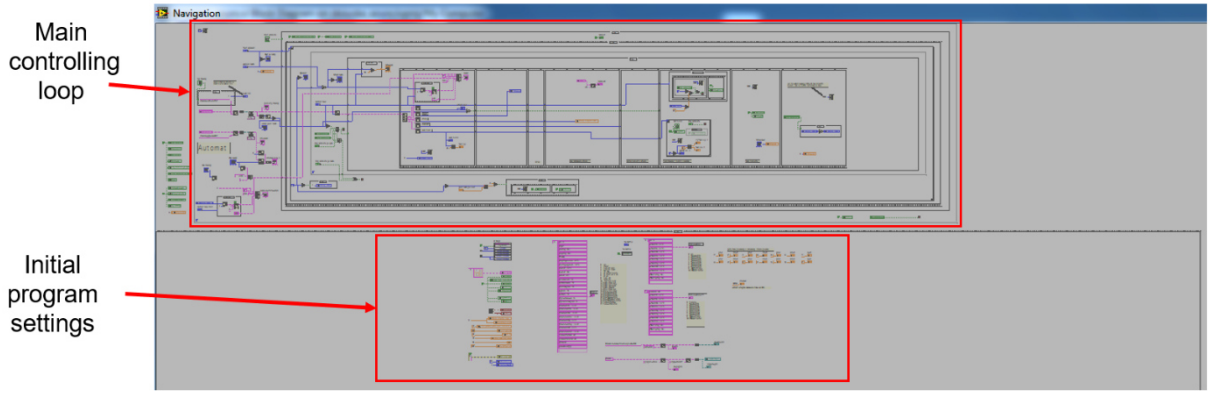

Figure 5-27: Block diagram of the controlling program initial step for the endurance testing in CTU labs

After the initial step, the program skips in the following stacked sequence, where it stays until the program stopping. The block diagram of this second phase is depicted in the Figure 5-28 with the description. It consists of more separate loops, which are used for special functions, e.g. the frequency convertor control, cooling fans control, vibrations acquisition and analysis, data files management, etc.

Independently at this stacked sequence was created the main controlling loop depicted in the upper part of both Figure 5-27 and Figure 5-28. In this loop it is set the precise course or the testing regime. Firstly, if the gearbox warming up is needed, it is either performed or skipped. In the next step the filename is created and subsequently the testing period starts. After this period either another period can start, or the testing cycle can be stopped due to either reaching desired number of testing cycles or some failure appearance and thus exceeding some limit. This "main controlling loop" communicates with the other part using "local variables".

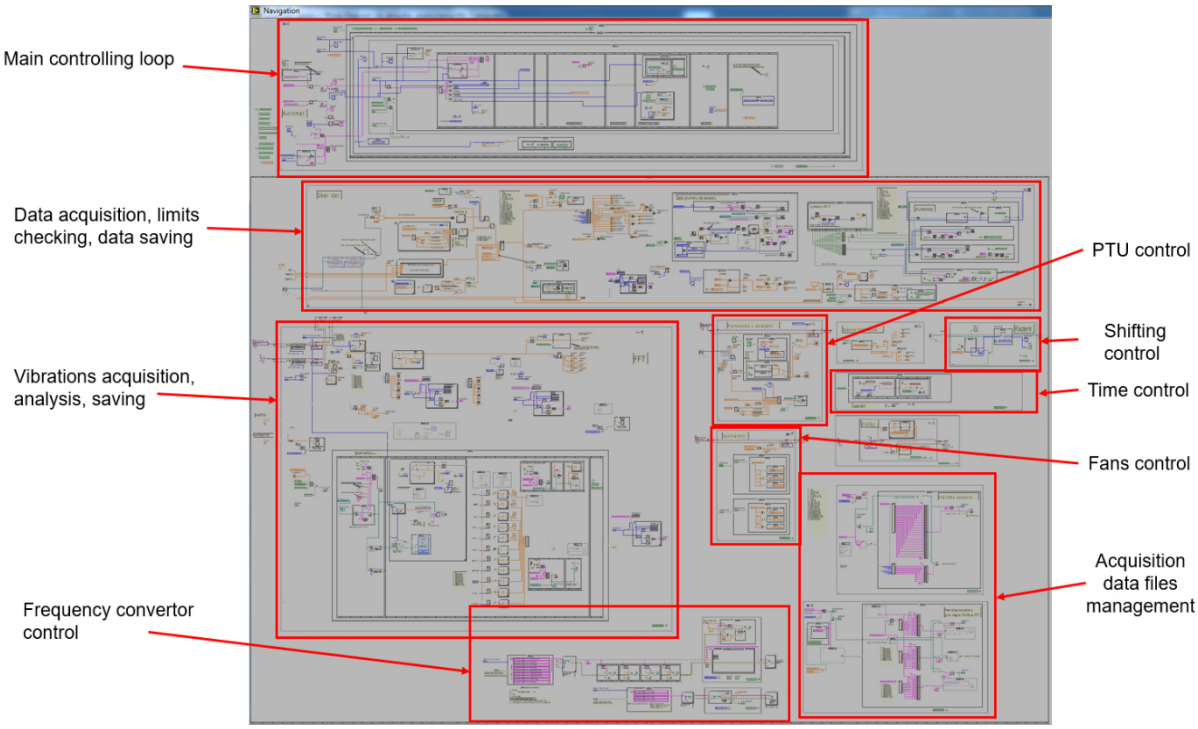

Figure 5-28: Block diagram of the following step - controlling program during the testing.

The last improvement of this program is the integration of the shifting robot control. This is done by more subordinate files, where the actuator's movement (shifting bowden's position) for each speed stage is defined. Real actuator control is performed using a NI cRIO with an FPGA (Field Programmable Gate Array) module NI cRIO-9024.

The shifting is possible only if the planetary torque unit (PTU) is mounted. Needed cooperation between the PTU and shifting robot is solved in this software too, because the shifting can be accomplished only if the loading torque is close to zero. The detailed shifting robot description can be seen in the Chapter 5.1.4.

6 Asymmetric Gearing

Within this thesis, involute gearing with an asymmetric profile had to be designed, manufactured and tested. First step to perform it was to design theoretical profile of this gearing. For this purpose, there was a need of a special software.

This "project" started in the spring of 2016. At that time, it still was not possible to use any commercial software for this purpose. The module in KissSoft for the gearing with an asymmetric profile (BETA Version) has been published only in the March of 2018, based on [26]. For this reason, special software for designing of the involute gearing with asymmetric profile had to be developed. The initial step was to describe the geometry of the asymmetric involute gearing.

6.1 Nomenclature and Usage of Asymmetric Gearing

Initially, the side (flank) nomenclature should be defined. When driving a car, the power is transmitted at the "drive" flank; with Internal combustion engine (ICE) braking (going downhill without the gas pedal pressed), power is transmitted from the wheels to the engine via the "coast" flank of the teeth. In the case of a passenger car, load conditions at both tooth flanks can be very different. This important difference is caused by ICE turbocharging (torque increase). This means that one tooth flank is used much more often and with higher loading torque than the opposite one. This situation is depicted in Figure 6-1. The recorded torque during a real test drive of a passenger car is used as input data. These measured torque values are then sorted into "load levels". At each load level is then calculated an average torque and number of occurrences – the "load level spectrum". The effect of this whole loading spectrum on the gearset can then be transformed into loading with constant "equivalent" torque M_e, which causes the same damage as the spectrum while undergoing the same number of cycles n. The exact procedure of its processing is described in [20].

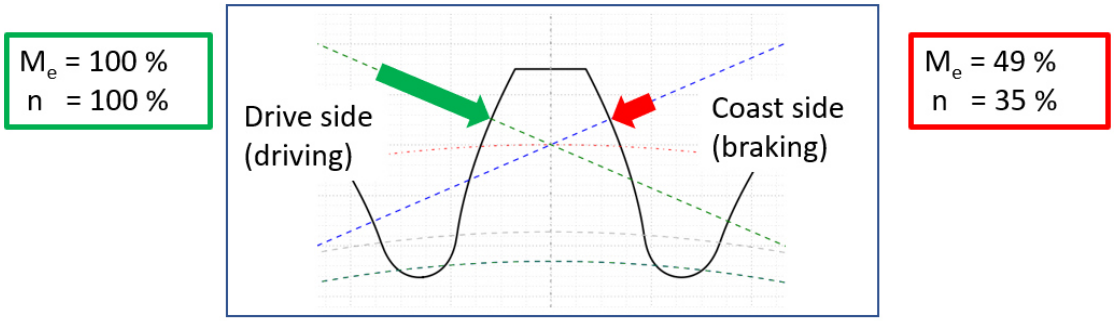

Figure 6-1: Loading conditions of the passenger car at both tooth flanks while driving and braking by ICE.

Figure 6-1 depicts a typical situation for a passenger car where the tooth flank at the coast side is loaded only with the torque value of 49% and only for 35% of loading cycles in comparison with the drive flank. In the case of lorries or electric cars, loading torque at the coast side increases due to usage of an engine brake, retarder or recuperation, so there are comparable loading conditions at both flanks. For this reason, a symmetric gearing profile makes sense is in these cases.

From the point of view of gearing durability, a symmetric profile in the case of passenger cars is not ideal. One side is always either overloaded or has excessive durability, particularly from the perspective of Hertzian (contact) stresses, which affect pitting formation. To optimize the durability

at both tooth sides according to loading conditions, it is useful to reduce the contact stress on the drive side. This reduction can be achieved using an asymmetric gearing profile. This means that the most important parameter of the rack profile - angle α_n (α_{P0}) - is not the same for both sides.

6.2 Geometry of Symmetric Involute Gearing

Before the macrogeometry of the gearing with an asymmetric profile will be described, the standard approach to symmetric involute gearing should be mentioned.

When designing the macrogeometry of a symmetric gearset according to applicable standards (e.g. DIN 3990:1987, Method B in KissSoft), all needed input parameters must be determined. The result is then the sum of required profile shift coefficients x_Σ for the gearset, which can be calculated using Formula (6-1).

$$x_\Sigma = x_1 + x_2 = \frac{z_1 + z_2}{2 \cdot tg\ \alpha_n} \cdot (inv\ \alpha_{tw} - inv\ \alpha_t) \tag{6-1}$$

where:

$x_{1,2}$	...	profile shift coefficients
$z_{1,2}$	...	number of teeth
α_n (α_{P0})	...	normal (tool) pressure angle
α_t	...	transverse pressure angle
α_{tw}	...	working transverse pressure angle

The value of x_Σ is calculated with the condition of no backlash and is then divided among each gearwheel according to loading or geometrical conditions and demands on the wheels. Finally, needed backlash is implemented to the final gear shape by the given standard (e.g. DIN 3967). An example of such gearing including the backlash can be seen in Figure 6-2.

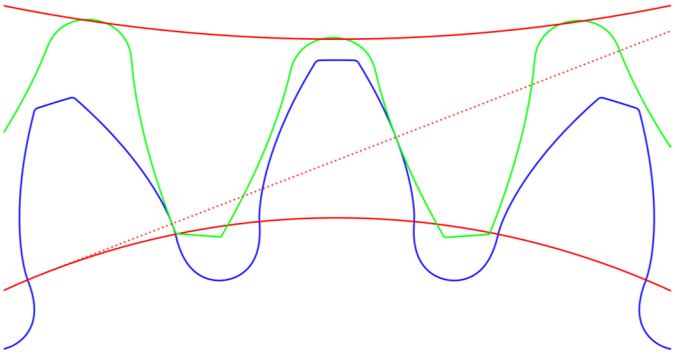

Figure 6-2: Example of the gearset appearance including the backlash designed in KissSoft.

6.3 Geometry of Asymmetric Involute Gearing

In the case of symmetric profile (rack), the tooth thickness is simply divided into two identical halves. In the case of asymmetric gearing, the situation is different. Figure 6-3 shows the situation in the transverse plane during manufacturing, i.e. the mesh of the tool (rack) with a gearwheel. All values with the symbol ”0” are related to a tool. The tool geometry description follows. A basic parameter is the thickness at tool’s reference plane s_{t0}, which equals half of the transverse pitch p_{t0}, as in the case of a symmetric version.

$$s_{t0} = \frac{p_{t0}}{2} = \frac{\pi \cdot m_t}{2} \tag{6-2}$$

where: m_t … transverse module

This tool thickness is a sum of partial tool thicknesses at both sides (drive and coast)

$$s_{t0} = s_{t0\ drive} + s_{t0\ coast} \tag{6-3}$$

Furthermore, the asymmetry ratio “A“ depends on the transverse profile angles and can be defined as the ratio of both these thicknesses

$$A = \frac{s_{t0\ drive}}{s_{t0\ coast}} = \frac{\tan \alpha_{t\ drive}}{\tan \alpha_{t\ coast}} \tag{6-4}$$

For symmetric gearing this value is $A = 1$. For asymmetric gearing there is standardly higher value of the profile angle α_t at the drive side. For this reason, also the thickness on the drive side is higher than on the coast side and thus the asymmetry ratio is standardly $A > 1$.

$$s_{t0\ drive} = s_{t0} \cdot \frac{A}{1+A} \quad , \quad s_{t0\ coast} = s_{t0} \cdot \frac{1}{1+A} \tag{6-5}$$

Regarding the tooth profile, the rack shift must be considered. If the profile shift coefficient is equal to zero, the tooth thickness s_t at the reference diameter *d* is the same as the thickness of the tool (gap) s_{t0}. If the rack is in a general position, i.e. shifted about the distance of *“x.m_n”* as depicted in Figure 6-3, tooth thicknesses at reference diameter on both sides are still divided in the same ratio *A* and their values are

$$s_{t\ drive} = s_{t0\ drive} + x \cdot m_n \cdot \tan \alpha_{t\ drive} = s_{t0\ drive} + x \cdot m_t \cdot \tan\ \alpha_{n\ drive} \tag{6-6}$$

and

$$s_{t\ coast} = s_{t0\ coast} + x \cdot m_n \cdot \tan \alpha_{t\ coast} = s_{t0\ coast} + x \cdot m_t \cdot \tan\ \alpha_{n\ coast} \tag{6-7}$$

where: m_n … normal module

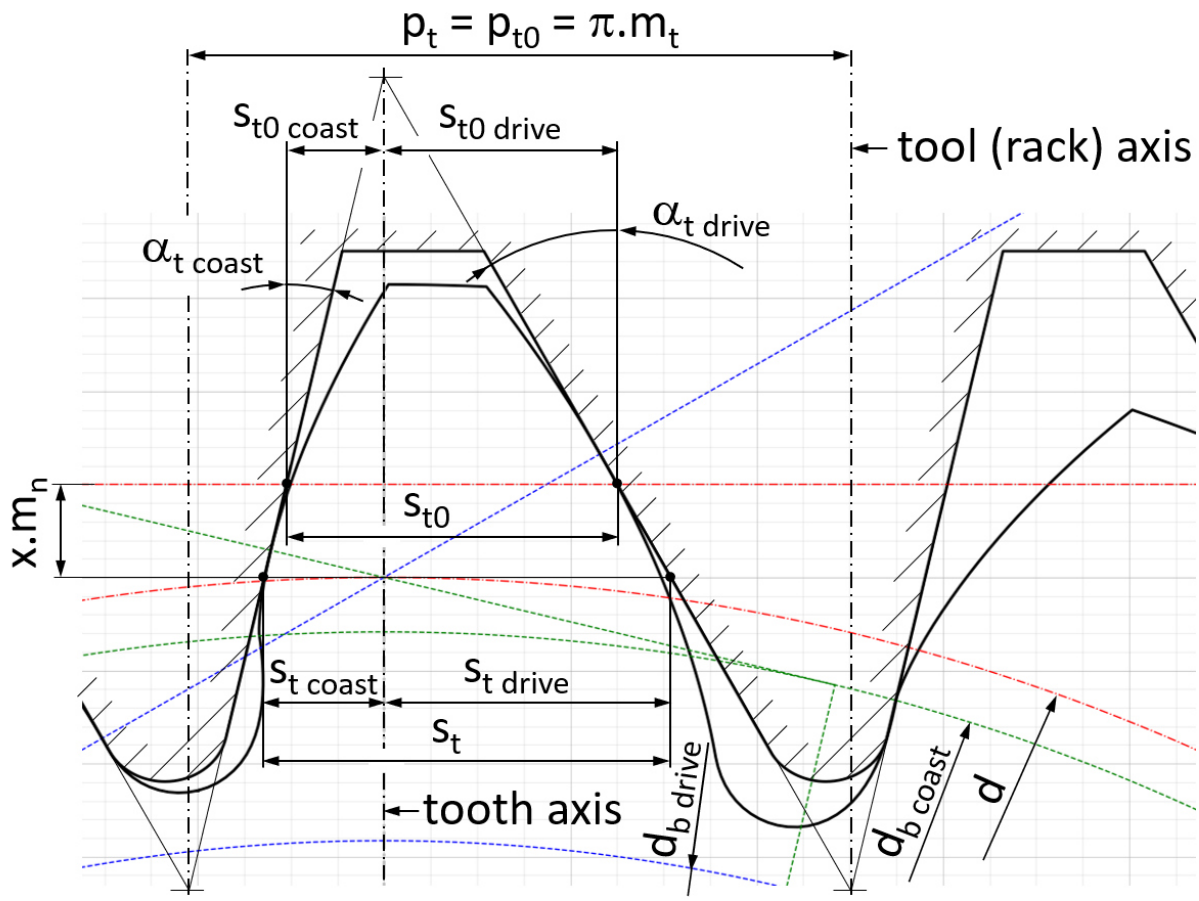

Figure 6-3: Situation in transverse plane while manufacturing of asymmetric gearing

To be able to derive a formula for a needed sum of both profile shift coefficients for the case of asymmetric gearing without a backlash, the basic condition of correct mesh must be used, Formula (6-8). The meaning is that the sum of tooth thicknesses of mating gears at their working pitch diameters must remain the transverse pitch.

$$p_{tw} = s_{tw1} + s_{tw2} \tag{6-8}$$

These working pitch diameters can be calculated purely from the kinematic ratio using of number of teeth as (6-9)

$$r_{w1} = \frac{a_w}{1 + \frac{z_2}{z_1}} \quad , \qquad r_{w2} = \frac{a_w \cdot \frac{z_2}{z_1}}{1 + \frac{z_2}{z_1}} \tag{6-9}$$

For a symmetric gearing, these thicknesses $s_{tw\ 1,2}$ can be computed using formula (6-10) as

$$s_{tw\ 1,2} = d_{w\ 1,2}\left(\frac{s_{t\ 1,2}}{d_{1,2}} + inv\ \alpha_t - inv\ \alpha_{tw}\right), \quad inv\ \alpha = \tan\alpha - \alpha\ [rad] \tag{6-10}$$

where working transverse pressure angle α_{tw} can be calculated using Formula (6-11) as

$$\alpha_{tw} = \arccos\left(\frac{a_n}{a_w} \cdot \cos\alpha_t\right) \tag{6-11}$$

where: $a_n = r_1 + r_2$ … nominal center distance

$a_w = r_{w1} + r_{w2}$ … working (real) center distance

For an asymmetric profile, these thicknesses $s_{tw\ 1,2}$ can also be computed, using Formula (6-10), but separately for each tooth side. Radii must be used instead of diameters, Formulas (6-12) and (6-13).

$$s_{tw\ drive\ 1,2} = r_{w\ 1,2}\left(\frac{s_{t\ drive\ 1,2}}{r_{1,2}} + inv\ \alpha_{t\ drive} - inv\ \alpha_{tw\ drive}\right) \tag{6-12}$$

$$s_{tw\ coast\ 1,2} = r_{w\ 1,2}\left(\frac{s_{t\ coast\ 1,2}}{r_{1,2}} + inv\ \alpha_{t\ coast} - inv\ \alpha_{tw\ coast}\right) \tag{6-13}$$

By the summing of these two parts, total tooth thickness can be defined at working pitch diameters $d_{w1,2}$ for both gearwheels, Formula (6-14)

$$s_{tw\ 1,2} = s_{tw\ drive\ 1,2} + s_{tw\ coast\ 1,2} \tag{6-14}$$

The aim is to determine needed sum of both profile shift coefficients. For this reason, these values $x_{1,2}$ must be used for description of the thicknesses $s_{tw\ 1,2}$, Formula (6-15).

$$s_{tw\ 1,2} = r_{w\ 1,2}\left(\frac{m_t \cdot \pi}{2 \cdot r_{1,2}} + \frac{m_t \cdot x_{1,2}}{r_{1,2}} \cdot (\tan\alpha_{n\ drive} + \tan\alpha_{n\ coast}) + inv\ \alpha_{t\ drive} - inv\ \alpha_{tw\ drive} + inv\ \alpha_{t\ coast} - inv\ \alpha_{tw\ coast}\right) \tag{6-15}$$

The sum of these two thicknesses follows in the Formula (6-16).

$$s_{tw\ 1} + s_{tw\ 2} = \frac{m_t \cdot \pi}{2} \cdot \left(\frac{r_{w1}}{r_1} + \frac{r_{w2}}{r_2}\right) + (x_1 + x_2) \cdot m_t \cdot \frac{r_{w1}}{r_1} \cdot (\tan(\alpha_{n\ drive}) + \tan(\alpha_{n\ coast})) + + (r_{w1} + r_{w2}) \cdot (inv\alpha_{t\ drive} - inv\alpha_{tw\ drive} + inv\alpha_{t\ coast} - inv\alpha_{tw\ coast}) \tag{6-16}$$

The value of $(r_{w1} + r_{w2})$ can be substituted using Formula (6-17). Values of appropriate mesh angles α_t and α_{tw} can be taken either from drive or coast side because their ratio used in Formula (6-17) remains same for both of them.

$$r_{w1} + r_{w2} = a_w = a_n \cdot \frac{\cos\alpha_{t\ drive}}{\cos\alpha_{tw\ drive}} = \frac{(z_1 + z_2) \cdot m_t}{2} \cdot \frac{\cos\alpha_{t\ drive}}{\cos\alpha_{tw\ drive}} \tag{6-17}$$

Transverse pitch p_{tw} at working pitch diameters $d_{w\ 1,2}$ can be then computed using Formula (6-18) as

$$p_{tw} = p_t \cdot \frac{d_w}{d} = \pi \cdot m_t \cdot \frac{d_w}{d} = \pi \cdot m_t \cdot \frac{\cos\alpha_{t\ drive}}{\cos\alpha_{tw\ drive}} = \pi \cdot m_t \cdot \frac{\cos\alpha_{t\ coast}}{\cos\alpha_{tw\ coast}} \tag{6-18}$$

Now it is finally possible to put all needed formulas into the Formula (6-8). The final result of this condition is the desired sum of profile shift coefficients $x_1 + x_2$ of both gearwheels, Formula (6-19).

$$x_\Sigma = x_1 + x_2 = \frac{(z_1 + z_2) \cdot (inv\alpha_{tw\ drive} - inv\alpha_{t\ drive} + inv\alpha_{tw\ coast} - inv\alpha_{t\ coast})}{2 \cdot (\tan\alpha_{n\ drive} + \tan\alpha_{n\ coast})} \tag{6-19}$$

As it was mentioned, value of x_Σ resulting from the Formula (6-19) is derived for the condition of theoretical mesh with no backlash between tooth flanks. Similarity with the Formula (6-1) is obvious at the first glance. The only difference is, that appropriate expressions are used separately for each tooth side, instead of one value identical on both sides as for symmetric profile. One of these two values $x_{1,2}$ must be set and the second one is then calculated from x_Σ.

6.4 Gearset Depiction including the Backlash

For assuring of correct gearset function some minimal backlash is needed between tooth flanks while meshing. To be able to determine and depict this circumferential transverse backlash j_t, the attention must be focused again on working pitch diameters $d_{w\,1,2}$ where thicknesses of mating gears are important. On these diameters transverse working pitch p_{tw} remains the same as for the case of meshing without a backlash and can be defined using Formula (6-18). Teeth thicknesses of both gears can be computed using Formula (6-15). Fundamental condition for meshing without a backlash expressed by the Formula (6-8) then changes to the Formula (6-20), where circumferential backlash j_t is already considered.

$$p_{tw} = s_{tw1} + s_{tw2} + j_t \tag{6-20}$$

Formula (6-20) can then be used to express the circumferential transverse backlash j_t as

$$j_t = p_{tw} - s_{tw1} - s_{tw2} \tag{6-21}$$

From Formula (6-21) it is clear, that the sum of both tooth thicknesses $s_{tw\,1,2}$ must be smaller than for the case without clearance. These thicknesses are influenced by the values of profile shift coefficients. This means that for this case, including the backlash, the Formula (6-19) cannot be used. When considering a real case including the backlash, both values of $x_{1,2}$ must be entered and resulting transverse backlash j_t can be then calculated.

More important than circumferential transverse backlash j_t is the normal one j_n. In the case of asymmetric gearing, the same formula is used as for a symmetric profile, but relevant angles differ at both sides, Formula (6-22).

$$j_{n\,drive} = j_t \cdot \cos\alpha_{tw\,drive} \cdot \cos\beta_w \quad , \quad j_{n\,coast} = j_t \cdot \cos\alpha_{tw\,coast} \cdot \cos\beta_w \tag{6-22}$$

The situation while recalculating backlashes is depicted in detail in Figure 6-4. This figure applies only for spur gearing, in the case of helical gearing the influence of helix angle β_w cannot be depicted in transverse plane. Nevertheless, in Formulas (6-22) it is included, so computed values of j_n are correct also for helical gearing.

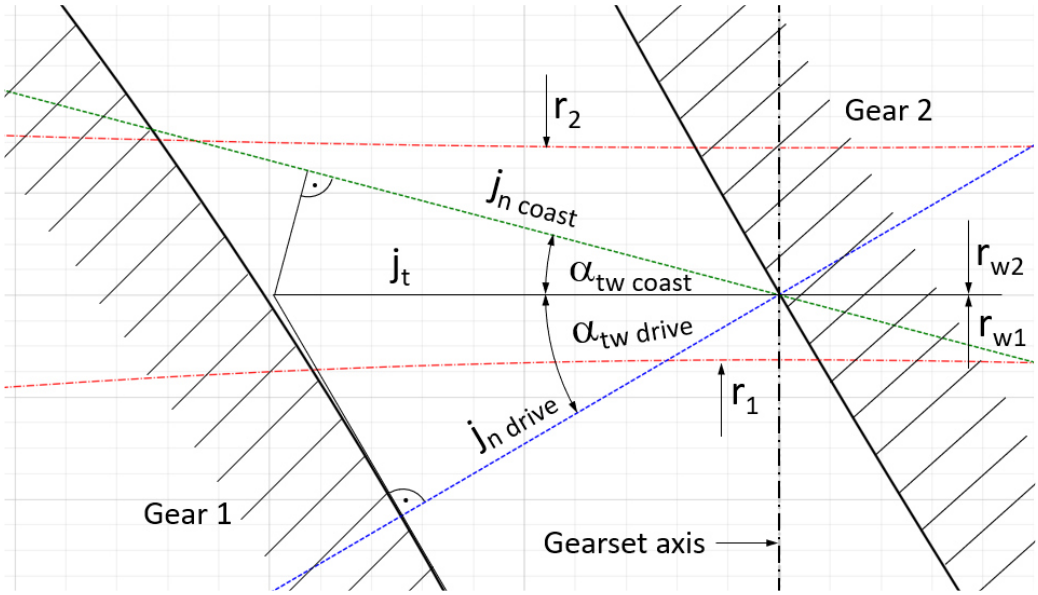

Figure 6-4: Recalculation from circumferential transverse backlash to normal backlash - detail

While meshing of drive flanks, the backlash between coast flanks appears (and conversely), Figure 6-5. Normally the drive side is the more important one and has a higher value of mesh angle than the coast one. For this reason, backlash at the coast side is standardly also higher, Figure 6-4.

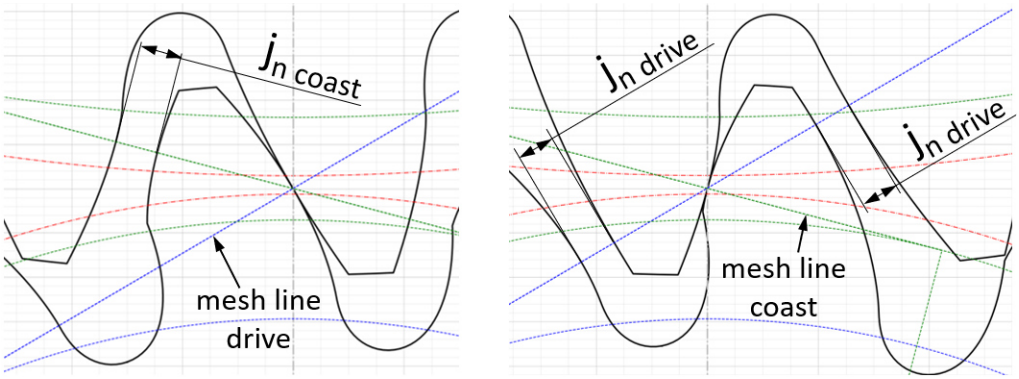

Figure 6-5: Normal backlash j_n between coast/drive flanks while drive/coast flanks meshing (left/right).

When designing a gearset, input parameters must be given. This is normally the ratio (number of teeth), working center distance and maximum addendum diameters restricted by space requirements. Subsequently, tooth profile (mesh angle) and helix angle are determined. The result of the gearset macrogeometry design is the sum of profile shift x_Σ for the condition of no backlash.

Real tooth profiles (values of profile shift coefficients) are subsequently changed according to related standards (e.g. DIN 3967) to reach desired backlash, which is crucial for correct gearset function.

In the case of the software described in next chapter, x_Σ can be either calculated directly using Formula (6-19) for the condition of no backlash or can be entered manually, separately for each gear including the profile shift coefficients. An exception to this are common parameters of both gears (e.g. helix angle). Gearwheel profiles are directly depicted including the backlash (if possible) and all needed parameters are calculated. Example of such case is depicted in Figure 6-5. Indeed, the situation when negative backlash appears can occur, Figure 6-6. Of course, in reality negative

backlash is not possible, its value must be always positive! For this reason, it is very important to check backlash values. The text of these values is enlarged in Figure 6-6.

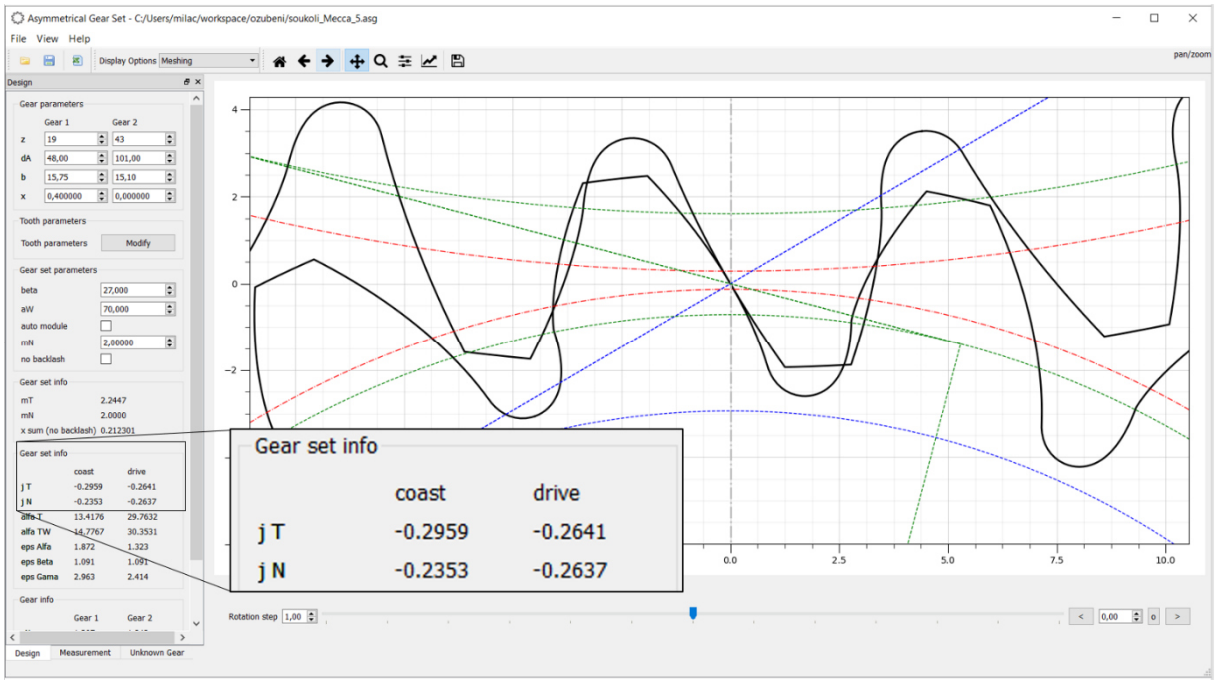

Figure 6-6: Example of the gearset with negative backlash value – not possible.

The geometry of asymmetric gearing and created software appearance were described in [41] and [44].

6.5 Software Description

The evolution of this software in few sequential versions is described in this chapter.

It is very important to include the influence of the production technology into the gearing design. Modern technologies allow the fine-tuning of the profile using CNC milling, electrical discharge machining (EDM) or grinding technology. In this software, the gearing profile is created purely by a trochoidal machining method with a cutting tool (rack).

The development process of this software was quite demanding. In the following text its appearance and parameters at given stages are depicted and described. In the final version the tool profile includes standard technological issues (properties) - the tip chamfer and the protuberance.

This software was developed in the Python programming software. Units of all used and displayed values are [mm]. The KissSoft program served as an example of its appearance. The first version is depicted in Figure 6-7.

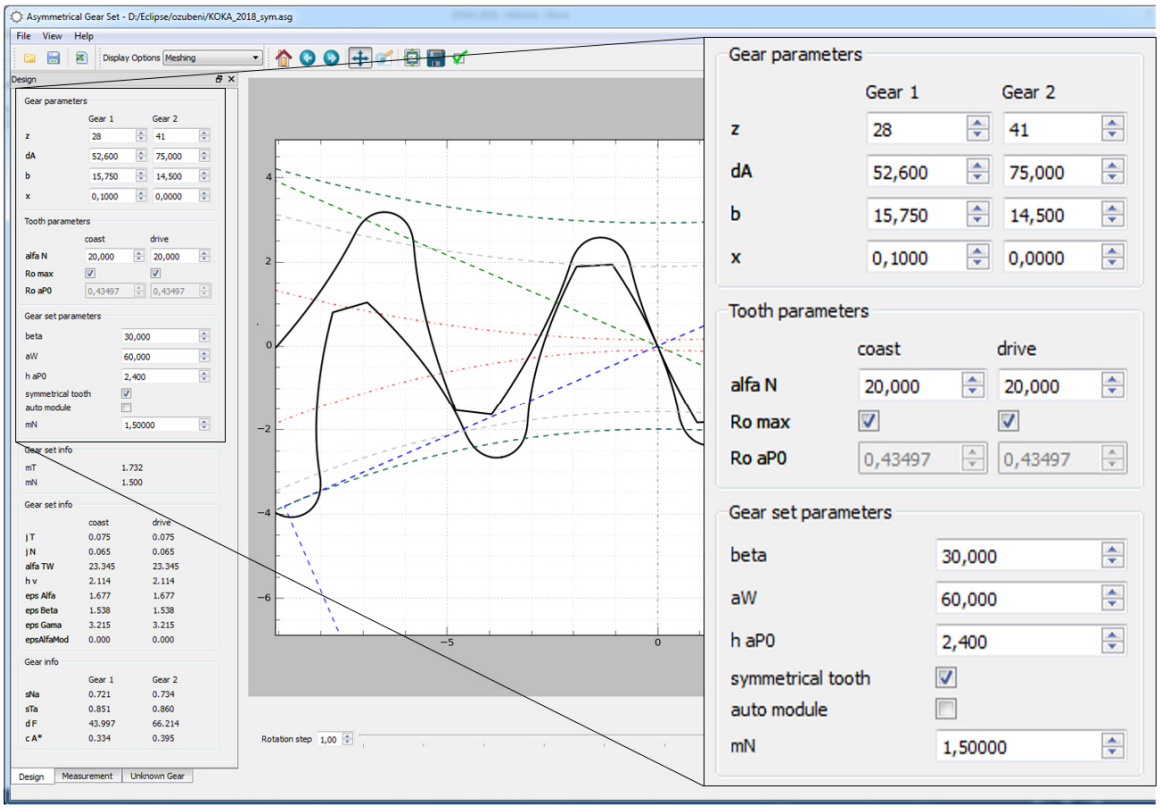

Figure 6-7: Appearance of the program initial version for depicting symmetric and asymmetric gearing – example of a gear mesh

parameter	sign	unit
Number of teeth	z_1, z_2	-
Normal module	m_n	mm
Rack profile angle - drive	α_{nD}	deg
Rack profile angle - coast	α_{nC}	deg
Helix angle	β	deg
Facewidth	b_1, b_2	mm
x – shift coefficient	x_1, x_2	-
Outer (tip) diameter	d_{a1}, d_{a2}	mm
Axes distance	a_w	mm
Addendum height of the rack (tool)	h_{aP0}	mm
Addendum radius of the rack (tool) - drive	ρ_{aP0_D}	mm
Addendum radius of the rack (tool) - coast	ρ_{aP0_C}	mm
Number of teeth to measure over	i	-
Ball diameter to measure over	D	mm

Table 6-1: Input parameters of the depicted gearset in Figure 6-7 – initial program version.

At this stage it was possible to set only the basic parameters of the rack. These input parameters are mentioned in Table 6-1. Furthermore, for the manufacturing of both gears only one (identical) cutting tool was considered. This issue can cause the tip – root interference. Besides all necessary parameters, there is also the option of some checkboxes - for choosing of symmetric/asymmetric profile, maximum addendum rack radii at both flanks and "auto module" checkbox. This enables selection of whether the value of the normal module is calculated from other given values with no clearance (particularly the working axes distance a_w) or can be strictly determined. The second variant enables creation of the clearance between flanks. This function is very useful for preliminary design of the gearset. In next steps, fine tuning of the profile can adjust this value to a more suitable one.

In addition to the gearing meshing, it is also very useful to see the situation while manufacturing. For this reason, more depiction options are possible – e.g. while manufacturing of both gears – the meshing of the gear with the tool (rack) – depicted in Figure 6-8. The displayed variant can be chosen by clicking the button "Display Options" in the upper-left corner.

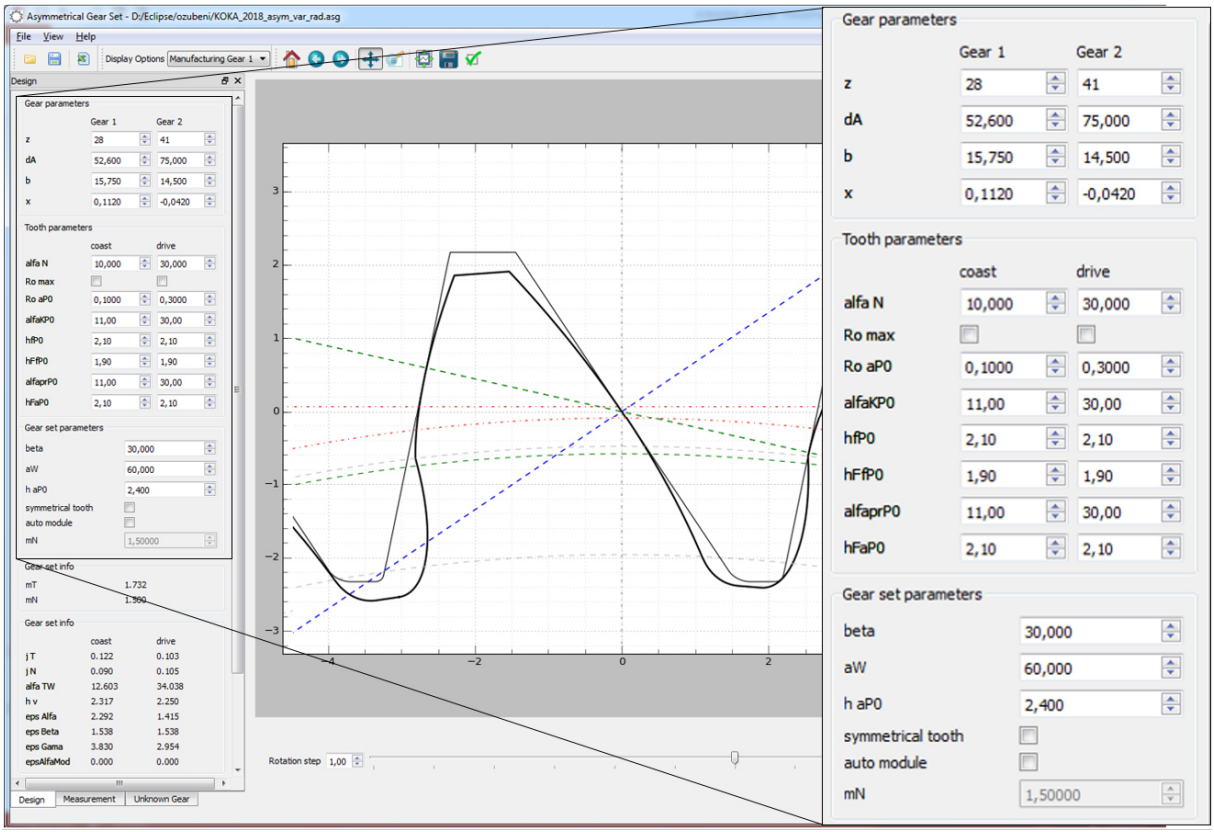

Figure 6-8: Asymmetric gear design - option "Manufacturing gear 1".

In the version depicted in Figure 6-8, an improvement in the tool geometry is visible in comparison with the previous version in Figure 6-7. It is already possible to set a tip chamfering and a protuberance. If these options are not needed, values of appropriate profile angles (α_{KP0} , α_{prP0}) are set to same value as α_n. The detailed appearance of a possible tool with tip chamfer and protuberance is depicted in Figure 6-9. Nevertheless, there is still only one common tool for manufacturing both gearwheels. This limitation led to an issue concerning non-equal tip – root clearance. To eliminate this issue another innovation was added to the final version. Each gearwheel has its own manufacturing tool. The only common parameters of these two tools are angles α_{P0} at both sides to assure correct mesh. All other parameters can be different, e.g. addendum and

dedendum heights. Furthermore, the option of tip chamfering and protuberance was maintained. In total, four separate profiles of tooth flanks can be defined. All these parameters can be set in a separate pop-up window after clicking the button “Modify”, which can be seen in Figure 6-11. Its appearance is depicted in Figure 6-10.

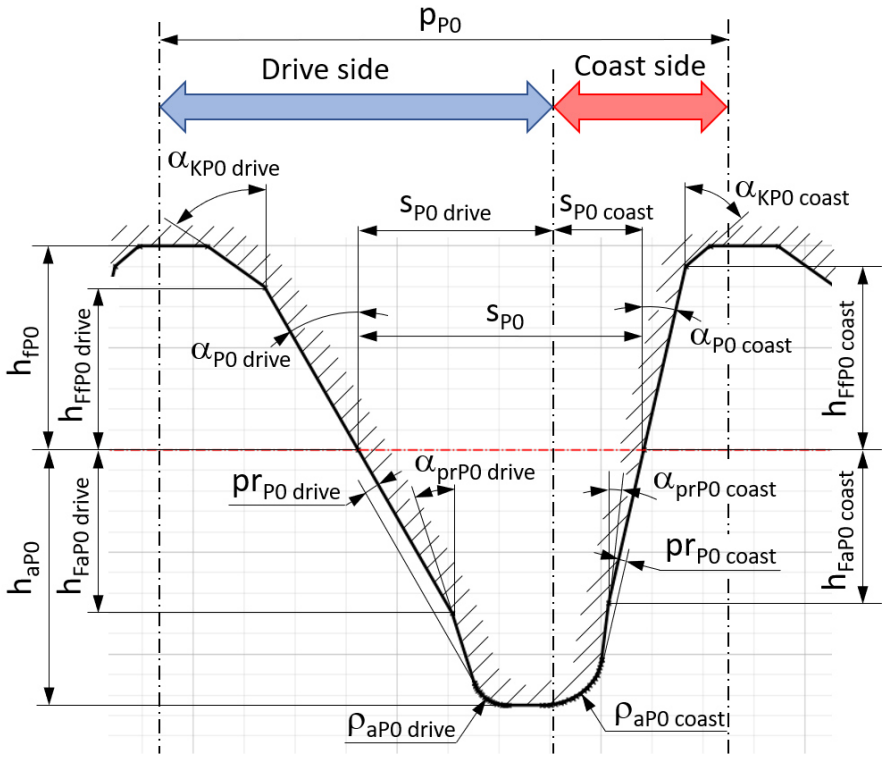

Figure 6-9: Complete appearance of manufacturing tool (rack) with asymmetric profile, tip chamfer and protuberance created by this software.

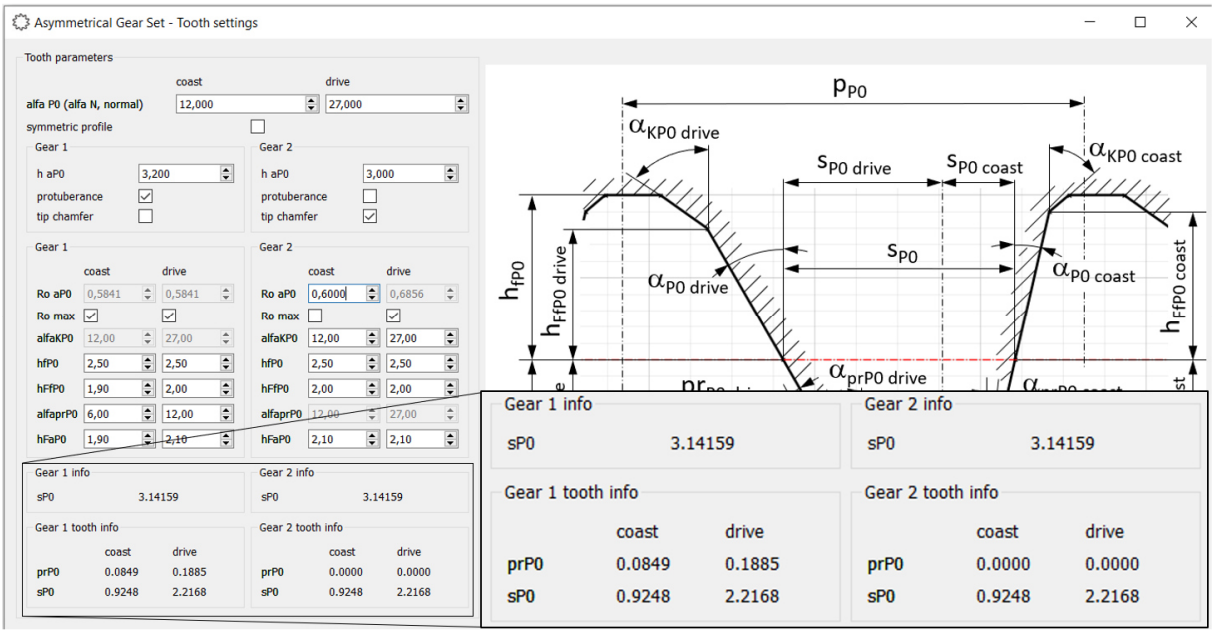

Figure 6-10: Appearance of the window for setting of a tool (rack) parameters with asymmetric profile. This window pops-up after clicking the button ”Modify”.

In Figure 6-11 can be also seen that the checkbox “no backlash” is checked. For this reason, the value of x_Σ was calculated and depicted in the tab „Gear set info“ and furthermore, it is possible to set only the value of x_1 and the value of x_2 is computed automatically without a possibility to be changed.

All angles mentioned in the pop-up window (Figure 6-10) are parameters of the tool, so they are defined in the normal plane (e.g. rack profile angles α_{P0}). From all these parameters results the final tool geometry. Important tool parameters are depicted in the lower part, i.e. the protuberance magnitude (prP0) and tool thickness (sP0) at the appropriate side (flank). Furthermore, total tool thickness (sP0) is displayed above too. The correctness of displayed values can be simply checked, because for the value of normal module for the depicted example is m_n = 2 mm, and thus the value of total tool thickness s_{P0} is precisely π mm. At the gear 1 protuberance was used, at the gear 2 there is no protuberance, so the value of prP0 is zero at both flanks (Figure 6-10).

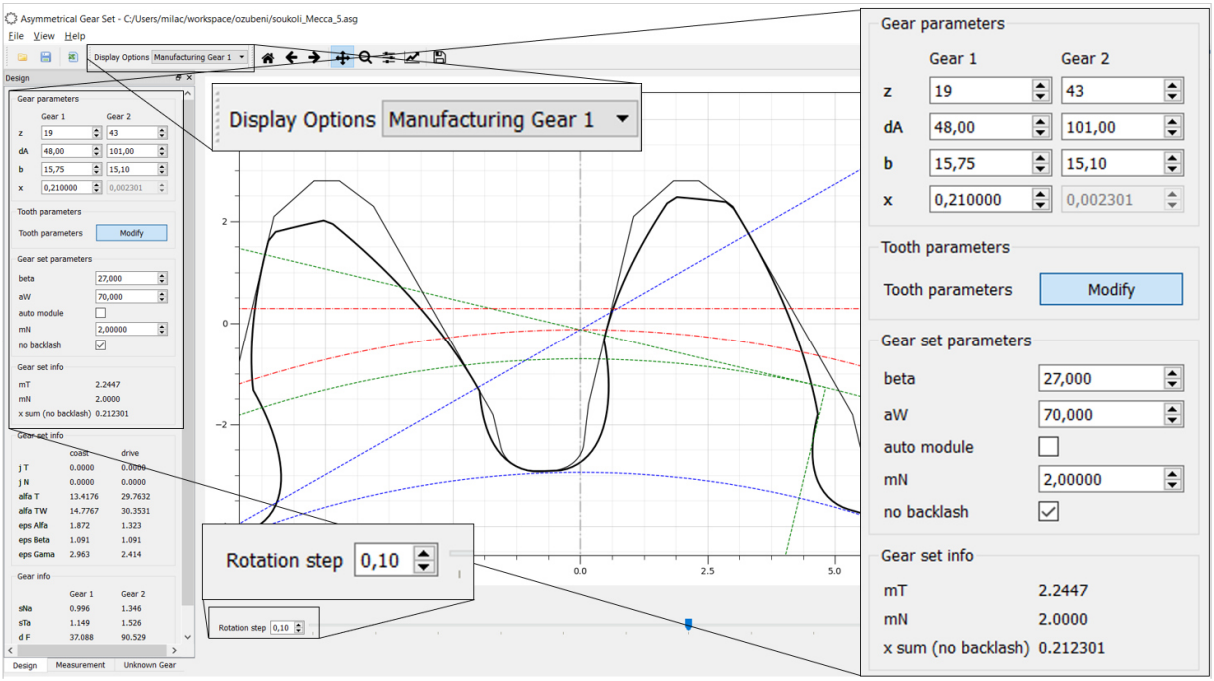

Figure 6-11: Appearance of the program including tip chamfer and protuberance – display option “Manufacturing gear 1”.

Regarding geometry calculations, in principle the same formulas are used as for symmetric gearing. For the symmetric case it is quite simple because all computed values are divided by “2” because of the symmetry. In the case of asymmetrical gearing, all these computations lead to a system of non-linear formulas which must be solved numerically by an appropriate solver. All used formulas for completing the geometry calculations were found in [25].

Today, it is possible to use it only for external, spur and helical, symmetric and asymmetric design. All necessary parameters of the gearset can be set on the left side. In the left bottom corner are three tabs: “Design”, “Measurement” and “Unknown gear”, Figure 6-15. In the tab “Design”, basic input parameters of the gearset can be entered.

Thanks to this program, it is also possible to calculate the value of the measurement over teeth (span measurement) and over balls. This can be seen in the tab ”Measurement” in the bottom-left corner. In the case of symmetric teeth both these variants are possible. In the case of asymmetric gearing, only the measurement over balls is possible because there is no common tangent between

opposite involute flanks. Graphical depiction of the situation with embedded ball with the diameter "D" is depicted in Figure 6-12 and is meaningful only for spur gearing when the depicted ball really touches both flanks. For helical gearing, the calculated value of the ball centers diameter d_g is correct, but because of the helix angle, the inserted ball does not touch the depicted transverse gear profile.

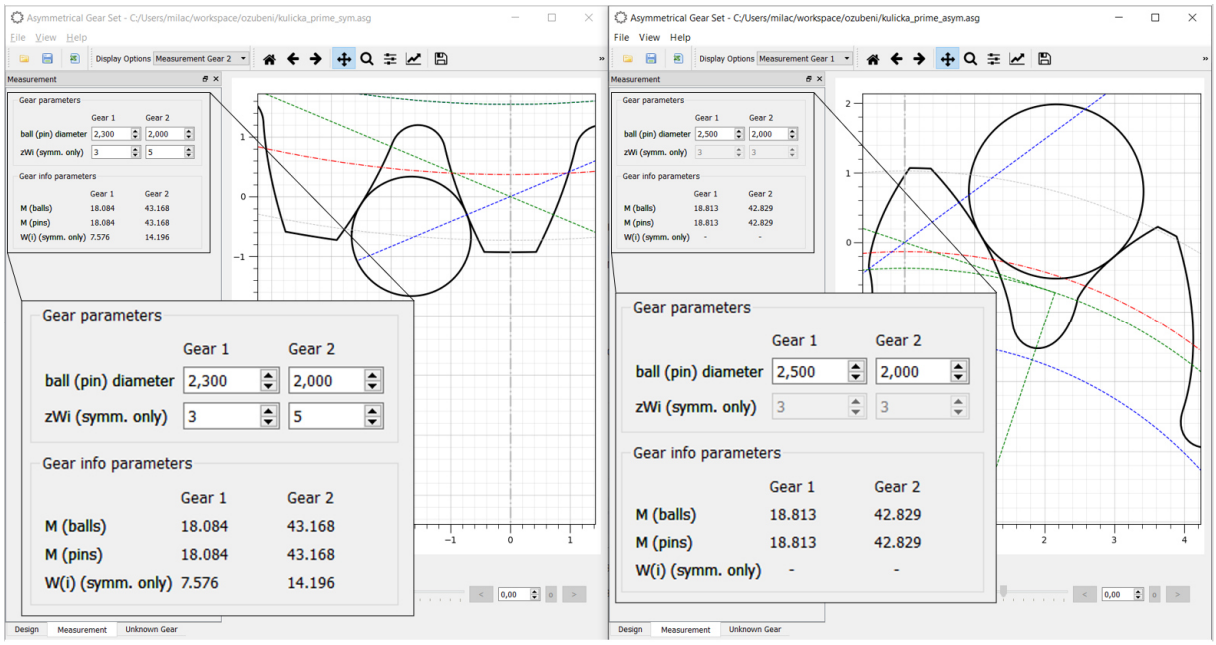

Figure 6-12: Appearance of the program tab „Measurement" for spur gearing with an symmetric (left) and asymmetric (right) profile. Embedded ball touches the transverse tooth profile.

For asymmetric profile, this ball center diameter d_g can be computed from the system of two formulas (6-23) and (6-24).

$$inv\ \alpha_{gd} + inv\ \alpha_{gc} = inv\ \nu_d + inv\ \nu_c + \frac{D}{d_{bd} \cdot cos\beta_{bd}} + \frac{D}{d_{bc} \cdot cos\beta_{bc}} - \frac{2 \cdot \pi}{z} \tag{6-23}$$

$$(d_g =)\quad \frac{d_{bd}}{cos\ \alpha_{gd}} = \frac{d_{bc}}{\cos \alpha_{gc}} \tag{6-24}$$

Used angles $inv\ \nu_d$ and $inv\ \nu_c$ in the Formula (6-23) can be computed using Formulas (6-25).

$$inv\ \nu_d = \frac{s_{td}}{r} + inv\ \alpha_{td}\ ,\quad inv\ \nu_c = \frac{s_{tc}}{r} + inv\ \alpha_{tc} \tag{6-25}$$

The angular position of embedded ball related to the tooth axis is for symmetric profile given quite easily as half of the angle related to the one tooth pitch, Formula (6-26).

$$\varepsilon_{ball,\ symm} = \frac{2 \cdot \pi}{2 \cdot z} = \frac{\pi}{z} \tag{6-26}$$

In case of asymmetric profile, this angle ε_{ball} can be derived from the Figure 6-13. If the diameter d_g is already known, we can focus only on the drive side, where the "touching" angle α_{tTd} can be computed as

$$\alpha_{tTd} = arctg\left(tg\ \alpha_{gd} - \frac{D}{d_{bd}}\right) \tag{6-27}$$

The radius of the touching point can be computed thanks to contact angle α_{tTd} as

$$r_{Td} = \frac{r_{bd}}{\cos \alpha_{td}} \tag{6-28}$$

Tooth thickness of the drive side at this radius s_{tTd} can be subsequently computed

$$s_{tTd} = r_{Td} \cdot \left(\frac{s_{td}}{r} + inv\ \alpha_{td} - inv\ \alpha_{tTd}\right) \tag{6-29}$$

To this thickness s_{tTd} relates at a radius r_{Td} an appropriate angle ε_{tTd}

$$\varepsilon_{tTd} = \frac{s_{tTd}}{r_{Td}} \tag{6-30}$$

And finally, the desired angle between the tooth axis and embedded ball ε_{ball} is

$$\varepsilon_{ball} = \varepsilon_{tTd} + \alpha_{gd} - \alpha_{tTd} \tag{6-31}$$

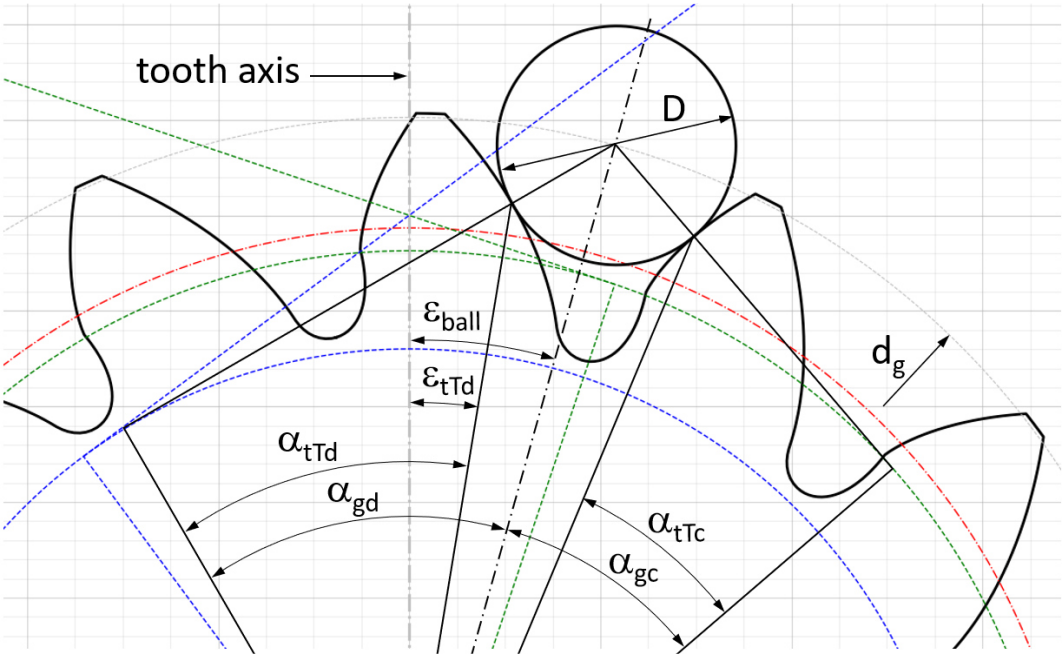

Figure 6-13: Geometry of the measurement over balls for the asymmetric profile.

The final formula for the measurement over balls "*M*" is then for even number of teeth

$$M = d_g + D \tag{6-32}$$

and for the gearwheels with odd number of teeth same recalculation formula as for standard symmetric profile holds true, Formula (6-33).

$$M = d_g \cdot \cos\frac{\pi}{2 \cdot z} + D \tag{6-33}$$

The tab "Unknown Gear" enables identification of unknown gear parameters using measured normal thickness at a given depth. The measured unknown gear profile can then be visually compared with the gear profile designed in the tab "Design". If both these depicted profiles match,

then parameters of the unknown gear are set. This method can only be used for spur symmetric gearing and is very inaccurate.

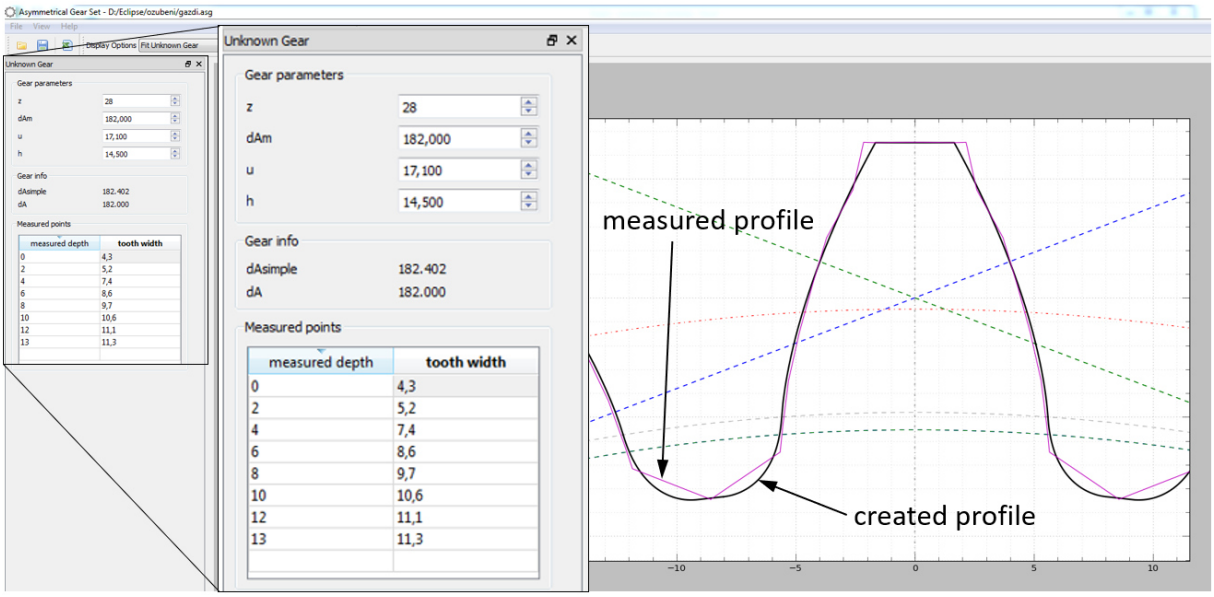

Figure 6-14: Appearance of the program – display option "Fit Unknown gear".

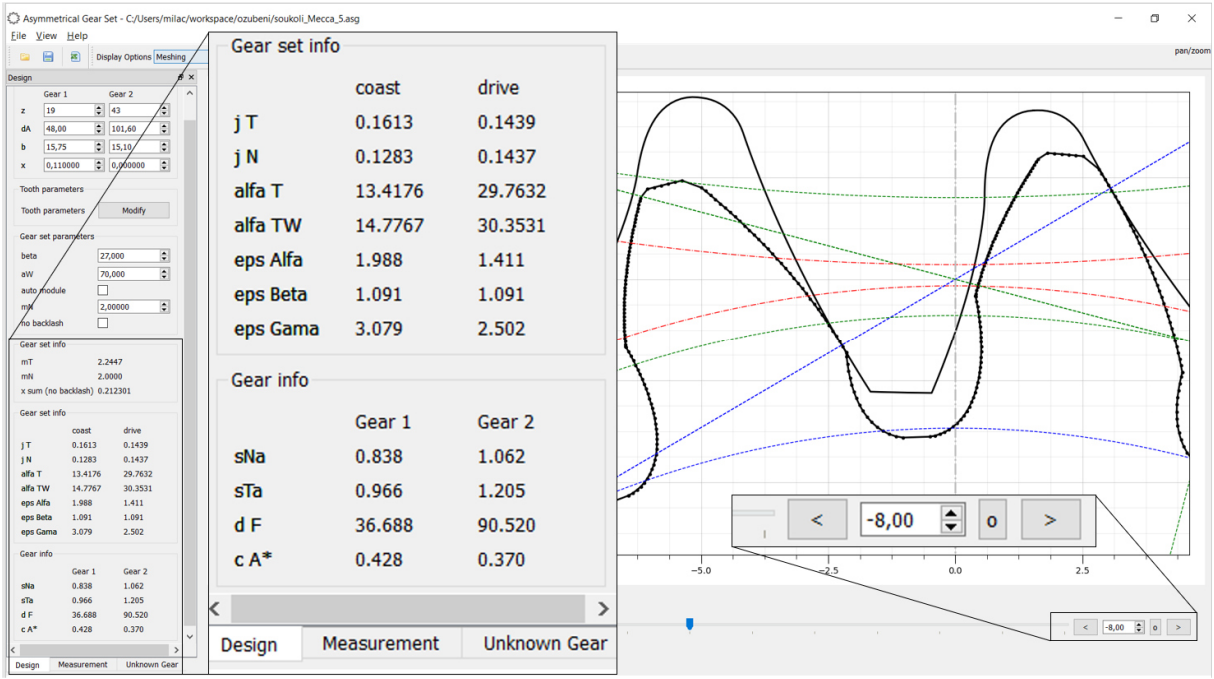

Figure 6-15: Appearance of the program including tip chamfer and protuberance – display option "Meshing". Gear 1 is depicted using interpolating spline with highlighted equidistant points.

For gearset optimizing from the perspective of qualitative properties, all necessary values are computed and depicted in the part "Gear set info" e.g. normal and tangential backlash (j_n - drive/coast), transverse contact ratio (ε_α - drive/coast), axial contact ratio (ε_β - drive/coast), total contact ratio (ε_χ - drive/coast), minimum tip thickness without chamfering (s_{na}) and relative minimum tip - root clearance (c_a* [-]), Figure 6-15.

Coordinates of tooth flank points, which are calculated analytically, don't have the same distance between each other. To assure correct depicting, these calculated points are interpolated using spline curves, whose intersections are subsequently computed. This approach is applied for

both intersections, i.e. for tip chamfer involute (α_{KP0}) and active involute (α_{P0}), and for active involute (α_{P0}) and tooth root fillet curve. Then these splines are defined by a given number of equidistant points. In some special cases there can occur a situation where active involute (α_{P0}) is shortened (cut) by an involute created by linear part of tool protuberance (α_{prP0}). Firstly, to find this intersection is numerically very problematic (unstable) and secondly, the magnitude of this phenomenon is very small. For both these reasons, this whole part of the tooth flank is neglected in this software. These equidistant points of the tooth profile are depicted for gear 1 in Figure 6-15.

The final interesting property of this program can be found in a very useful function – "kinematics". It is possible to change the angular position of the gearset, so the whole "passing through the mesh" of a gear pair or the gearwheel – rack meshing, can be observed. It can be done with arrows in the bottom-right corner, Figure 6-15. To be able to set a precise gear mesh position, it is possible to set the magnitude of rotational step (bottom-left corner of Figure 6-11) and absolute angular position of the gearset (bottom-right corner of the Figure 6-15). This function is very illustrative for students during lessons. Furthermore, tip root interference can be visually detected while rotating the gearset.

Finally, it must also be mentioned that no commonly used deviations of all important dimensions (e.g. backlash magnitude j_n or working center distance a_w) are included in the finally designed profile. Both these gear profiles are purely theoretical.

To be able to determine desired values (e.g. normal backlash j_n) including tolerances, all input values must be set to their both tolerance extremes (maximum and minimum value in the appropriate tolerance range).

6.6 Reliability Computation Method for Asymmetric Gearing

Analytically, the Hertzian stress at a single tooth contact can be computed using a standard Formula (6-34), where both osculation radii of touching bodies are known. In the case of a helical gearset, these bodies are cylinders with radii $\rho_{1,2}$.

$$\sigma_H = \sqrt{\frac{F_n}{\pi \cdot b} \cdot \frac{E}{2 \cdot (1-\nu^2)} \cdot \left(\frac{1}{\rho_1} + \frac{1}{\rho_2}\right)} \tag{6-34}$$

where:

σ_H	…	Hertzian stress
F_n	…	normal force
b	…	facewidth
E	…	Young's modulus of elasticity
ν	…	Poisson's ratio
$\rho_{1,2}$	…	osculation radii.

For involute gearing, the values of these osculation radii depend on its geometry. This case is depicted in Figure 6-16. This figure shows that these values are given, based on the involute geometry, as

$$\sigma_H = \rho_{1,2} = r_{w\,1,2} \cdot \sin \alpha_{tw} \tag{6-35}$$

where $r_{w1,2}$ … working pitch radii of both gearwheels

α_{tw} … working transverse pressure angle

This means that the contact stress can be reduced while maintaining the gearset's main dimensions only by increasing the working transverse pressure angle α_{tw}. It is also clear that these osculation radii are much larger at the drive side (blue) than at the coast side (green).

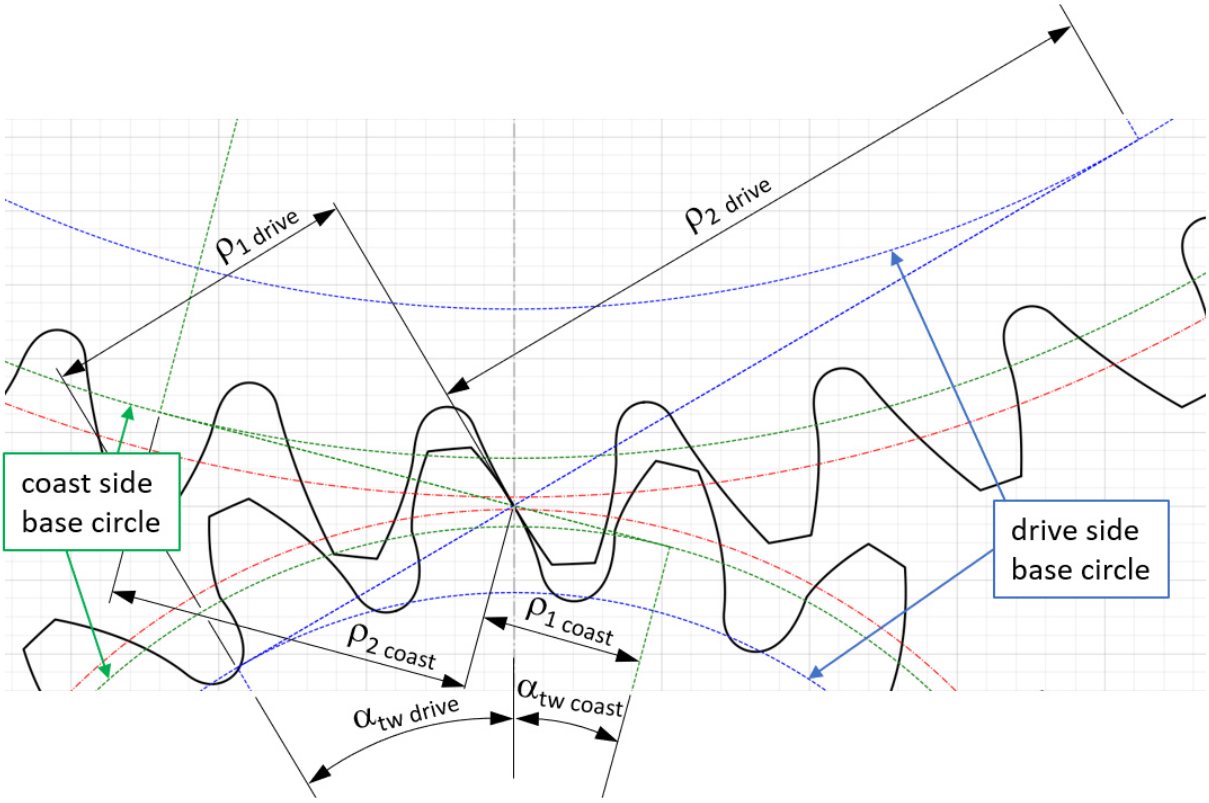

Figure 6-16: Osculation radii of involute gearset for single tooth contact in the mesh point.

Unlike for symmetric gearing, at the time when this thesis was created, no standardized method for calculation of the strength of involute gearing with an asymmetric profile existed. For this reason, FEM simulation must be firstly used for symmetric gearing. These results must be compared with the stress obtained from a standardized calculation. In this calculation are included all meshing and loading conditions using necessary coefficients (e.g. software KissSoft). By comparing both these results, recalculation coefficients are defined using Formula (6-36) for contact stresses and Formula (6-37) for root bending stresses at each gearwheel.

$$k_{H\,FEM} = \frac{\sigma_{H\,KissSoft}}{\sigma_{H\,FEM}} \tag{6-36}$$

$$k_{F\,FEM_{1,2}} = \frac{\sigma_{F\,KissSoft_{1,2}}}{\sigma_{F\,FEM_{drive\,side_{1,2}}}} \tag{6-37}$$

These coefficients are then used for backward recalculation of FEM results of asymmetric gearing to be comparable with symmetric gearing results.

The Figure 6-17 depicts an example of gearset FEM analysis. It's a comparison of symmetric and asymmetric variants of a gearset. The decrease in the contact pressure by the same load (torque)

for the asymmetric variant is approx. 9.3%. Text with values of maximum stresses (von Mises [GPa]) are enlarged to be readable.

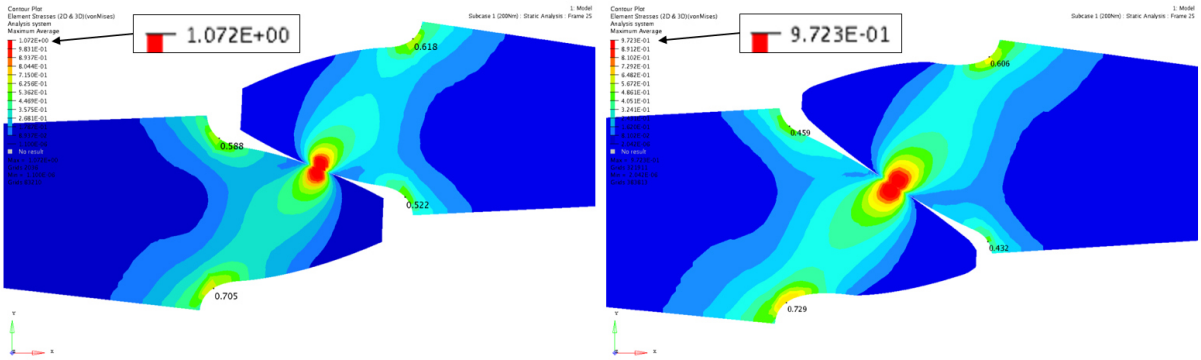

Figure 6-17: Example of FEM analysis of symmetric and asymmetric gearing, both profiles were designed using developed program.

On the other hand, asymmetric profile (higher pressure angle) also has one negative consequence - the increase in radial forces, which cause higher loading at bearings.

The method of strength calculation for gears with asymmetric profile was published in [42].

6.7 Selection of Asymmetric Gearing Profile Parameters

In this state the tool for designing of the gearing with an asymmetric profile was prepared. The question was - what exact values of parameters determining the profile should be set. One of the most important parameters is the profile angle α_n on both tooth flanks.

As input data for the profile determination the loading spectrum for 6th speed was measured at the testing circuit. The drive flank was loaded while driving the car by the ICE, the coast flank is loaded only by braking by the ICE. Resulting values of equivalent torques are stated in Table 6-2.

Tooth side (flank)	drive	coast
Equivalent torque [Nm]	195,32	62,99
Cycles [-]	50 237 000	5 530 000

Table 6-2: Table of loading conditions on both tooth sides

According to the methodic used in [25] with the condition of the same safety against pitting at both sides using Life factor Z_{NT} can be determined the asymmetry ratio. This means that the drive angle is chosen, and the coast angle is according to this methodology calculated. For example, for 25° at the drive side, results the value of 3,5° at the coast side for given loading conditions. This value is really small and leads to large undercut. But from the point of view of flank safety it is correct. For this reason, this value of the coast angle can be taken only as the smallest possible value. By increasing this coast angle value, also the safety against pitting on the coast flank increases.

The target while the profile angles choice was to reach as high asymmetry ratio as possible to highlight the advantage of the asymmetric profile in the resistance against pitting. Of course, some limitations had to be observed. Firstly, no undercut was allowed. Next crucial condition was to assure minimal normal tip (addendum) thickness s_{na}* due to heat treatment, which was approximately 0,4*m_n. The target was also to keep the backlash at the same value as at the original gearset and total contact ratio ε_χ approximately at the value 3,05 to assure smooth running.

The tip edge should be chamfered with the height of 0,2 mm by additional angle of 20°. This operation should be done to avoid tip interference. Negative impact of this operation is in shortening of the active tooth flank, which leads to decreasing the transverse contact ratio ε_α. For this reason, the tip diameter d_a used for this calculation was smaller by 0,4 mm.

Next chamfering should be done on the side edges. On each side this side chamfering takes 0,3 mm which leads to reducing of the active facewidth by 0,6 mm. This issue was also considered while the overlap ratio ε_β calculation. The appearance of the final gearing's shape is depicted in Figure 6-18.

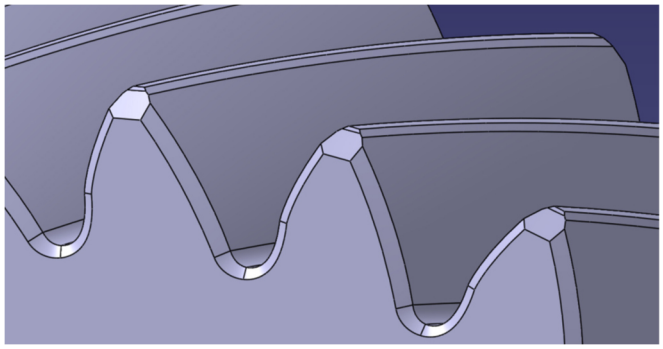

Figure 6-18: Appearance of the designed gearing considering the tip and side chamfering.

Regarding the backlash, in working position drive flanks are in the contact, so the backlash appears between coast flanks. For this reason, the more important backlash value, considered while designing, is the one on the coast side.

In the next step three gearset's geometries were designed and one of them was selected to be produced. These variants are described in the Table 6-3. Due to the confidentiality purposes only some data of the original symmetric gearing can be published in this thesis.

Variant of 6th speed	original	A	B	C
z_1 / z_2	48/31	48/31	48/31	48/31
Tip diameter d_{a1} / d_{a2} [mm]	-	82,6 / 54,9	82,6 / 54,8	82,6 / 54,8
Rack profile angles α_n [°] drive/coast	symmetric	**30/10**	**29/11**	**28/11**
Helix angle β [°]	-	33	33	33
profile shift coefficient gear 1 / gear 2	-	-0,106 / 0,030	-0,102 / 0,026	-0,100 / 0,023
Normal module m_n [mm]	-	1,38	1,38	1,38
Addendum height of the rack h_{aP0} [mm]	-	2,2	2,2	2,2
Addendum radius of the rack ρ_{aP0} [mm]	-	max. 0,35978 used 0,35	max. 0,36832 used 0,36	max. 0,40016 used 0,4
normal backlash (coast) j_n [mm]	0,068	0,068	0,068	0,068
ε_α with tip chamfering (transverse, drive)	1,565	1,319	1,315	1,332
ε_β with side chamfering (overlap)	1,734	1,734	1,734	1,734
ε_χ with chamfering (total)	3,298	3,052	3,049	3,066
min. tip thickness without chamfering s_{na} [mm]	-	0,474 (gear2)	0,541 (gear2)	0,579 (gear2)
min. tip thickness without chamfering s_{na}* [-]	-	0,343	0,392	0,420
minimal tip - root clearance c_a* [-]	-	0,256	0,260	0,263
recalculated contact pressure [MPa]	**1131**	**965**	**971**	**978**
recalculated root stress (σ1) gear1/gear2 [MPa]	**608** / 578	449 / **480**	457 / **485**	459 / **492**

Table 6-3: Parameters of the original and three proposed asymmetric gearset variants.

Very important for the final variant choice was the stress comparison. All profile variants were generated in newly created software (including original symmetric one). The geometry data (coordinates) were exported as text file to **MS Excel**, subsequently imported into **CATIA** using a "Design table". Here were these points interpolated using a spline function and exported as *.stp file. In this format the geometry was imported to the software **Hypermesh** and **Optistruct**.

The transversal gear profile is in Catia only purely drawn along the helix so at this 3D model there are **no modifications**! For this reason, it was meaningless to make FEM analysis in 3D, the stress distribution doesn't correspond to reality.

Other option was to use the 2D geometry and simply enter it into 3D for 1 mm as a spur gearing. The loading torque (200 Nm) applied at this thin slice was then divided by the width of the

gearset's thinner gear. An example of this computation is depicted in Figure 6-19 for contact stress and in Figure 6-20 for root bending stresses.

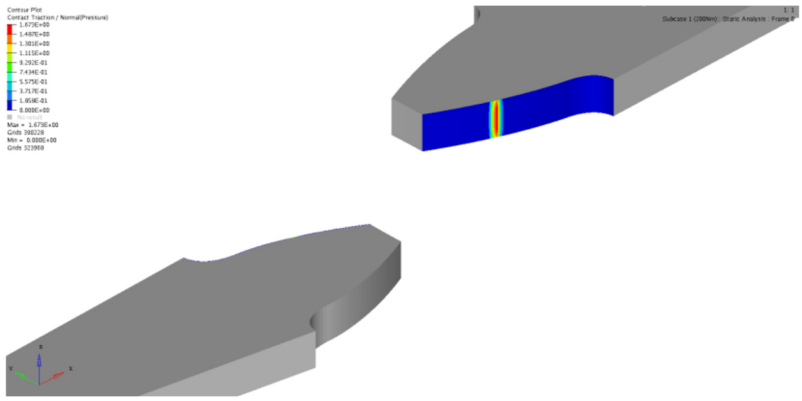

Figure 6-19: FEM contact analysis of the original symmetric gearing

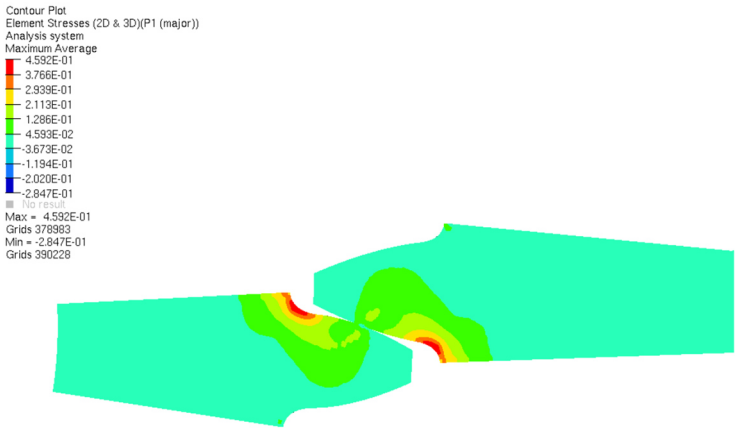

Figure 6-20: FEM root bending analysis of the original symmetric gearing

The same symmetric gearset was also computed in KissSoft. Obtained stress values from this computation include complete geometry (helix angle) and all standard stress and durability requisites, i.e., material properties and all necessary coefficients describing the geometric and loading conditions in the mesh according to the standard DIN 3990.

By comparing both these results (KissSoft, FEM), the recalculation coefficients can be defined according to Formula (6-36) for contact stress and using Formula (6-37) for root bending stress at each gearwheel. All these stress values are stated in Table 6-4.

Gearing Strength [MPa]	KissSoft (DIN 3990)		FEM (Optistruct)		k_{FEM}	
	gear1 z=48	gear2 z=31	gear1 z=48	gear2 z=31	gear1 z=48	gear2 z=31
Sigma H	1131,24		1401		**0,807452**	
Sigma F	607,91	577,73	443,1	459,2	**1,371948**	**1,258123**

Table 6-4: Comparison of bending and contact stresses at original (symmetric) gearing of 6^{th} speed.

Using these coefficients were recalculated stresses obtained from the FEM analysis of all asymmetric variants. These recalculated stresses are stated in the lower part of the Table 6-3.

By usage of an asymmetric profile the significant decrease of the contact stress is obvious (153 - 166 MPa). The same holds true also for the bending stresses. On the gear 1 (z=48) the decrease is larger (149 – 159 MPa), on the gear 2 (z=31) the decrease is smaller (86 – 98 MPa). The differences between all three asymmetric variants are very small.

From the point of view of the contact and root stresses, the variant A (30/10) would be the best choice. On contrary, from the point of view of the manufacturing (rolling) technology, the variant without undercut would be the best choice. This depends mainly on the coast profile angle, which is the same (11°) for the variant B and C. Final variant choice was a compromise between these two conditions, the variant B (29/11°).

6.8 Asymmetric Profile Adjusting

As it was already mentioned, the profile generated using this newly developed software supposes, that the gearing will be manufactured by chip forming using rolling milling cutter or grinding. For this type of technology, the undercut is no problem. But the gearing described in this thesis, should be in the first step ground (macrogeometry) and afterwards the surface should be densified using rolling. For this reason, the undercut and standard tip chamfer, e.g. depicted in Figure 6-15 is not allowed and the final transverse profile had to be adjusted to be rollable. This was accomplished by the specialist in the field of the rolling technology – the company Profiroll Technologies. These profile changes are depicted in Figure 6-21 and Figure 6-22.

After this profile change should be standardly performed next FEM analysis with new modified profiles. Regarding the contact stress, there is no change, because the geometry in contact points hasn’t been changed. In case of the root stresses, the change is very small (hundredths of a millimeter) and furthermore, the material in the root has been added, not removed. This profile change has positive impact (decrease) on the root stresses.

For these two reasons, FEM analysis wasn’t performed once again. The only operation performed with modified profiles, was the interference check performed visually in Catia while passing through the mesh.

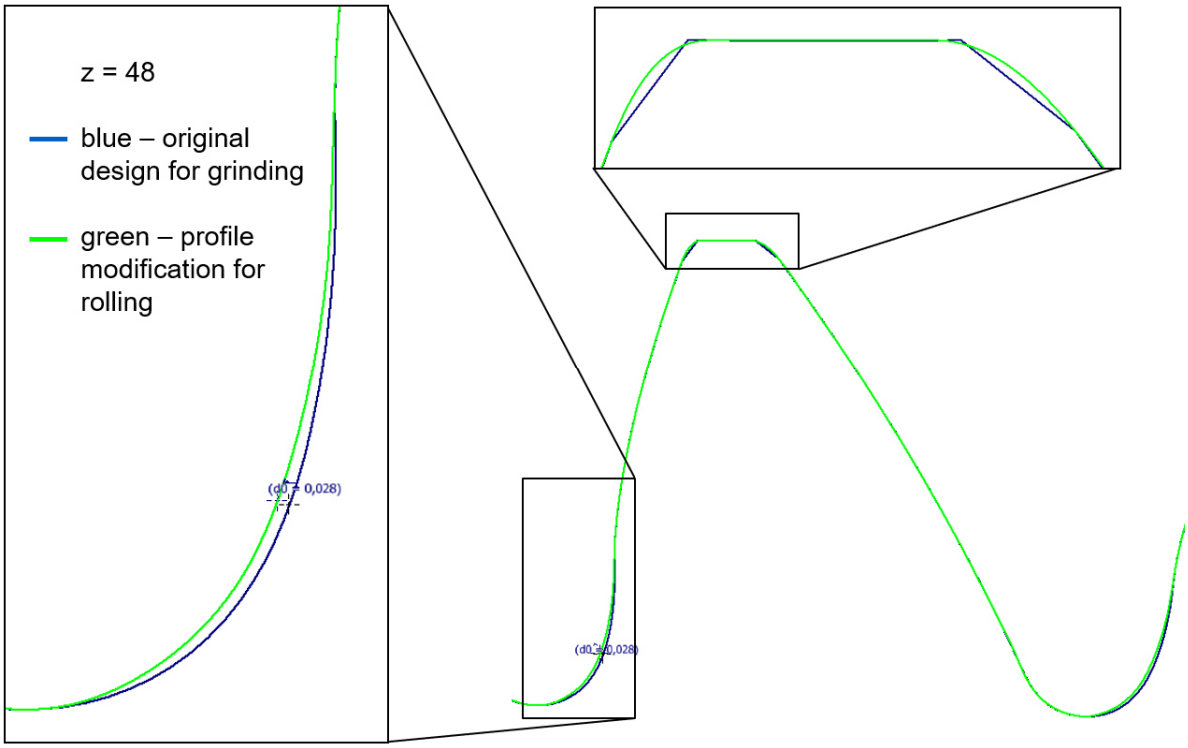

Figure 6-21: Profile modification to enable rolling technology application – gear1, z=48

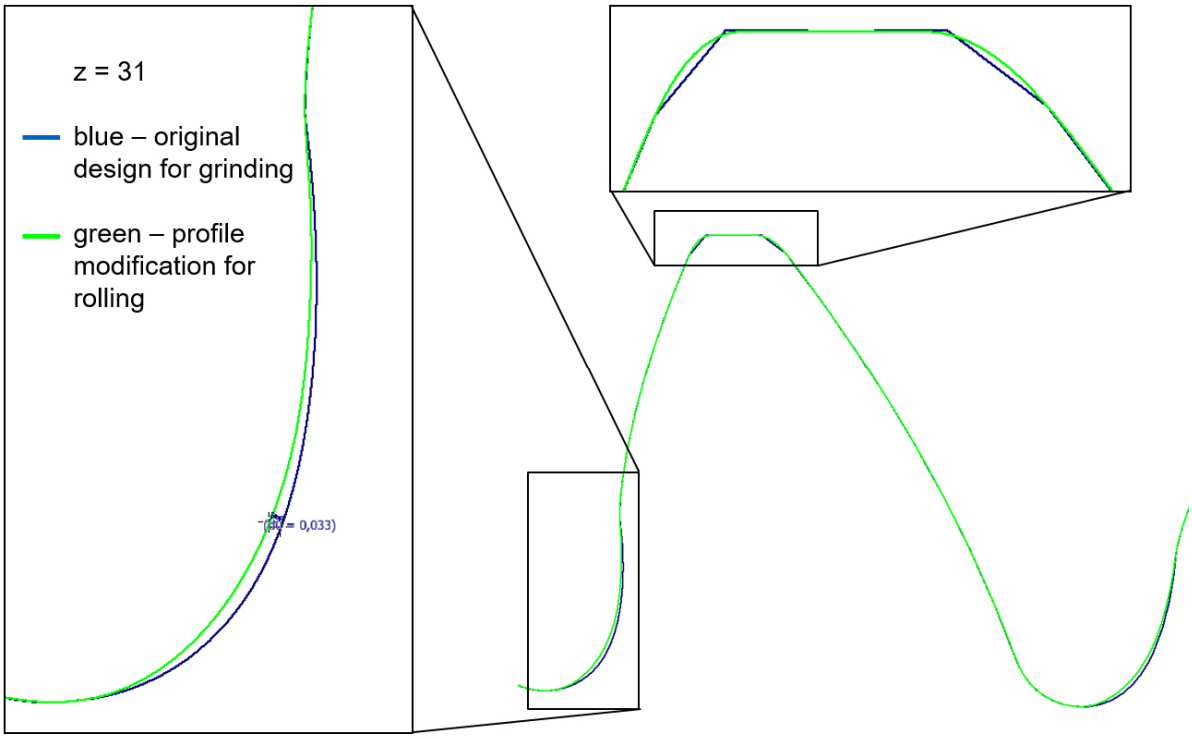

Figure 6-22: Profile modification to enable rolling technology application – gear2, z=31

6.9 Microgeometry Design Proposal

After designing the gear profiles macrogeometry, the problem of the modifications (microgeometry) had to be solved. For this purpose, the software **MDesign – module LVR** was used. This software computes shaft deformations and subsequently creates stress distribution diagrams over the tooth flank. Unfortunately, in this software the asymmetric gearing cannot be simulated. For this reason, each tooth side was simulated separately as symmetric profile with appropriate value of profile angle. In case of the coast flak it wasn't problem. The problem arose with the drive flank, because there was a limitation regarding the tip tooth thickness. It wasn't possible to create symmetric profile with the profile angle of 29° with desired addendum height. For this reason, this addendum height was used as large as possible, until the tip thickness equaled to zero (s_{ta} = 0). Because this was a preliminary proposal, this approach was sufficient.

As an input to this software was used the model of the gearbox including the shafts geometry, Figure 6-23. By this simulation the gearbox casting and bearings are ideally stiff (no deformations). Results from this simulation are expected diagrams of the load distribution as results of contact pattern test. Example of this predicted load distribution is depicted in Figure 6-24.

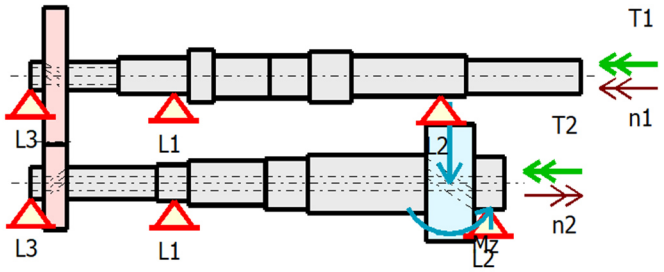

Figure 6-23: Internal gearbox arrangement including bearings and tested gearset loading

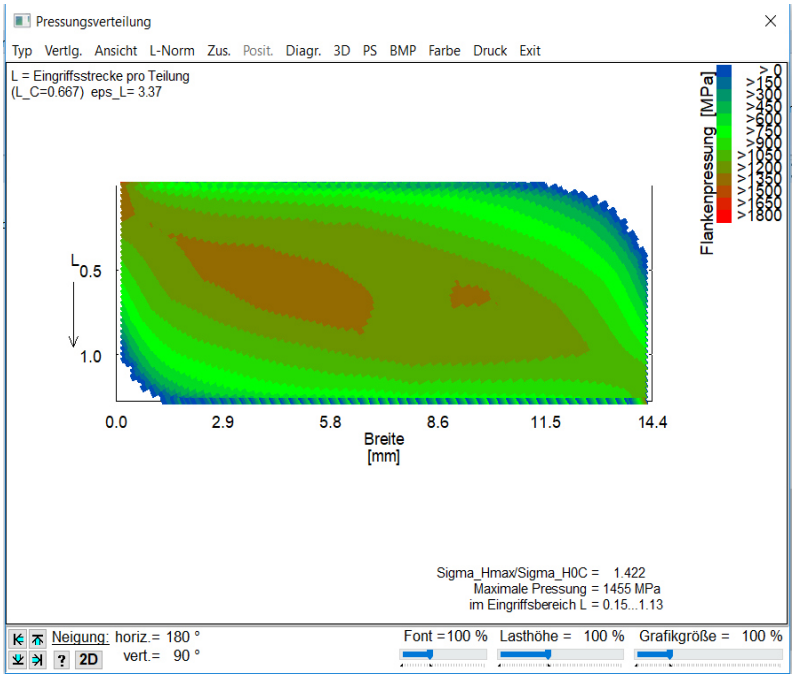

Figure 6-24: Result of the load distribution simulation performed in software MDesign – module LVR

Final parameters of the tooth flank's microgeometry are the crowning magnitude and lead and profile modifications. These values are listed in Table 6-5.

modification values are in [μm]		z = 48		z = 31	
		drive (29°)	coast (11°)	drive (29°)	coast (11°)
Profile modification	$f_{H\alpha}$	0	0	-8	5
	c_a	10	2	10	2
Lead modification	$f_{H\beta}$	20	5	0	0
	c_b	10	2	10	2
Positive value of profile modification $f_{H\alpha}$ decreases profile angle α_n Positive value of lead modification $f_{H\beta}$ increases helix angle β					

Table 6-5: Values of tooth flank modification magnitudes (microgeometry)

7 Tested Gear Selection

This dissertation thesis is a result of the common project of CTU in Prague, Swedish company Höganäs AB – an expert in the field of PM technology, German company Profiroll Technologies GmbH – an expert in rolling technology and a car producer.

The target of this project is to replace the gearset in an automotive gearbox with its variant made by PM technology and investigate its endurance properties while testing at the special test bench in the laboratories of the CTU in Prague.

Within this project, two gearsets should be tested. The choice was limited by their geometry and usage. Firstly - both the gearwheels had to be dismountable from the shafts, and secondly, they had to be well accessible – to be able to make visual inspection during testing. Finally, the selected speed had to be very often used while driving – to get significant results. For these reasons, the 3rd and 6th speeds were selected. The 3rd speed it is very often used during acceleration and uphill ride, the 6th speed is then mostly used at highways. Both these gearsets are depicted in Figure 7-1.

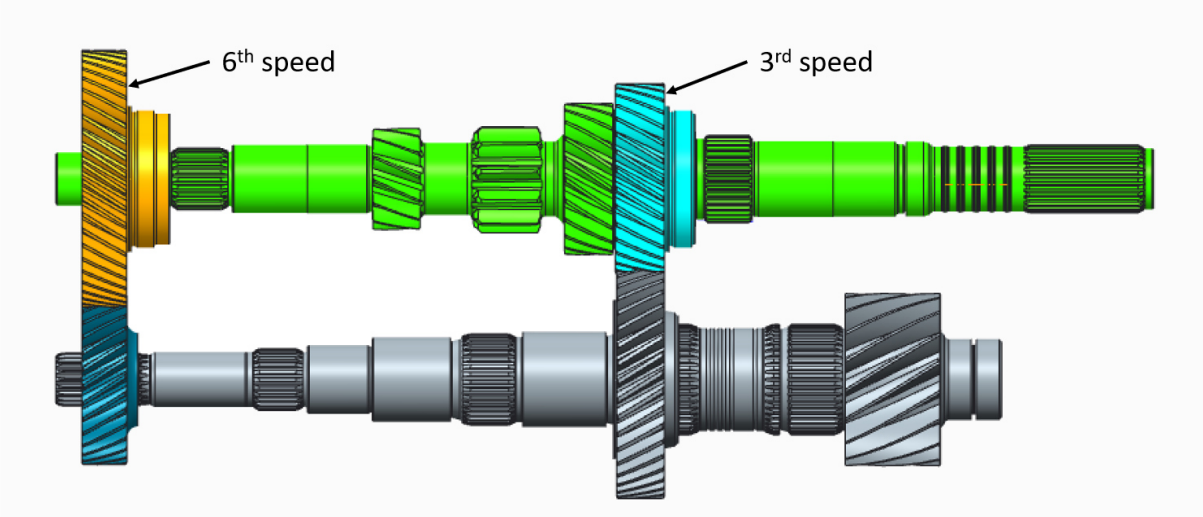

Figure 7-1: Two selected gearsets to be replaced with the gearsets made from the PM material instead of standard wrought steel.

At both gearsets another PM technology was used. In case of the 3rd speed the original symmetric geometry was maintained, the surface densification was performed by HIP technology by the company Höganäs AB. In case of the 6th speed the approach was different. The gearing geometry was changed to asymmetric one and the surface densification was performed by rolling technology by the company Profiroll Technologies GmbH. Detailed description of both these partial projects follows in next chapters.

7.1 HIP Project Description

This whole project was created in cooperation with the Swedish company Höganäs AB, which is one of the leaders in the PM technology field. In general, PM gears are being tested at back-to-back rigs according to FZG test method directly in this company. The target of this project was to perform dynamic test of PM gears directly in the car. For this reason, our next partner is a car manufacturer who had provided all necessary technology for manufacturing, assembling

(disassembling) and measuring of gearwheels during all performed endurance tests. Because such "in car" driving test is very expensive, we have decided to start with a constant load level test to verify the material potential. Next dynamic tests should follow. To be as close as possible to real condition in automotive gearbox, special back-to-back test rig, which is located in laboratories of CTU in Prague, was an ideal device for such testing. This test was performed on two gearsets for each speed stage (3rd and 6th).

7.1.1 PM Material Determination

The exact PM material and its heat treatment was determined by the company Höganäs AB. For all PM gearwheels in this investigation the material was **Astaloy® 85Mo** with additional application of **HIP technology**, which was performed by the company Bodycote in Sweden. Detailed HIP process parameters were:

temperature:	1130 - 1160°C
pressure:	100 MPa
holding time:	min. 3 hours
inert gas:	argon
HIP type:	in a capsule

Before HIP:ing (after sintering) the pucks density was around 7,25 g/ccm, after HIP:ing it has increased to 7,85 g/ccm (full density) in the whole part. The capsule serves as a prevention against the gas entering the part's body voids between its particles.

The assumption of the test results is that HIP:ed PM gears will have approximate strength (resistance against pitting) as gears manufactured conventionally from wrought steel.

7.1.2 HIP:ed Gears Manufacturing Process

In general, in the mass production PM parts are compacted in a final shape and afterwards they are sintered. In this case we have assumed to produce 10 gearsets for each speed. For such a small number of pieces, the compaction die and the appropriate press tool with final gearwheel shape would be too expensive. For this reason, instead of the final shape gearwheels were compacted only PM pucks, which were sintered and HIP:ed and roughly turned – Figure 7-2.

Figure 7-2: Semi-finished blanks – sintered, HIP:ed and turned PM pucks.

The parameters of these blanks sintering process were 1120°C for 45 minutes. These PM pucks were subsequently turned to a rough shape, the gearing was milled and the internal splines was machined – Figure 7-3.

Figure 7-3: Turned basic gear shape with milled gearing and machined splines (3rd speed).

With these gearwheels was then performed a heat treatment - case hardening of the gearing by Höganäs AB, Figure 7-4. Its parameters were 920°C for 130 minutes with a carbon potential of 0.95%. Then followed the tempering at 180°C for 120 minutes.

Figure 7-4: Gearset of the 3rd speed after the heat treatment.

Afterwards, the gearing was ground to a final shape (microgeometry – crowning, etc.) and prepared for synchroring welding. Gears in this manufacturing stage are depicted in Figure 7-5.

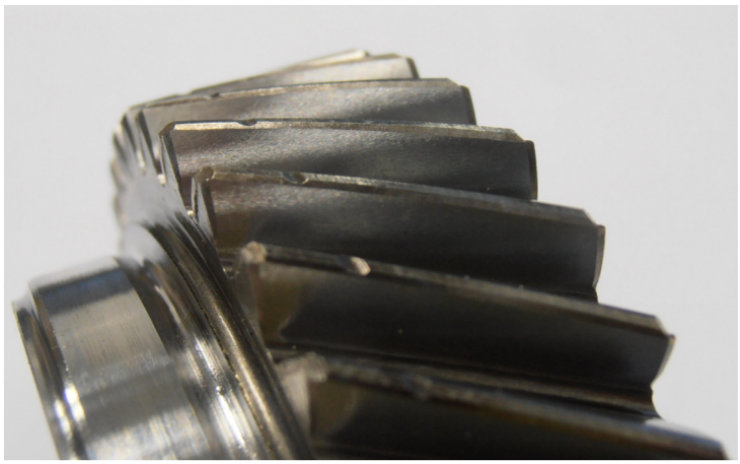

Figure 7-5: Final ground gearing and preparation for the synchroring welding (3rd speed).

Next step was the synchroring welding, performed by Höganäs AB. After this operation the gearwheel of the 6th speed is depicted in Figure 7-6.

Figure 7-6: Welded synchroring to a gearwheel (6th speed).

To be able to check the weld quality, one of the gearwheels had to be damaged – cut, Figure 7-7. The section was polished for investigation in light optical microscope (LOM) – Figure 7-8. As can be seen, the welding operation was successful.

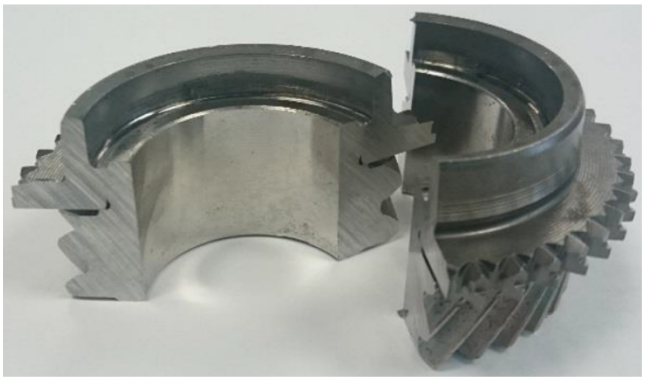

Figure 7-7: Section for checking the weld quality between the synchroring and PM gearwheel (3rd speed)

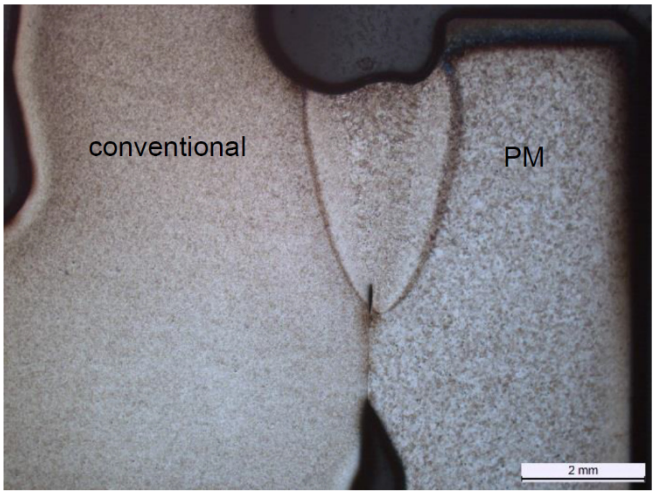

Figure 7-8: Detail of the weld between the synchroring from conventional steel and the PM gearwheel (3rd speed)

The last operation was the grinding of the inner diameter (for needle bearings) and grinding of the conical synchronizing surface. In this state gearsets were finally ready to be measured and tested.

For this project, the target was to test more gearwheels to be able to repeat the test for results verifying. We started with a number of 10 pieces for each gearset. During the production some parts had to be destroyed, e.g. while checking the synchroring weld quality. Finally, we had for each speed stage 6 gearsets ready for testing.

7.1.3 Stress Comparison between PM HIP:ed and Standard Gears

The geometry of tested gearing and loading conditions are “identical” – if all standard deviations which appear during standard mass production of gearwheels are neglected. So, the difference lies only in gearwheels material. It is possible to provide a stress calculation in the software KissSoft. In the material library there is already an option to choose the material “ASTALOY 85Mo, Dry powdered metal, case-hardened by Höganäs AB, Sweden”. But for this material additional HIP technology is not considered for the calculation. For this reason, this calculation is meaningless.

Since HIP:ing produces a pore free material, the elastic properties will be the same as for wrought steel. For this reason, also stresses will be the same as for the reference original gears.

7.1.4 HIP:ed Gears Test Results – 3rd Speed

During tests performed in laboratory at CTU in Prague there were used accelerometers applied on the gearbox casing. Thanks to this fact there could be observed the RMS and FFT of their signals for failure detection. This works great e.g. for bearing failure detection where acceleration signal RMS increase is significant and well detectable in FFT. But in case of pitting detection this method is not sufficient. For this reason, pitting had to be inspected optically after certain number of hours directly in the gearbox using a videoscope with low resolution. For this reason, the quality of the figures is quite poor. But for pitting detection it was enough.

Before each endurance test of PM HIP:ed gearset the contact pattern test was performed to depict real load distribution in the gearing’s mesh. The results of both these summative contact pattern tests for the 3rd speed sets are depicted in Figure 7-9 and Figure 7-10. In case of the serial gearsets these weren’t performed.

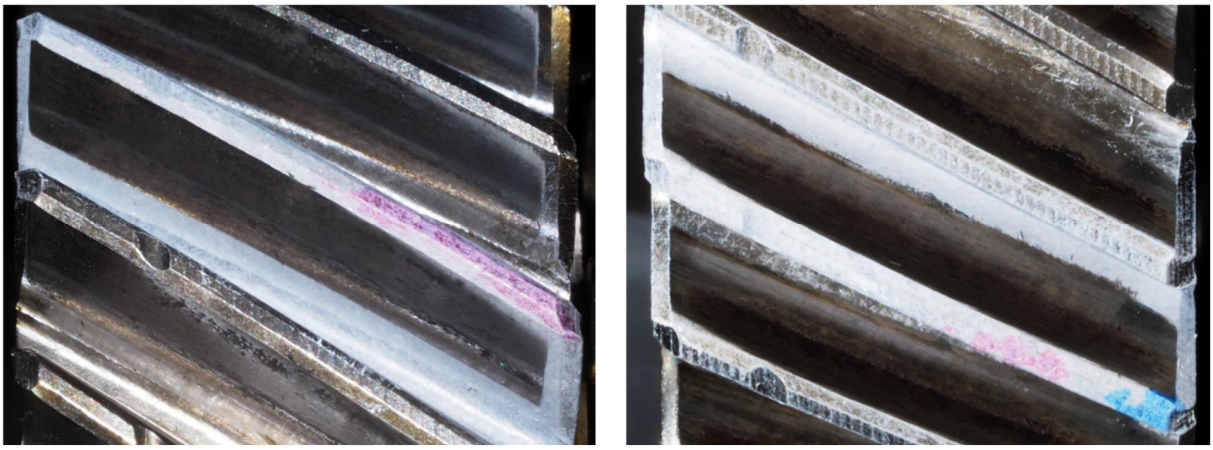

Figure 7-9: Result of the PM HIP:ed gears summative contact pattern test (3rd speed) by nominal test load (torque), gearset 1, gear 1 (z=32, left), gear 2 (z=41, right)

Figure 7-10: Result of the PM HIP:ed gears summative contact pattern test (3rd speed) by nominal test load (torque), gearset 2, gear 1 (z=32, left), gear 2 (z=41, right)

As a starting point it was necessary to have some reference test results. For this reason, there were performed identical endurance tests with serial gearing for both speed stages. In case of the 3rd speed three gearsets were tested. Afterwards two PM HIP:ed gearset tests followed. Test results (number of hours until pitting detection) for the 3rd speed are stated in Table 7-1 and are graphically depicted using a bar diagram in Figure 7-11.

gearset number	hours until pitting	
	serial	PM HIP:ed
1	43	115
2	28	100
3	135	-
arithmetic mean	68,7	107,5

Table 7-1: Test results of the 3rd speed - serial and PM HIP:ed gearsets – hours until pitting

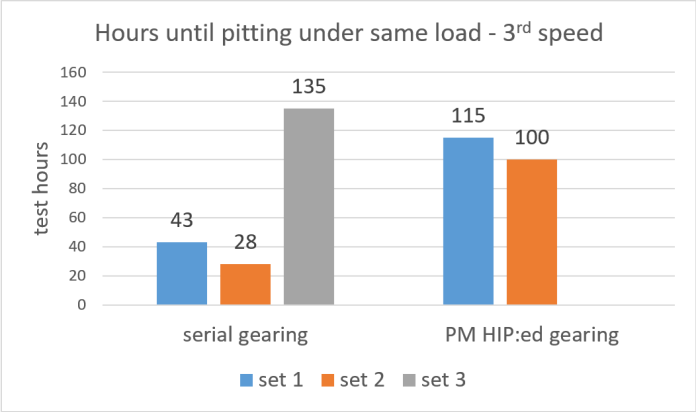

Figure 7-11: Test results of the 3rd speed - serial and PM HIP:ed gearsets – hours until pitting.

The appearance of pits on gearwheel's flanks after certain number of testing hours is depicted in following figures. In case of the serial gearsets only the first one is depicted due to similarity – Figure 7-12.

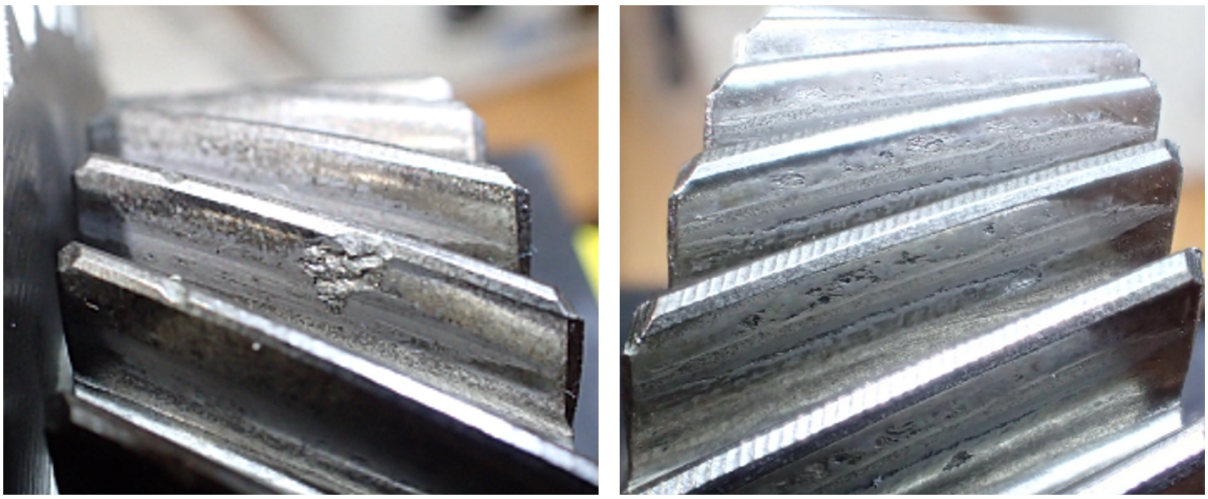

Figure 7-12: Pitting on serial gearwheels (pinion left) of 3rd speed – gearset 1 - after 52 hours. Pitting was detected already after 43 hours.

In the Figure 7-13 is depicted the pitting, which was observed after 115 testing hours directly in the gearbox using a videoscope.

Figure 7-13: Pitting on PM HIP:ed gearwheel (3rd speed pinion) – gearset 1 - after 115 hours

After observing the pitting on the PM HIP:ed gearset there was a question how long can such PM gearset work. For this reason, test continued and was stopped after 412 hours because of another issue in the gearbox. The aim of the test continuing after the pitting has appeared, was to verify whether the tooth breakage occurs. Gearset appearance after this number of hours is depicted in Figure 7-14, when the gears were removed from the gearbox. There is pitting almost on all teeth. The gearbox was already quite noisy but still in working order.

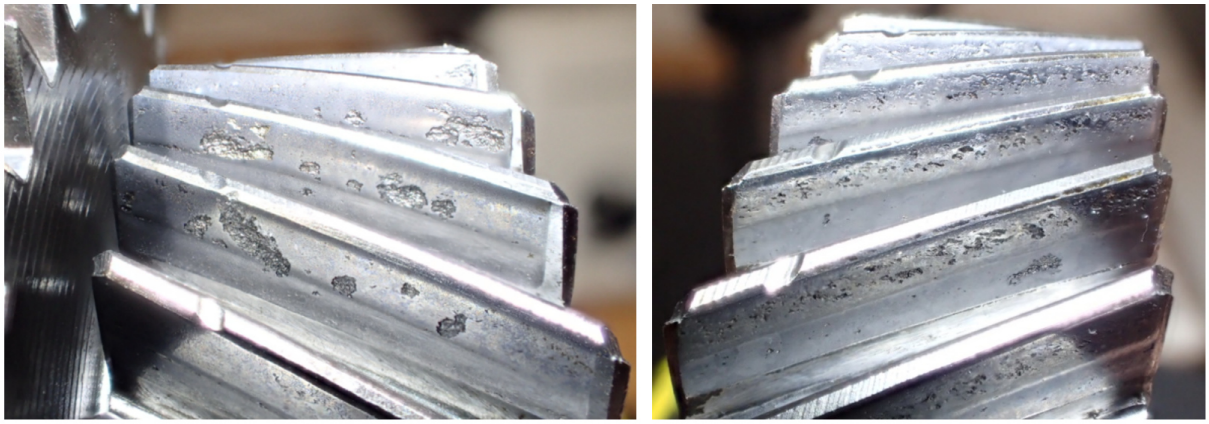

Figure 7-14: Pitting on PM HIP:ed gearset 1 of 3rd speed (pinion left) - after 412 hours. Pitting has been detected already after 115 hours (Figure 7-13).

Figure 7-15: Pitting on PM HIP:ed gearwheel (3rd speed pinion) – gearset 2 - after 100 hours

In case of the second PM HIP:ed gearset the pitting was detected directly in the gearbox using a videoscope after 100 test hours (Figure 7-15) and the test was stopped after 217 hours (Figure 7-16).

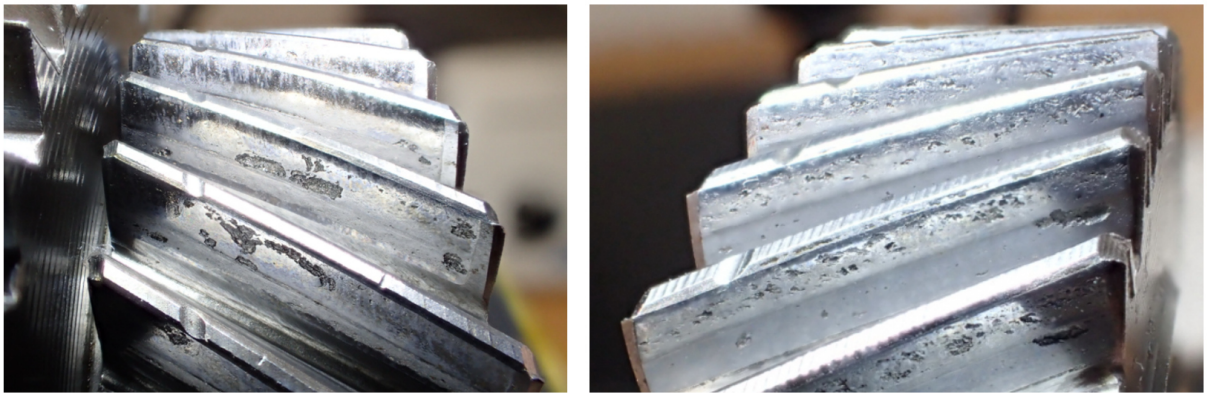

Figure 7-16: Pitting on PM HIP:ed gearset 2 of 3rd speed (pinion left) - after 217 hours. Pitting has been detected already after 100 hours (Figure 7-15).

In both cases the position of initial pitting (Figure 7-13, Figure 7-15) corresponds to the contact pattern test result (Figure 7-9), where it is visible, that higher load is not in the middle of the gear's facewidth but slightly shifted to the left side - to the synchroring.

7.1.5 HIP:ed Gears Test Results – 6th Speed

In this chapter the test of the 6th speed is described. As in the case of 3rd speed – comparative test with serial gearing was performed. After the pitting detection the gearset was replaced with another one, to get more results. In this case pitting occurred 6 times. Results of these tests are stated in Table 7-2 and are graphically depicted using a bar diagram in Figure 7-19. Afterwards, two tests with PM HIP:ed gearsets were performed. Firstly, there are depicted results of the contact pattern tests performed before testing for both tested gearsets, Figure 7-17 and Figure 7-18.

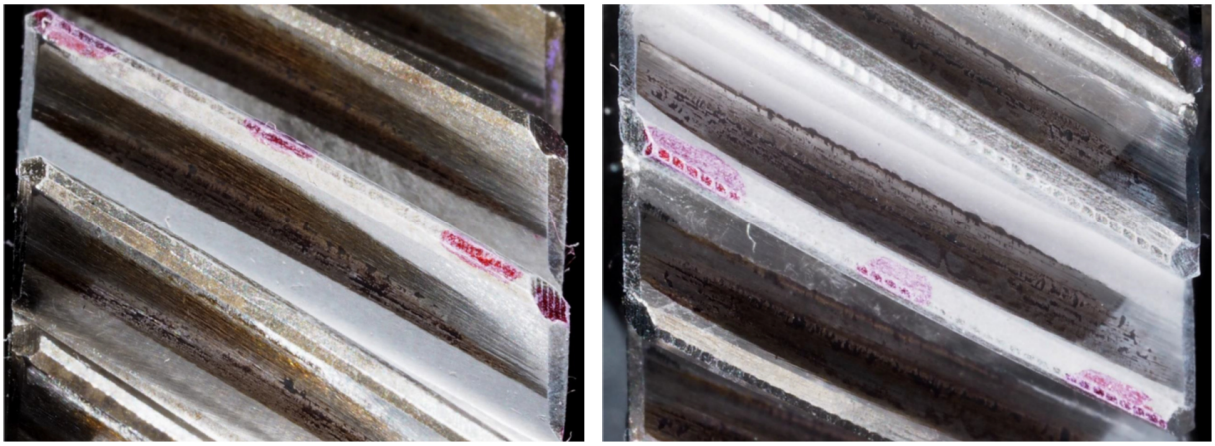

Figure 7-17: Result of the PM HIP:ed gears summative contact pattern test (6th speed) by nominal test load (torque), gearset 1, gear 1 (z=48, left), gear 2 (z=31, right)

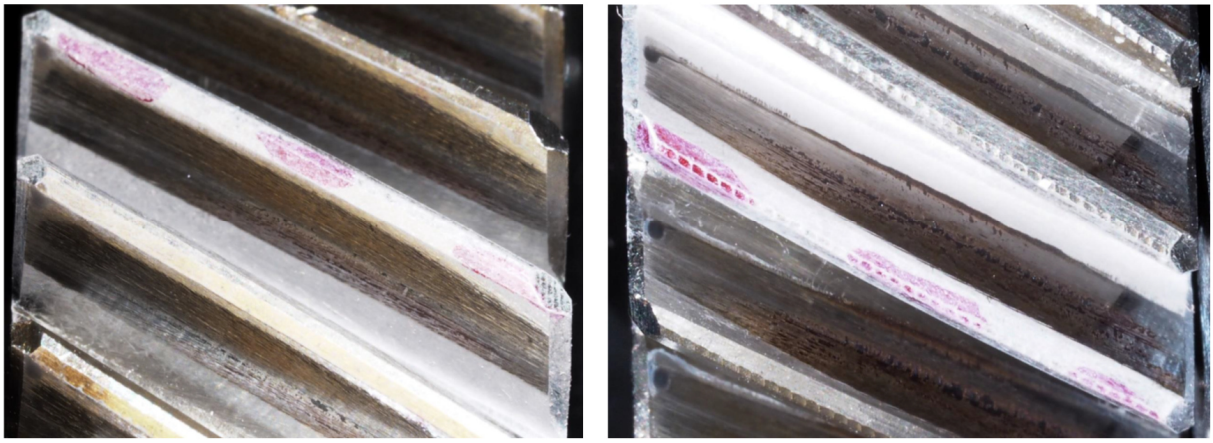

Figure 7-18: Result of the PM HIP:ed gears summative contact pattern test (6th speed) by nominal test load (torque), gearset 2, gear 1 (z=48, left), gear 2 (z=31, right)

Gearset Number	Hours until Pitting	
	serial	PM HIP:ed
1	60	85
2	62	41
3	30	
4	30	
5	34	
6	29	
7	34	-
arithmetic mean	39,9	63

Table 7-2: Test results of the 6th speed - serial and PM HIP:ed gearsets – hours until pitting

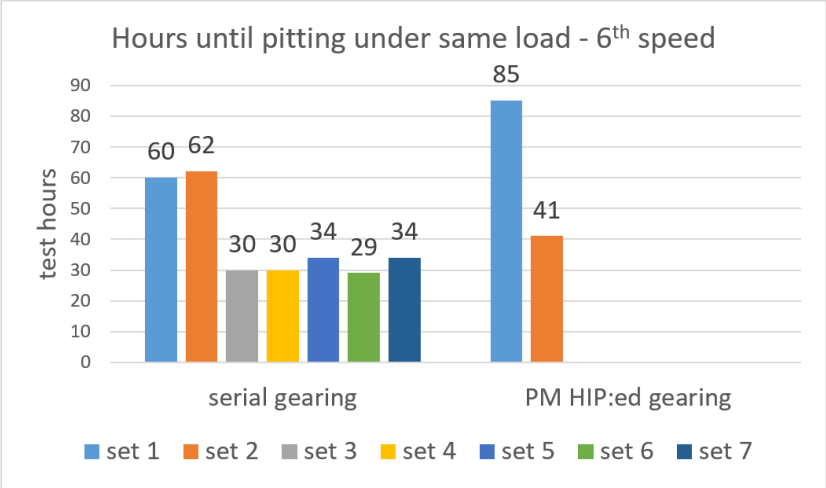

Figure 7-19: Test results of the 6th speed - serial and PM HIP:ed gearsets – hours until pitting

An example of the serial comparative test result there is depicted in the Figure 7-20. In this case of the gearset 1, the pitting was detected after 60 hours.

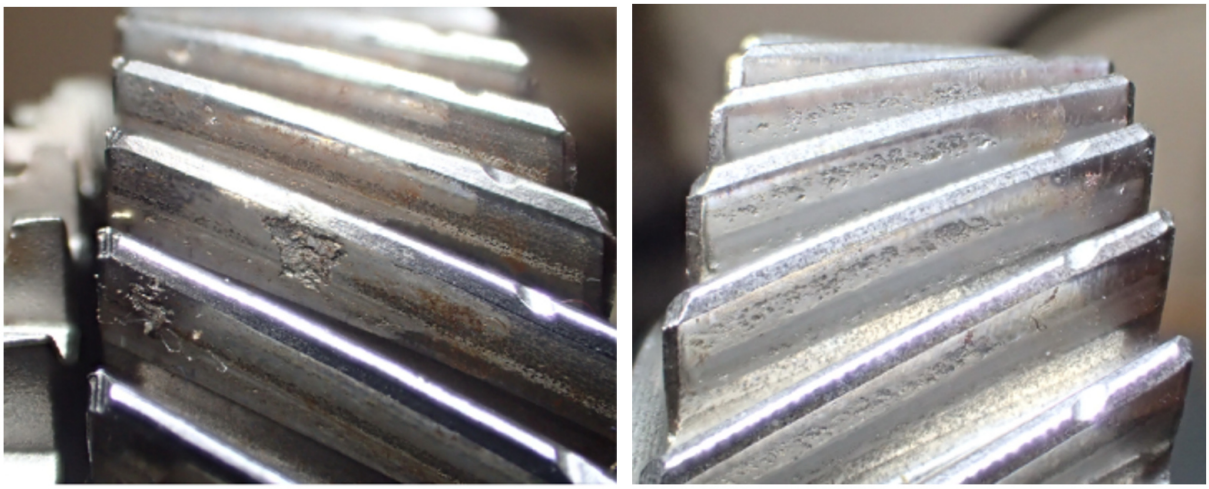

Figure 7-20: Pitting on serial gearwheels (pinion left) of 6th speed – gearset 1 - after 60 hours.

In Figure 7-21 there is depicted pitting on the first PM HIP:ed gearset, which was detected directly in the gearbox using a videoscope after 85 testing hours. Afterwards the test continued in the same way as for 3rd speed to prevent the tooth breakage. Finally, this test was stopped after 217 hours. Its appearance after this number of hours is depicted in Figure 7-22.

Figure 7-21: Pitting on PM HIP:ed gearwheel (6th speed) – gearset 1 - after 85 hours

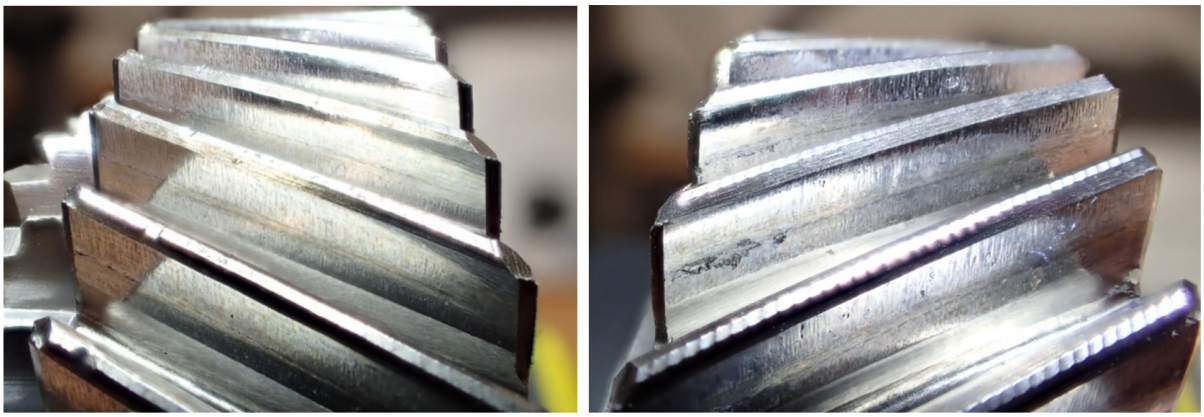

Figure 7-22: Pitting on PM HIP:ed gearset 1 of 6th speed (pinion left) - after 217 hours. Pitting has been detected already after 85 hours (Figure 7-21).

Next test was performed with the second gearset. In Figure 7-23 is depicted the pitting on this second PM HIP:ed gearset, which was detected directly in the gearbox using a videoscope already after 41 test hours. Afterwards, the test continued and was stopped after reaching 213 hours. Both gearwheels after this number of testing hours are depicted in Figure 7-24.

Figure 7-23: Pitting on PM HIP:ed gearwheel (6th speed) – gearset 2 - after 41 hours

Figure 7-24: Pitting on PM HIP:ed gearset 2 of 6th speed (pinion left) - after 213 hours. Pitting has been detected already after 41 hours (Figure 7-23).

Again, as in case of the 3rd speed, for both gearsets the position of initial pitting (Figure 7-21, Figure 7-23) is located slightly to the left side of the gear's facewidth, which corresponds to the contact pattern test result (Figure 7-17), where can be observed, that higher load is not in the middle of the gear's facewidth but also slightly shifted to the gear's left side.

7.1.6 PM HIP:ed Gears Test Conclusion

In laboratories of CTU in Prague were performed test of gearsets made from PM HIP:ed material. In this case its natural porosity was eliminated by technological operation called “Hot Isostatic Pressing”. Tests were performed at special back-to-back test rig, where whole automotive gearbox were used. For this reason, loading conditions applied at the gearset are very close to real ones while car driving.

The aim of these tests was to prove whether gearwheels made from this PM material have comparable loading capacity with the serial ones made of wrought steel.

From tests results it is clear, that in case of the 3rd speed the resistance against pitting was even higher by 56 %, in case of the 6th speed it was by 58 % higher in comparison with serial gearing. This holds true if the values of arithmetic means of test results (hours until pitting) are compared.

Of course, these results are based only on low number of performed tests. To increase the probability, the number of performed tests would have to be increased accordingly.

Results of both symmetric HIP:ed gears testing were published in [43].

By describing the results of performed tests of symmetric PM HIP:ed gears was accomplished thesis target number 1.

7.2 Asymmetric PM Gearwheels Project Description

The second part of this thesis deals with the rolling technology, which is also very specific industrial field. For this reason, the cooperation in this project to a specialist in this branch was offered. For testing of symmetric HIP:ed gears were chosen 3rd and 6th speed. Same speeds were selected also for the application of the rolling technology, each of them should be produced by another company. Originally, we have cooperated with the company **Miba AG** from Austria, which was to produce the 3rd speed and the German company **Profiroll Technologies GmbH**, which was to produce the 6th speed. But after a short time Miba AG has left this project, so we have continued only with the 6th speed.

The aim was to produce a PM gearset with an asymmetric profile and densify its surface using the rolling technology. This gearset should be then tested in the laboratory at CTU in Prague to compare its strength with original and HIP:ed PM gears.

In case of the PM gearing with an original symmetric profile the natural porosity was eliminated using the HIP technology. In the case of asymmetric gears this issue (porosity) was reduced thanks to rolling technology. There is an obvious difference in the porosity removing between both these technologies. In comparison to HIP:ing, when the porosity is removed in the whole parts volume, rolling is only a surface operation. This means that original porosity inside the part stays unchanged. Only a very thin surface layer can be densified to a 100% density by rolling technology. In case of the gearwheels this issue is not so important, because the most important areas with highest stresses influencing the lifetime strength, are always at the tooth profile surface. This applies to both contact and bending (tensile) stresses in the tooth root, Figure 6-17. Furthermore, the Hertzian stress is reduced thanks to asymmetric design.

7.2.1 Rolled Asymmetric PM Gearset Production Process

The manufacturing process of these gears was very close to the one for HIP:ed gears. Blanks were compacted from a material **Astaloy® 85Mo** to a density of 7.25 kg/m^3 and sintered at the temperature of **1120°C** for **45 minutes**. Regarding the heat treatment, the parameters were: temperature **920°C** for **60 minutes** with 0.95% carbon potential. Afterwards the tempering at **180°C** for **120 minutes** followed. All these conditions related to the material treatment were defined by Höganäs. These parameters are adjusted for a number of different reasons. They depend on things such as density and required case depth, but also the type of surface (machined, rolled etc.). That's why they were adjusted between the HIP:ed and rolled gears.

All steps of this process chain are in chronological order listed in following steps:

1) compacting, sintering and turning base blanks (Höganäs)
2) turning base gearwheel's shape (Profiroll)
3) grinding the gearing macro shape (Profiroll)
4) densification rolling + measurement (Profiroll)
5) heat treatment + material investigation (Höganäs)
6) welding of synchro rings (Höganäs)
7) final grinding of synchronization cone and inner diameter
8) measurement (Profiroll)

Real situation during the rolling process is depicted in Figure 7-25.

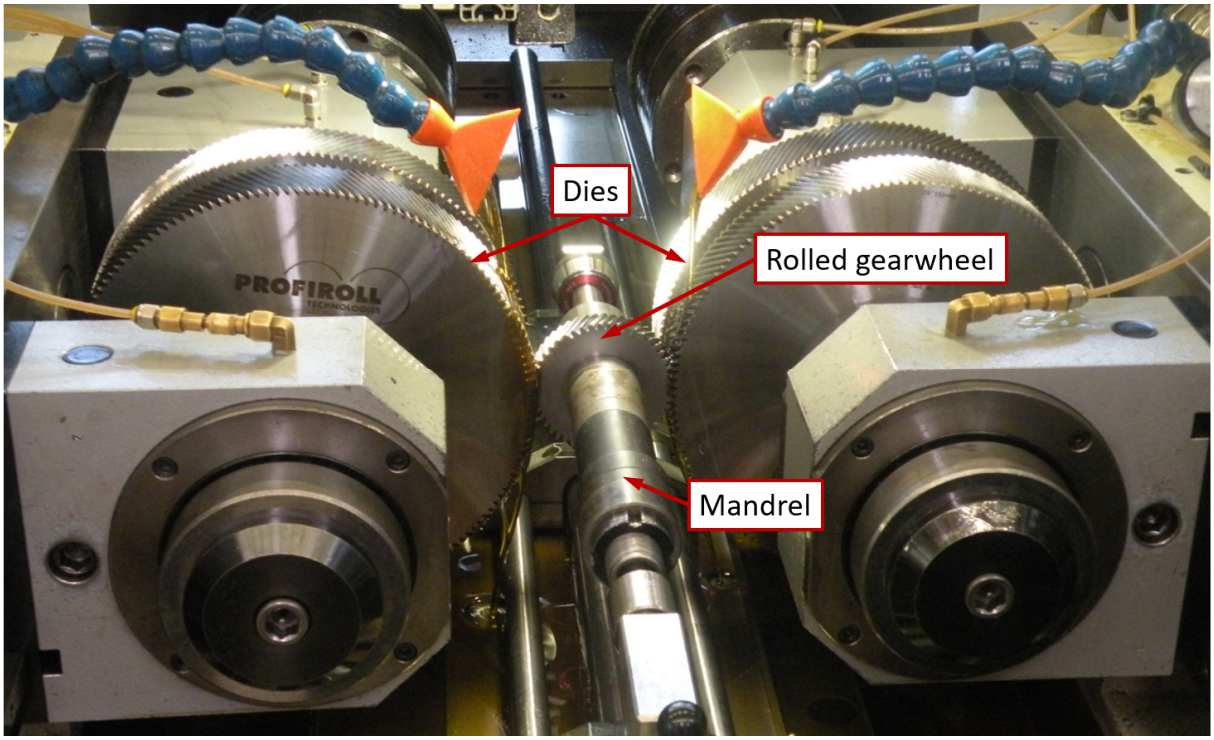

Figure 7-25: Gearwheel (z=48) during the rolling operation in the company Profiroll Technologies

7.2.2 Material Structure Analysis of Rolled PM Gears

In Figure 7-26 is depicted the asymmetric rolled PM gearset of the 6th speed after all necessary technological operations ready for material properties investigation.

Figure 7-26: Asymmetric rolled PM gearset of the 6th speed ready for material properties investigation

To gain more pieces of information about the rolled gearwheels material structure, these gears were investigated by Höganäs AB in LOM (Light Optical Microscope) and density profiles were measured on both flanks and in the root. In following figures are depicted besides the tooth overview also the details of all important areas of the tooth profile, i.e. the root, and both flanks. In Figure 7-27 is depicted the larger gearwheel (z=48).

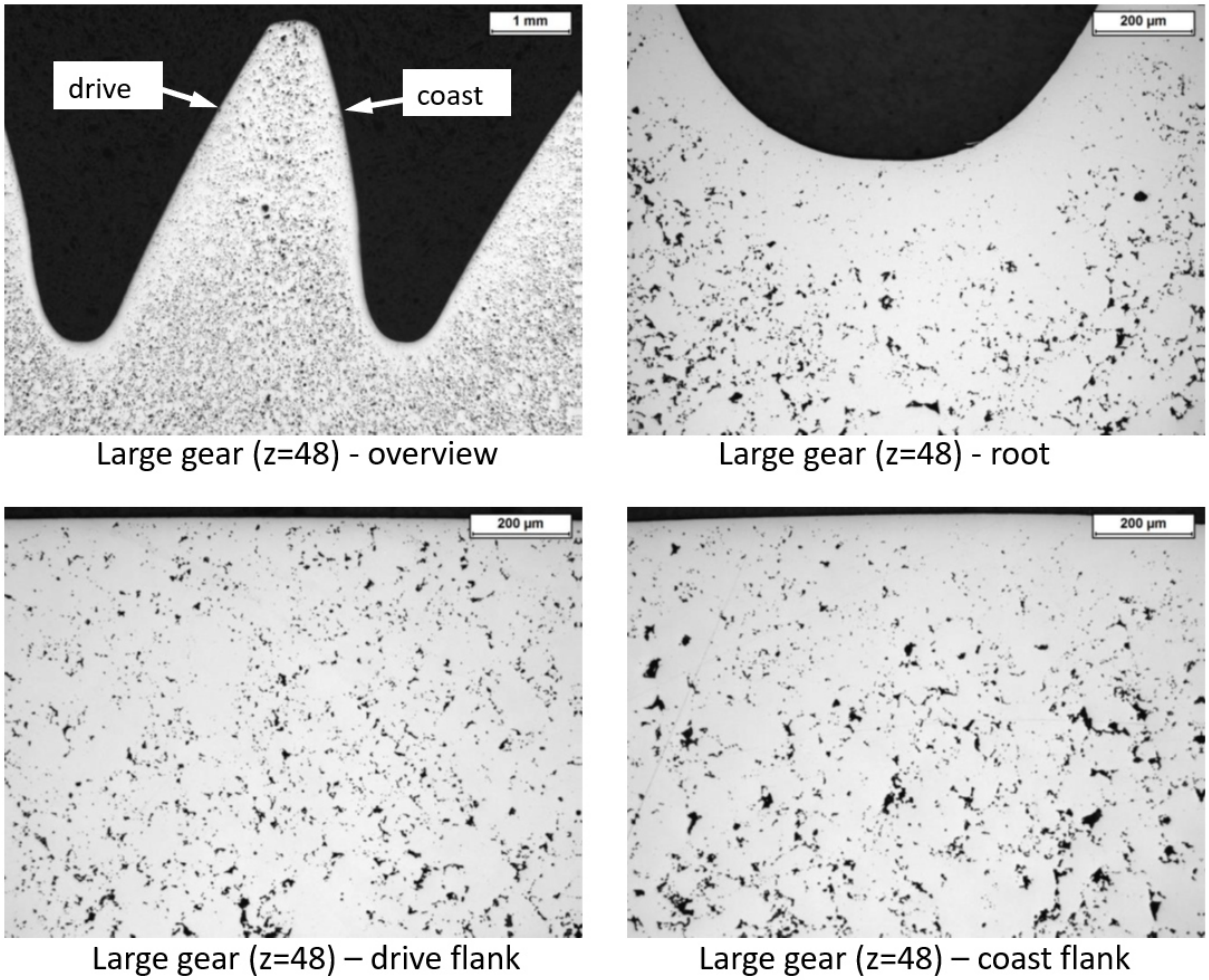

Large gear (z=48) - overview

Large gear (z=48) - root

Large gear (z=48) – drive flank

Large gear (z=48) – coast flank

Figure 7-27: Structure analysis result from LOM of the rolled large gear (z=48)

The same figures of the gearwheel's structure, but for the small gear (z=31), are depicted in the Figure 7-28.

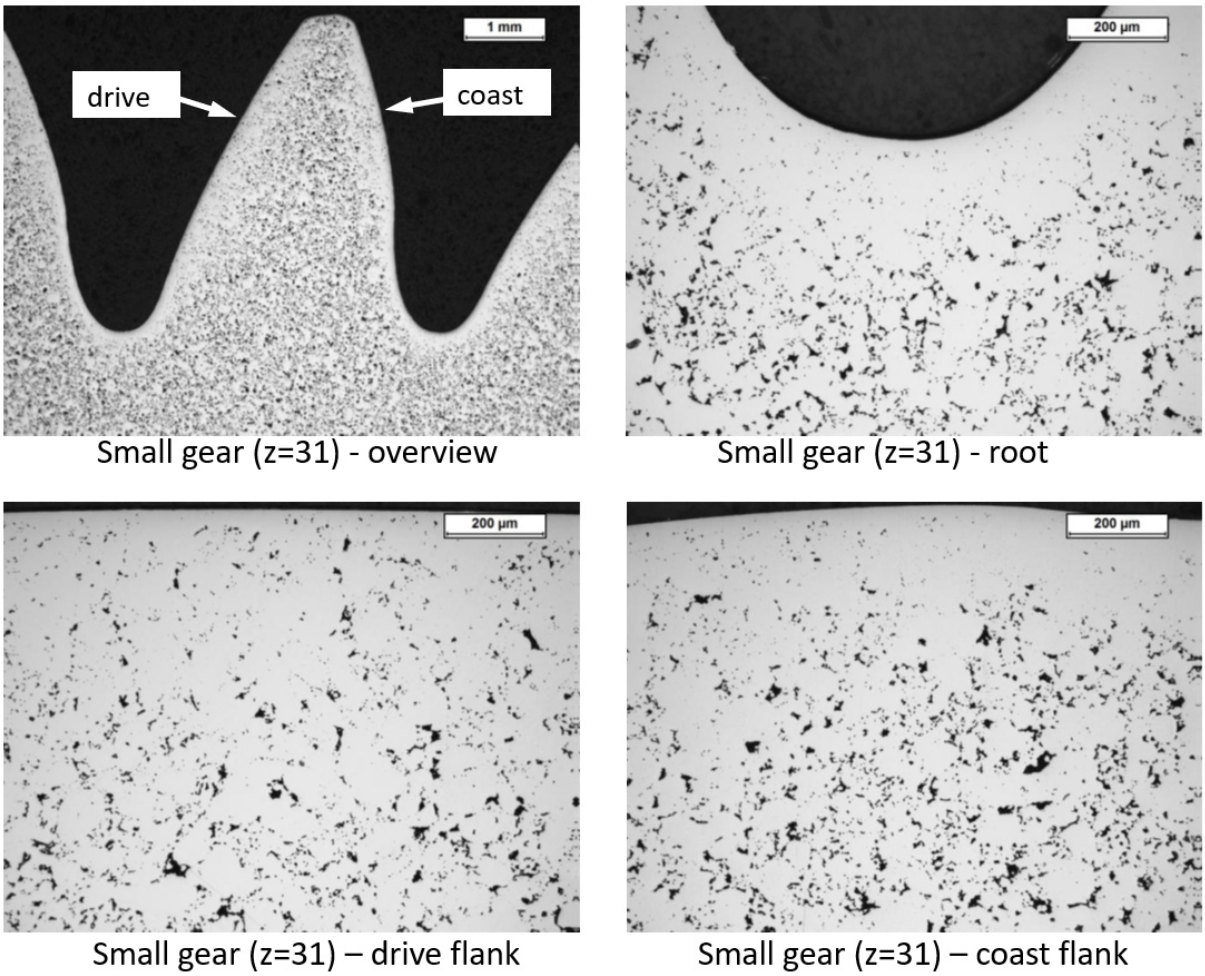

Small gear (z=31) - overview | Small gear (z=31) - root

Small gear (z=31) – drive flank | Small gear (z=31) – coast flank

Figure 7-28: Structure analysis result from LOM of the rolled small gear (z=31)

In the large gear the drive flank has thicker densified layer but with higher number of smaller pores compared to the other side, Figure 7-27. In the small gear the drive flank has thicker densified layer but with higher number of smaller pores compared to the other side Figure 7-28.

After etching all surfaces were martensitic with only low number of retained austenite, Figure 7-29 and Figure 7-30a) and Figure 7-31. In the centre of the teeth in both parts the microstructure was martensite with lower carbon content, Figure 7-30b) and Figure 7-32a). In the centre of the part the microstructure was martensite with bainite, Figure 7-30c) and Figure 7-32b).

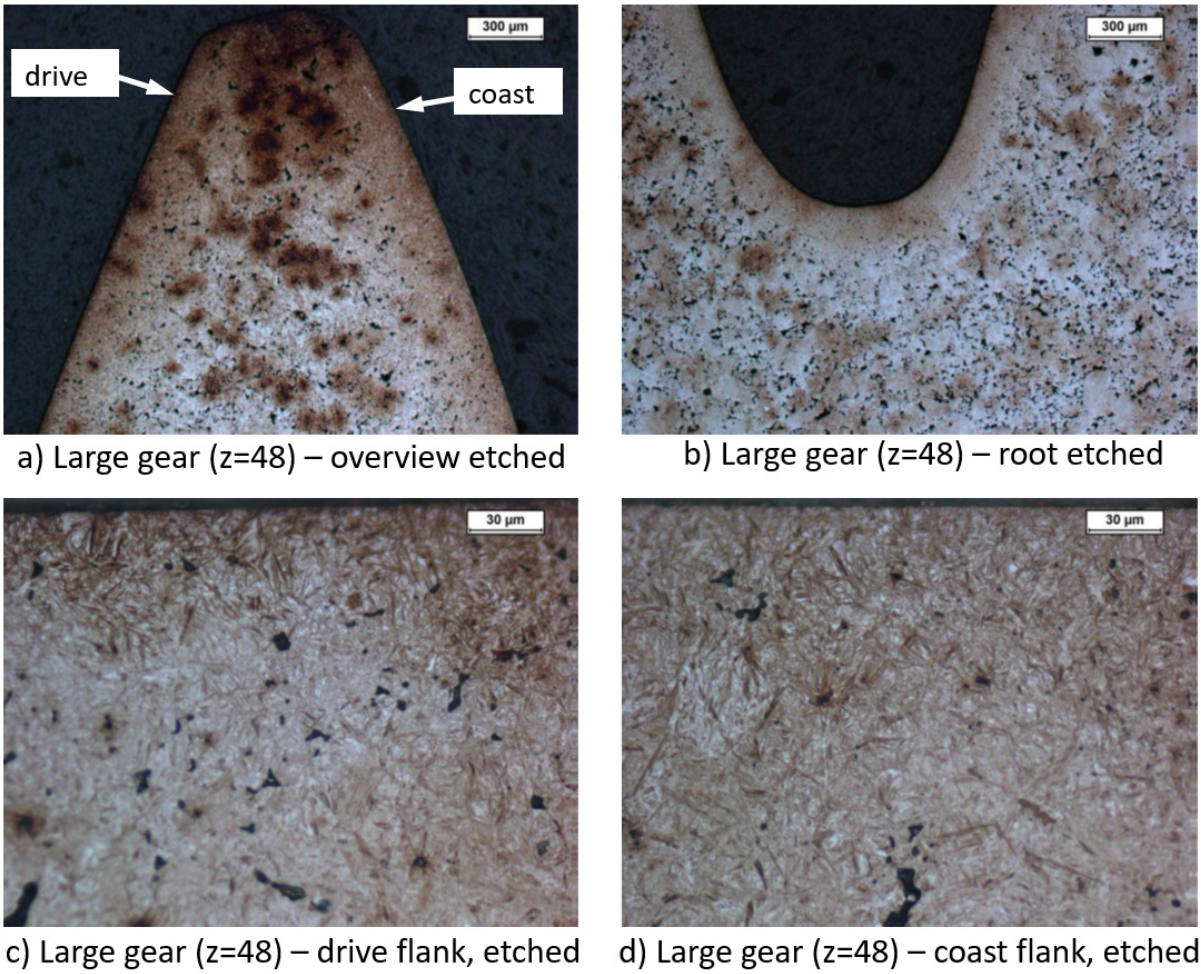

a) Large gear (z=48) – overview etched

b) Large gear (z=48) – root etched

c) Large gear (z=48) – drive flank, etched

d) Large gear (z=48) – coast flank, etched

Figure 7-29: Material structure of the large gear's surface (z=48) - etched

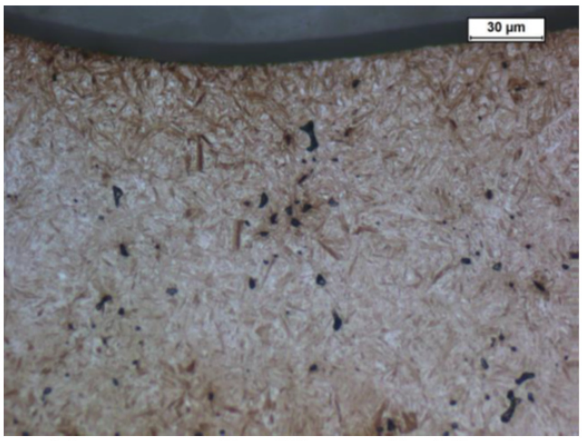

a) Large gear (z=48) – root etched

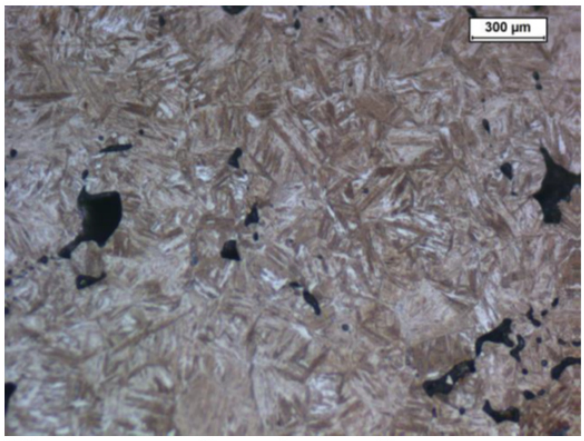

b) Large gear (z=48) – tooth centre, etched

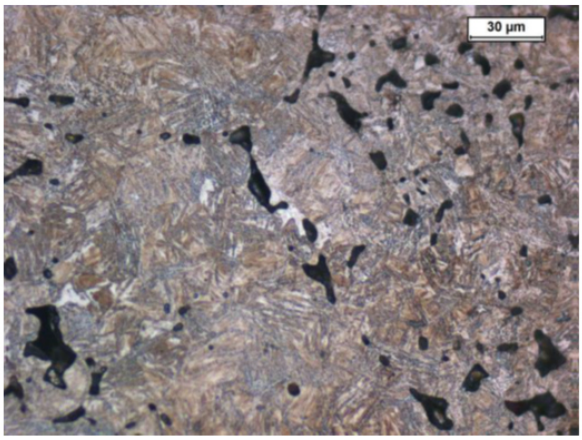

c) Large gear (z=48) – part centre, etched

Figure 7-30: Material structure of the large gear's surface + centre (z=48) - etched

The density profile measurement on the large gear (z=48) showed that on the drive flank the densification depth with 98% full density was 50 µm, on the coast flank and the root it was 150 µm, Figure 7-33.

On the small gear (z=31) on the drive flank the densification depth with 98% full density was again 50 µm, on the coast flank and the root it was 150 µm, Figure 7-34.

At both these measured gears is visible, that the surface densification on drive sides is lower than on coast sides. This phenomenon can be logically explained. It is caused by the magnitude of the curvature radius in the contact. This radius is larger on the drive side (Figure 6-16), and thus the local contact pressure while rolling decreases on the drive side. And on contrary, using the same principle, the densification is higher on the coast side due to smaller curvature radius.

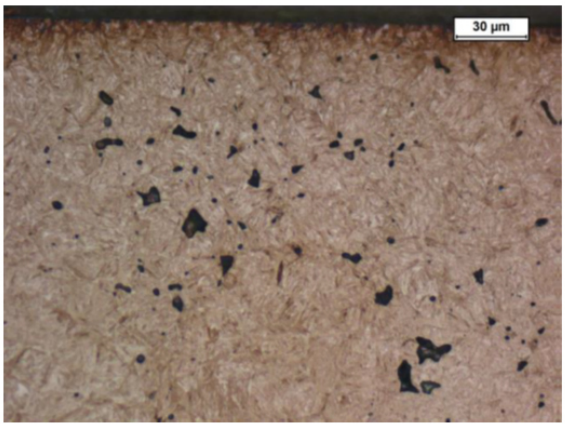

a) Small gear (z=31) – drive flank, etched

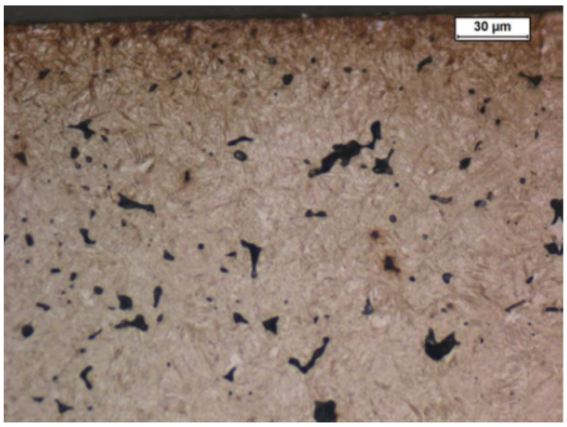

b) Small gear (z=31) – coast flank, etched

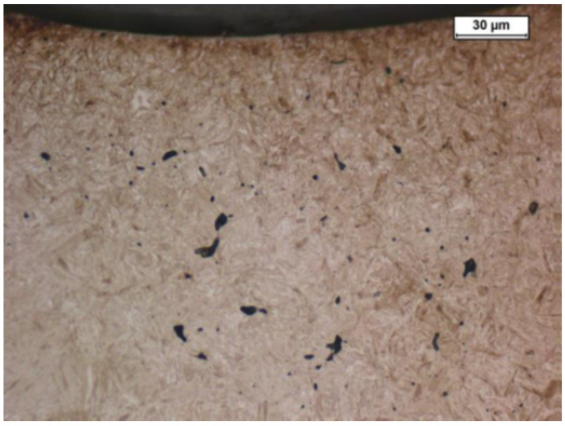

c) Small gear (z=31) – root etched

Figure 7-31: Material structure of the small gear's surface (z=31) - etched

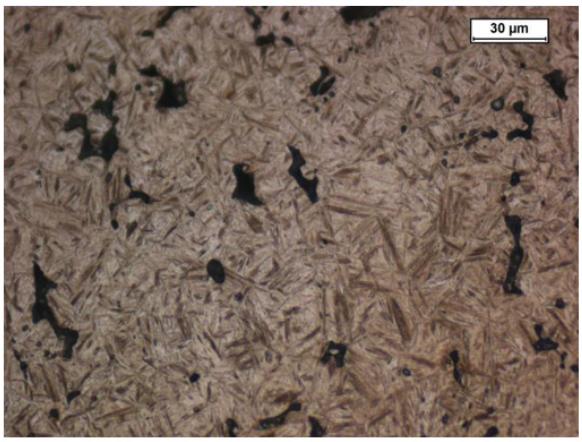

a) Small gear (z=31) – tooth centre, etched

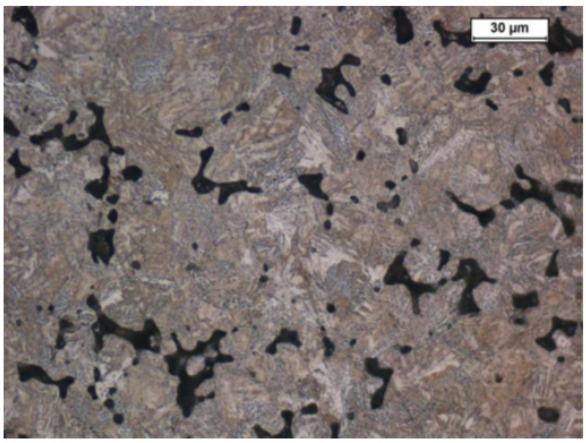

b) Small gear (z=31) – part centre, etched

Figure 7-32: Material structure of the small gear's centre (z=31) - etched

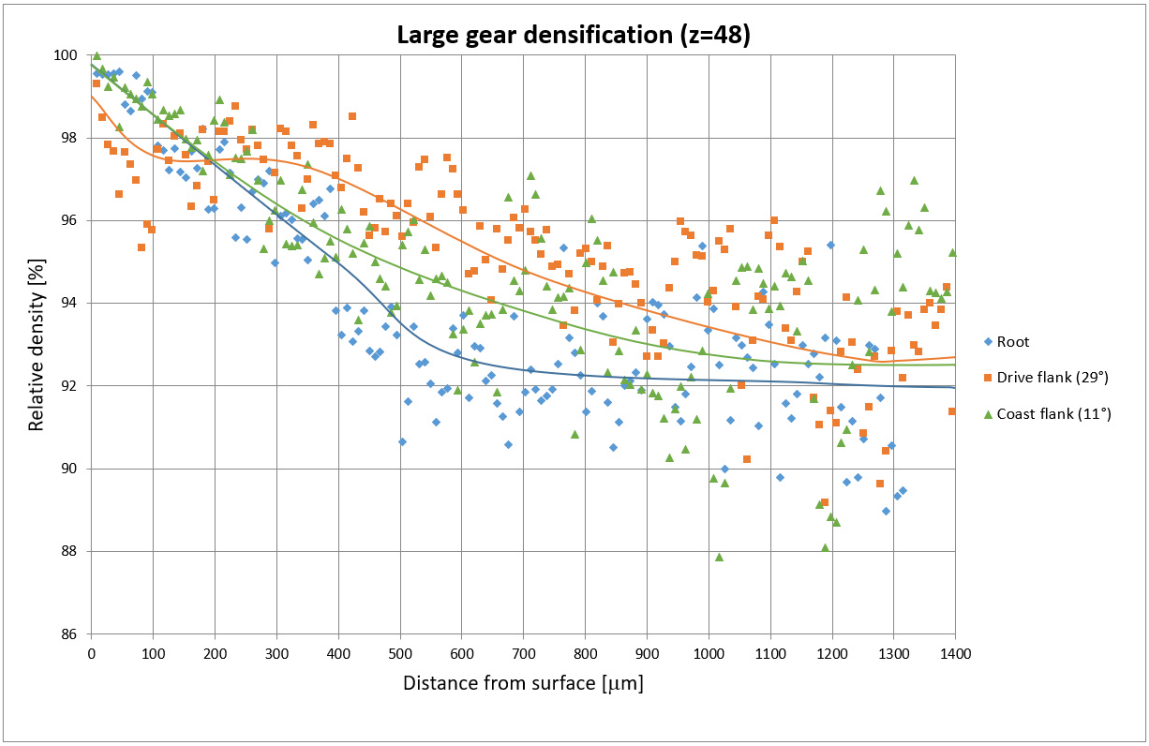

Figure 7-33: Density profiles measured on the large gear (z=48) on both flanks and the root

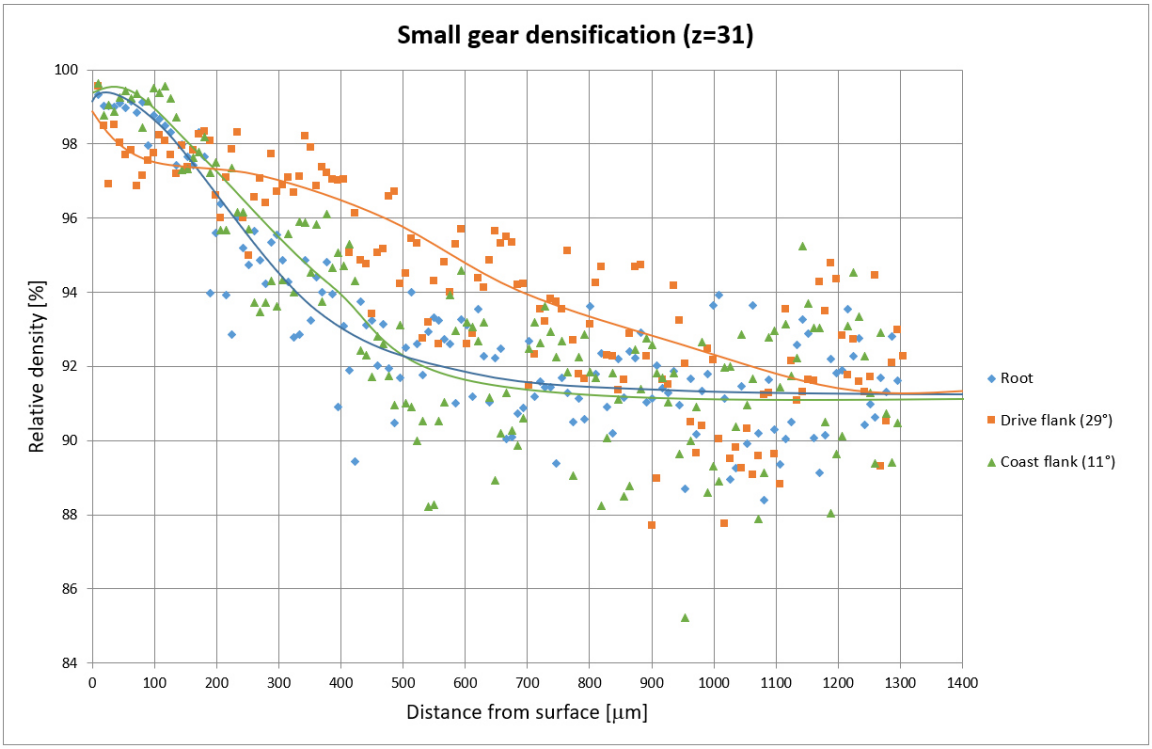

Figure 7-34: Density profiles measured on the small gear (z=31) on both flanks and the root

Required radial force during rolling was adjusted according to performed measurement of the densification depth. The target was to reach the relative density of 98% into the depth of 0,05 mm.

The case depth in the large gear (z=48) was 0.6 mm in both flanks and 0.4 mm in both roots. It is depicted in the Figure 7-35.

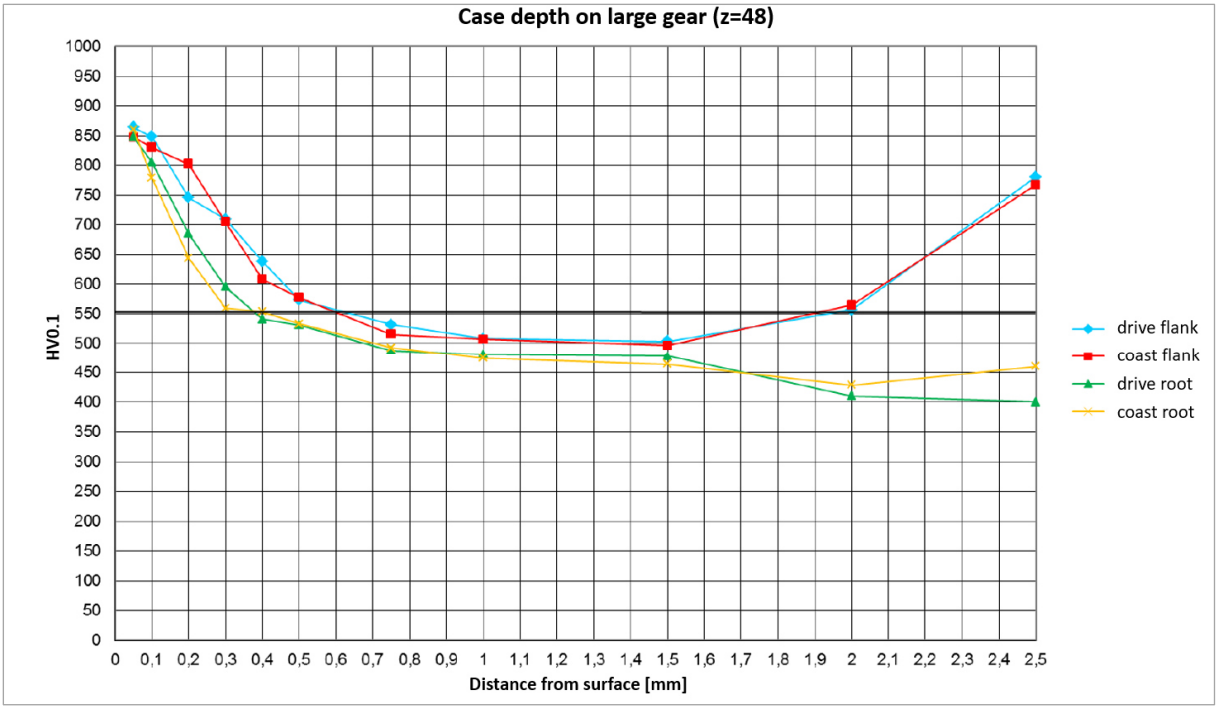

Figure 7-35: Case depth measured in the large gear, it was 0.6 mm in both flanks and 0.4 mm in both roots.

In the small gear (z=31) the teeth were through hardened, while the case depth in the coast root was 0.5 mm and in the drive root it was 0.3 mm, Figure 7-36.

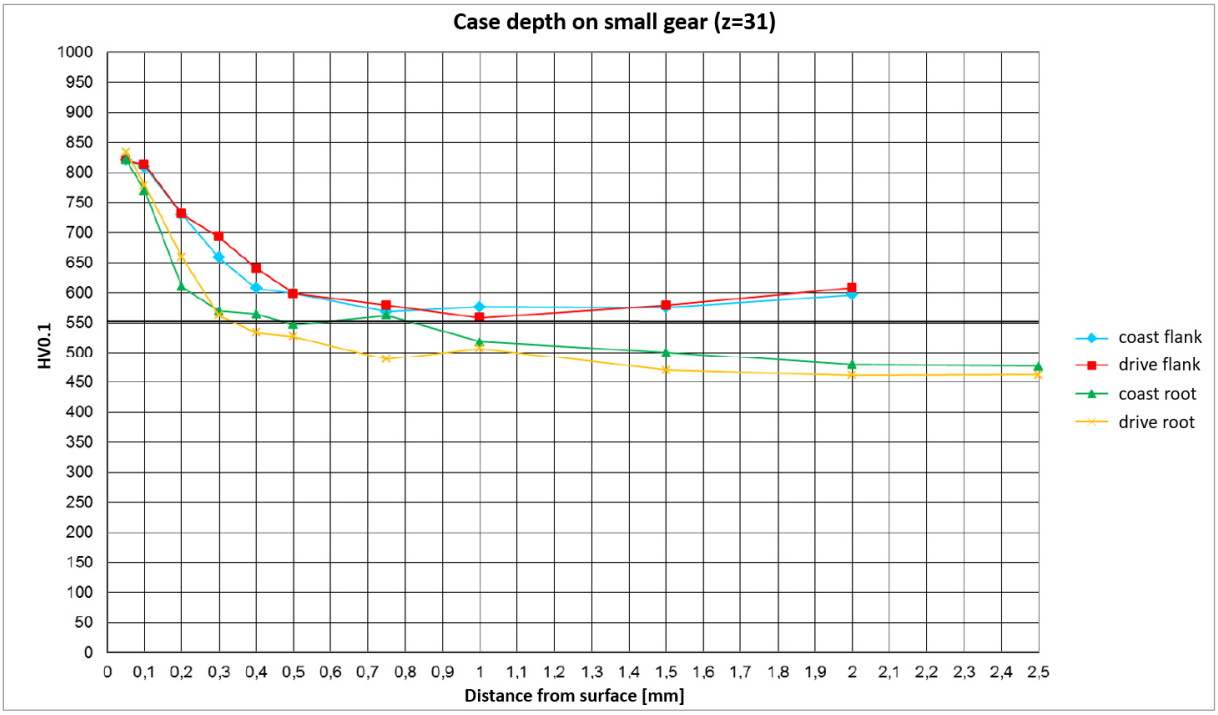

Figure 7-36: Case depth measured in the small gear. It was through hardened in the teeth and the case depth was 0.5 mm in the coast root and 0.3 mm in the drive root.

In Figure 7-37 is depicted the asymmetric gearset after all necessary production operations. In this state the gearset was finally ready to be installed in the gearbox and tested.

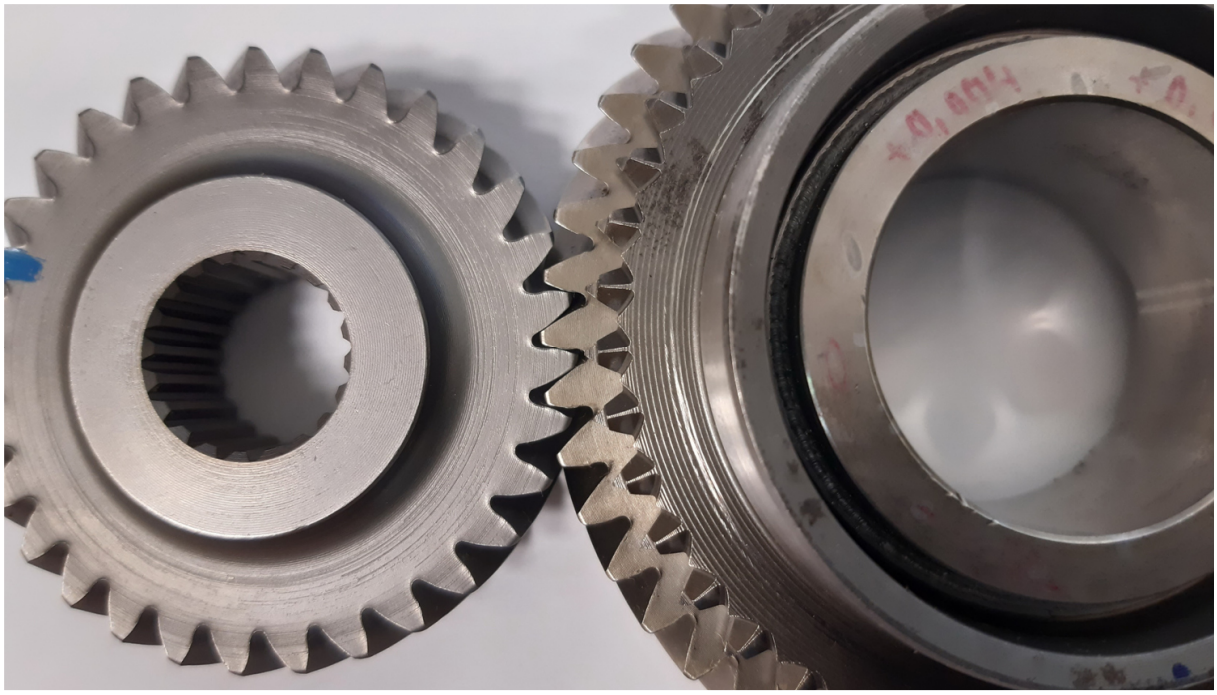

Figure 7-37: Asymmetric rolled PM gearset of the 6th speed ready for testing

7.2.3 Weight Comparison of both Gear Variants

As it was mentioned, the basic material of these gears is **Astaloy® 85Mo**. Its natural property is the porosity, which logically leads to the density reduction (**7,25 g/cm^3**) and thus also the weight reduction. This fact has positive influence on passive resistances and fuel consumption of the vehicle.

To investigate the weight reduction potential of this new gearset, these gears were weighed. To get more precise results, 5 gearwheels were weighed together, and the result was subsequently divided by 5. Results can be seen in Table 7-3.

[g]	original symmetric gears		rolled asymmetric PM gears	
	pinion (z=48)	gear (z=31)	pinion (z=48)	gear (z=31)
weight of 5 gears	2914	1057	2826	990
avg. weight of 1 gear	**582,8**	**211,4**	**565,2**	**198**

Table 7-3: Weight comparison between PM rolled asymmetric and serial gears of the 6th speed.

For the smaller gear (z=31), the material change relates to the whole volume. In case of the pinion (z=48) this change was present just partly, because original synchrorings made from steel were used. By subtracting of values from the Table 7-3 can be determined the weight reduction.

This weight saving is - for the pinion (z=48) **17,6 g** (3 %)

- for the gear (z=31) **13,6 g** (6,4 %).

7.3 Asymmetric Gears Test Results

The aim of these gears testing was to find out the potential of the rolling technology application on PM gears. For this reason, no additional flank surface treatment was performed after rolling.

First pair of gears was selected, assembled into the gearbox and tested in the laboratory of the CTU in Prague under same loading conditions as both HIP:ed gears. Surprisingly, this test ended after 1 hour and 35 minutes (380 000 cycles) by a tooth breakage, Figure 7-38.

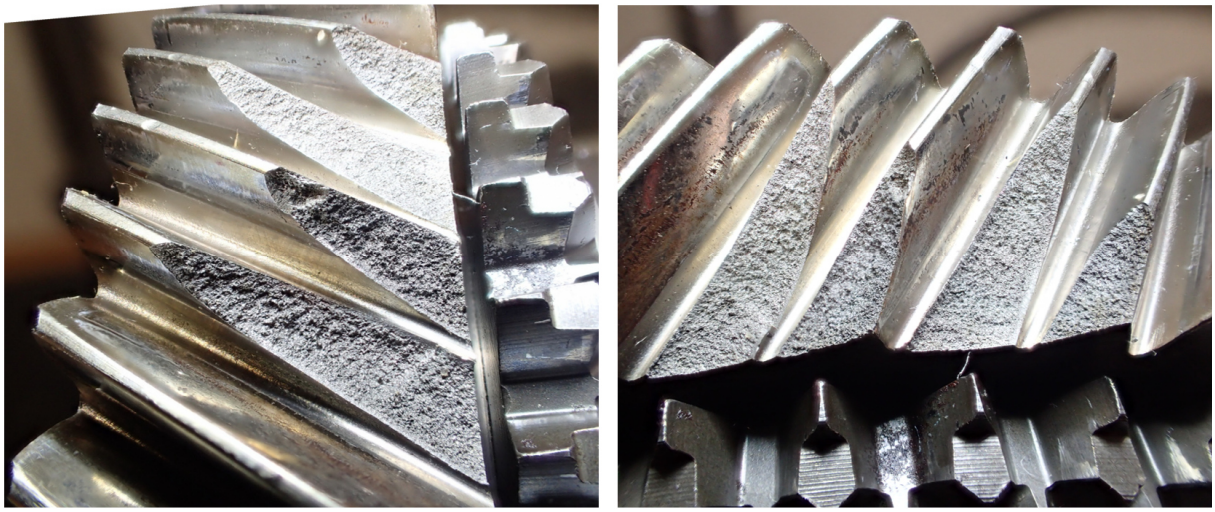

Figure 7-38: Test result of the first asymmetric rolled gearset – tooth breakage after 1h and 43min

In Figure 7-39 is depicted the testing process during the second testing hour. There is clearly visible the sudden increase of the accelerations RMS of both accelerometers glued on the tested gearbox. During the first step (increase) first two teeth broke, five minutes after next two teeth broke as well, Figure 7-38.

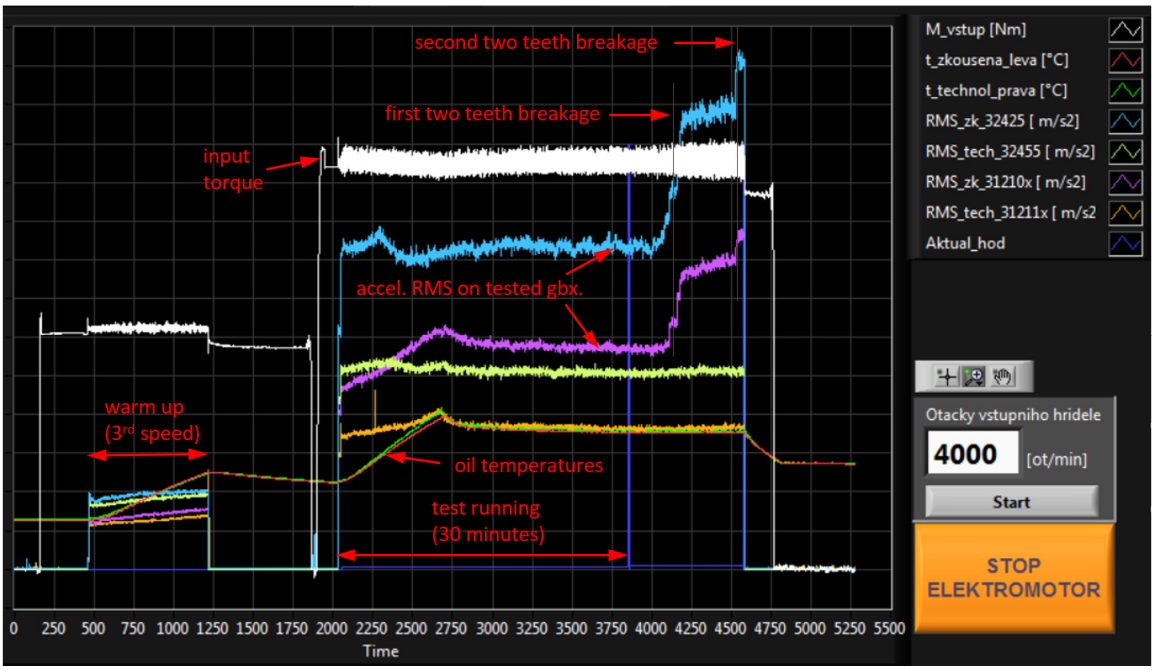

Figure 7-39: Test process conditions during the second testing hour of the first asymmetric gearset. Tooth breakage started after 35 minutes (1 hour and 35 minutes in total).

Due to this unexpected test result, the contact pattern test was performed once more on this gearset. This time, not only on the loaded drive flank to investigate the load distribution in the mesh, but also on the coast flank, to verify that the backlash is sufficient (to avoid the interference). This test was performed as usual for more load levels. In one of them – by free rotating (torque = 0 Nm) there was found some imprint (trace) on the coast side of the small gear (z=31). To validate this result, this test was performed repeatedly with same result. It is depicted in Figure 7-40.

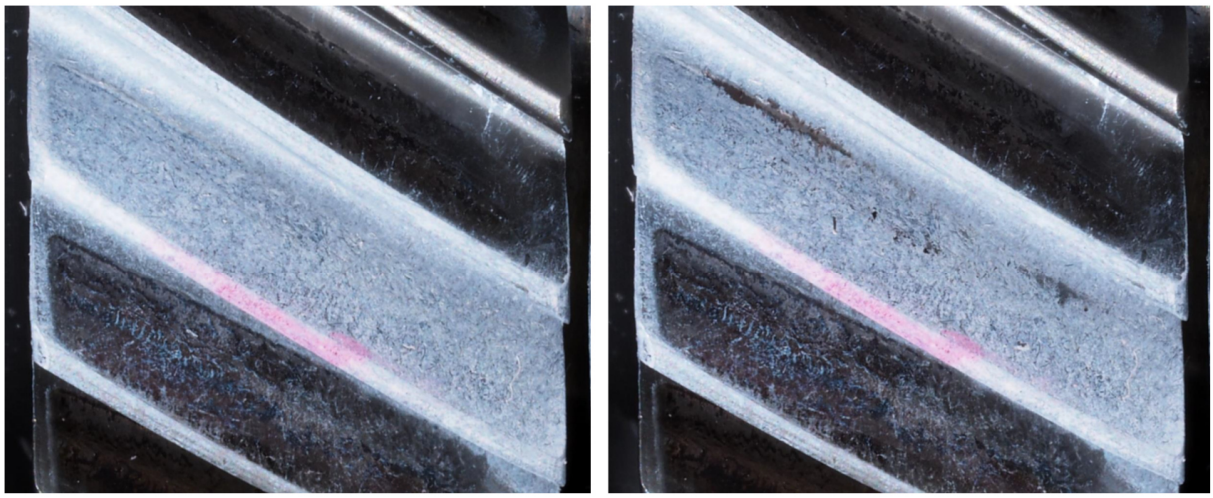

Single mesh pattern (coast) Summative mesh pattern (coast)

Figure 7-40: Contact pattern test result on coast flank (z=31) after tooth breakage – single (left) without touching, summative (right) – with touching (interference occurred)

In the case of the single contact pattern test (left) there is no trace, thus no contact occurs. In case of the summative contact pattern test some trace was detected. This means that the backlash between tooth flanks is not sufficient and therefore interference occurs. As can be seen, the contact area was detected close to the small gear's dedendum. This means that it was done by the pinion's addendum. This corresponds to the fact that the tooth breakage appeared on the pinion (z=48). This issue documents the fact, that the theoretical backlash (j_n = 0,068 mm) would be sufficient only if tooth flanks geometry and gears placement is ideal. In reality there is always some radial runout between the shaft and the gear, and imperfections on tooth flanks. Furthermore, these flank deviations cause local overloading which can cause the tooth breakage initiation.

To solve this interference issue, additional grinding of the coast flank was performed to assure sufficient backlash in the gear mesh. Because these gears have very thin densified layer, it was decided that the grinding magnitude will be divided to both gears into the depth of 0,05 mm. This should increase the backlash about 0,1 mm to final theoretical value of j_n = 0,168 mm.

The grinding was performed by the company Profiroll Technologies. Its accuracy obviously depends on the used equipment. In this case the standard chuck was used for gear's clamping. For this reason, some misalignment (radial runout) appeared while grinding. The consequence of this issue is, that the grinding has been performed unevenly around the gear's circumference. It is clearly visible especially on the small gear (z=31), when the gear had to be clamped using the tip diameter of the internal involute splines. It is depicted in Figure 7-41. In its left part is depicted a gear's part where tooth flanks weren't ground, in the middle they are ground only partly and in the right figure there is depicted a gear's part, where tooth flanks were ground completely.

Similar situation was unfortunately also on the drive flank, which shouldn't be ground at all.

Figure 7-41: Small gear (z=31) after coast flank grinding. Gear's part not ground (left), partly ground (middle) and fully ground (right).

In the case of the large gear (z=48) the situation was much better, because as the clamping surface was used already ground surface for the needle bearing. This grinding result is depicted in Figure 7-42. It can be seen, that on the drive flank was maintained the original rolled surface (left) and the coast flank has been ground completely (right).

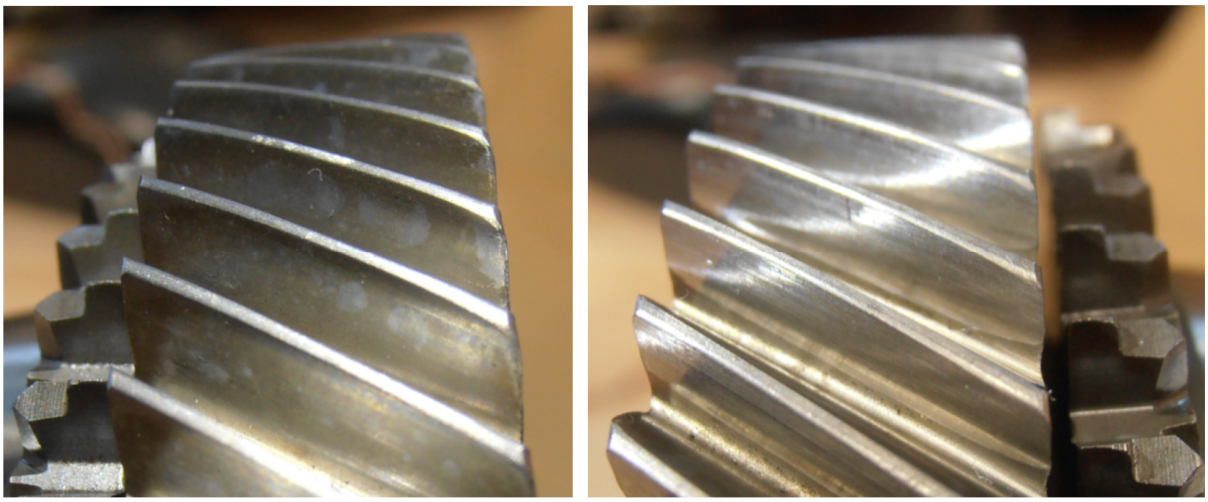

Figure 7-42: Large gear (z=48) after coast flank grinding. Original rolled (not ground) drive flank (left), ground coast flank (right).

The flanks geometry can be also depicted using measurement protocol. Its shortened version for both gears is depicted in Figure 7-43. The figures in its upper part depict the profile modifications, lower figures depict lead modifications. There are four flank profiles, which were measured evenly around the gear's circumference (by 90°). Flanks which were ground are highlighted by red rectangles. On the small gear (z=31) can be seen, that also drive flanks were ground. This issue happened unintentionally on the opposite flanks of teeth which weren't ground on the coast side. It was caused thanks to clamping misalignment while grinding (circumferential runout).

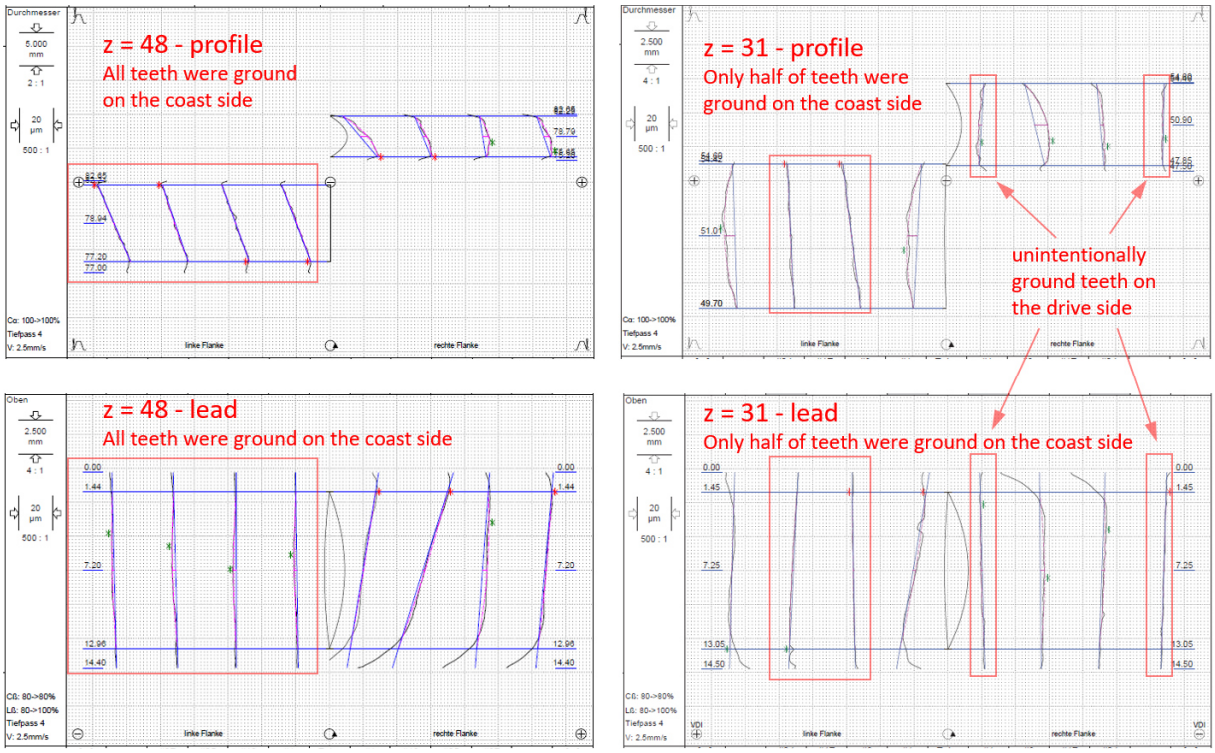

Figure 7-43: Large gear (z=48, left) and small gear (z=31, right) after coast flank grinding. Upper figures depict profile modifications, lower figures depict lead modifications. Ground surface is highlighted by red rectangles.

After this grinding the contact pattern test was performed. On coast flanks no contact (imprint) was detected which confirmed sufficient backlash. Working areas on drive flanks by nominal test load (torque) are depicted in Figure 7-44.

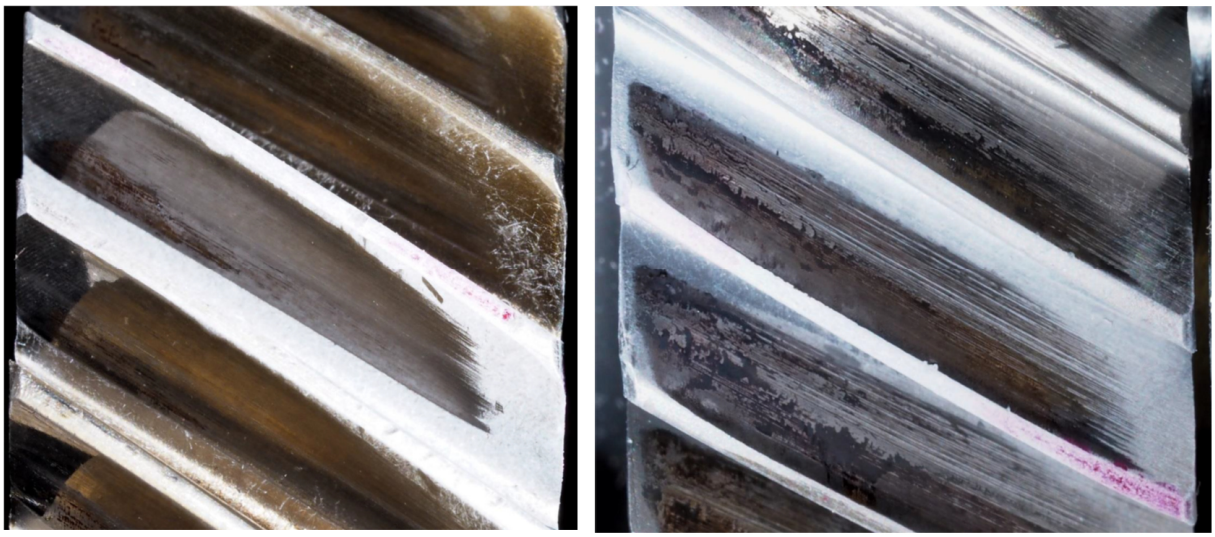

Figure 7-44: Result of summative contact pattern test of asymmetric rolled gearset after coast flank grinding – large gear (z=48, left), small gear (z=31, right)

In the Figure 7-44 is clearly visible, that on both gears is the left side (by the synchroring) overloaded, especially on the pinion (z=48). On contrary, on the opposite side the tooth flanks aren't used for a few millimeters. This fact led to the suspicion that the tooth breakage on the left side appears as in previous test.

The test was stopped after one hour to document the testing process. Loading conditions are depicted in Figure 7-45. Everything was going well.

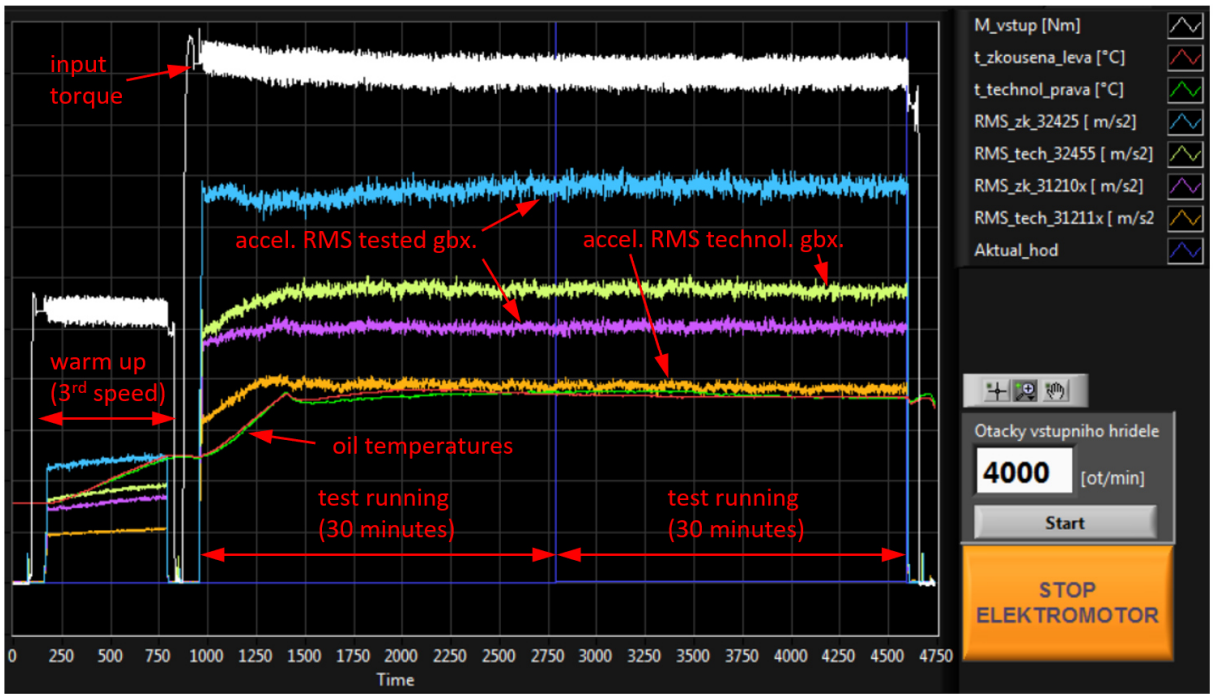

Figure 7-45: Test conditions during the first testing hour of second asymmetric gearset with ground coast flanks.

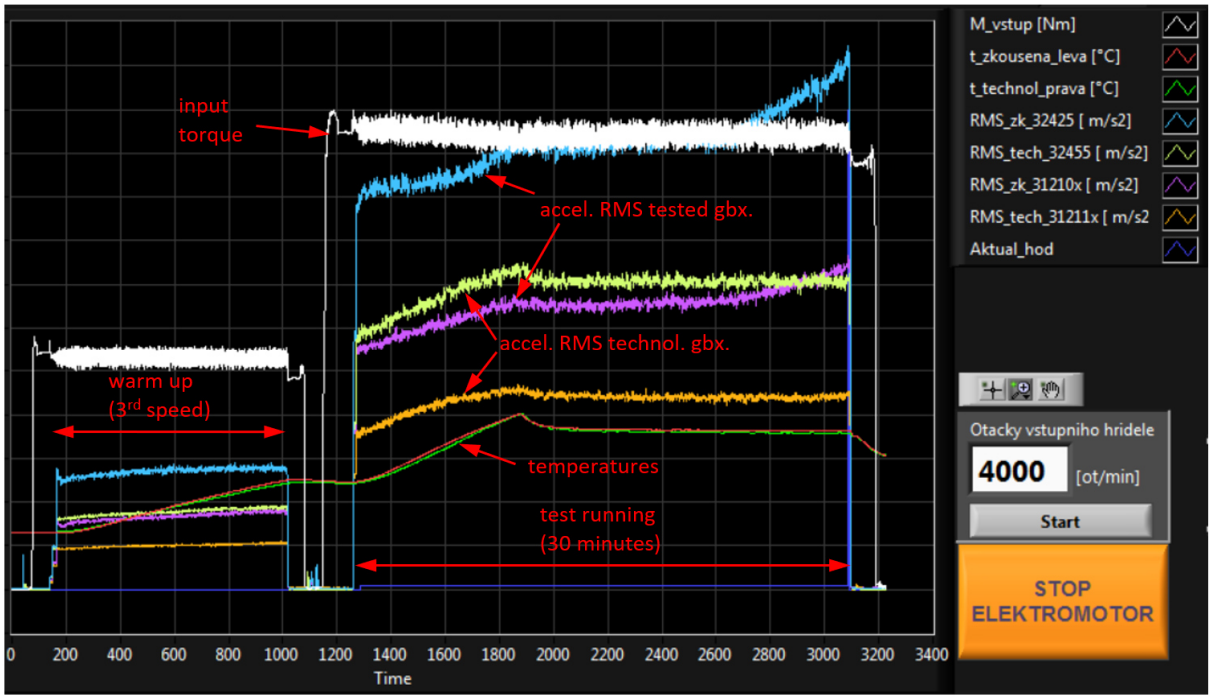

Figure 7-46: Test conditions during the second testing hour of second asymmetric gearset with ground coast flanks. Test was stopped after 30 minutes (1,5 hour in total).

During the test continuation, after the temperature stabilization (10 minutes) also values of acceleration's RMS have stabilized. The test went in this regime approximately for 10 minutes. Afterwards, both acceleration RMS signals on tested gearbox started to rise slowly. The test was

preventively stopped after 30 minutes. The gearset was tested in total only for 1,5 hours (360 000 cycles). This situation while testing is depicted in Figure 7-46.

In Figure 7-47 is depicted tested gearset after 1 hour (left) and after 1,5 hours (right). In both figures is clearly visible unused area on the right side. The tooth breakage is highlighted by red ellipse. In detail is the crack depicted in Figure 7-48.

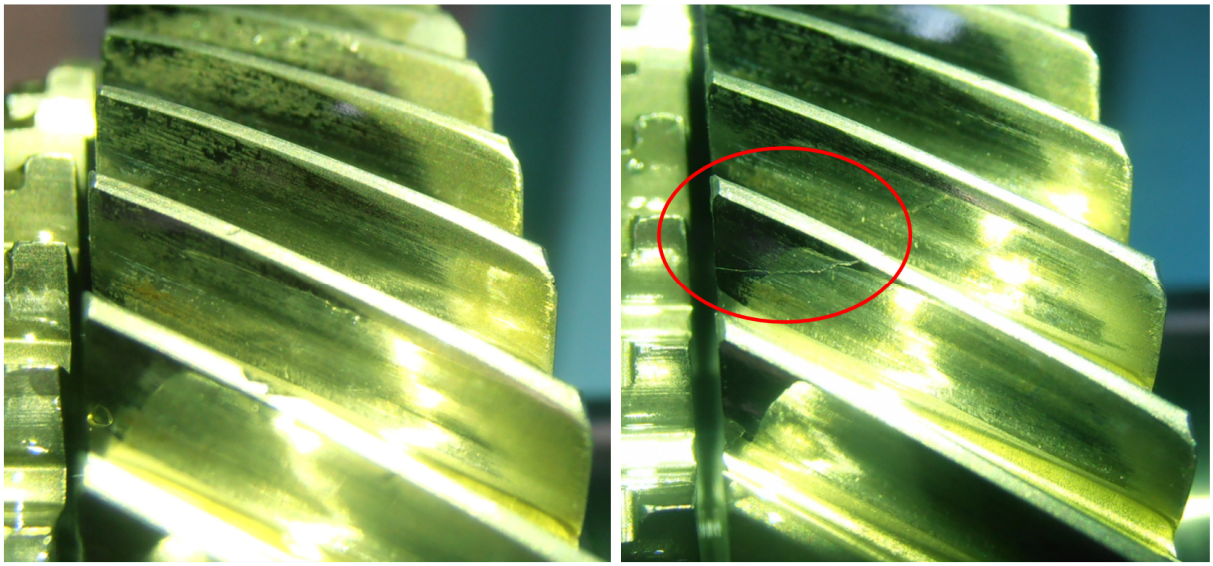

Figure 7-47: Gearing appearance during the test of asymmetric rolled PM gears with ground coast flanks after 1 hour (left) and after 1,5 hours (right, tooth breakage).

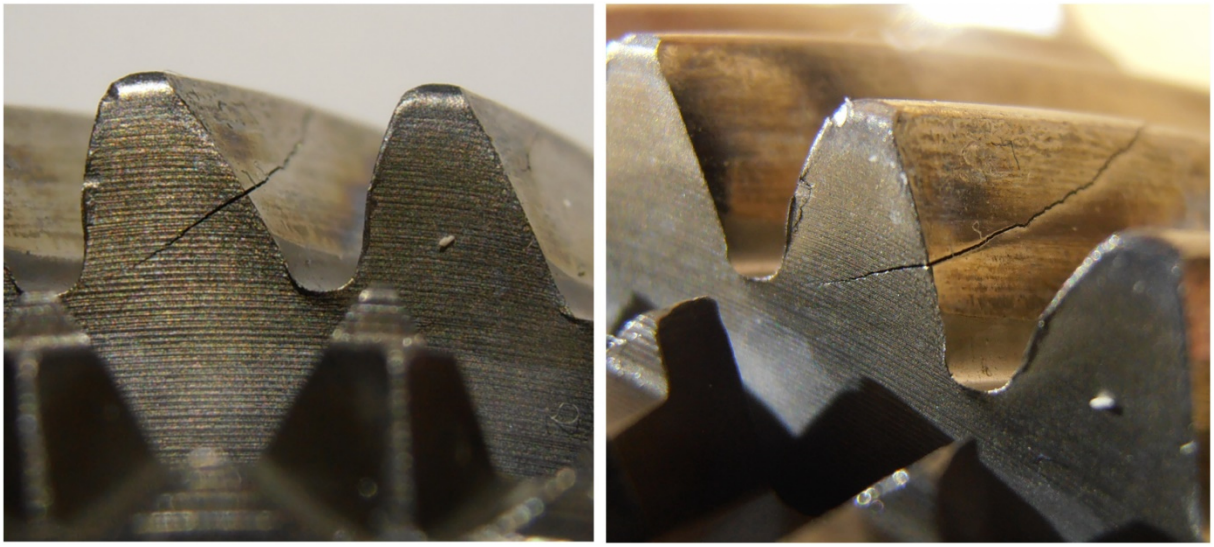

Figure 7-48: Tooth breakage of asymmetric rolled PM gear with ground coast flanks after 1,5 hours.

The crack structure was investigated by Höganäs. The result is that this was a fatigue crack, because directly in the corner there is a small area with very smooth surface, Figure 7-49.

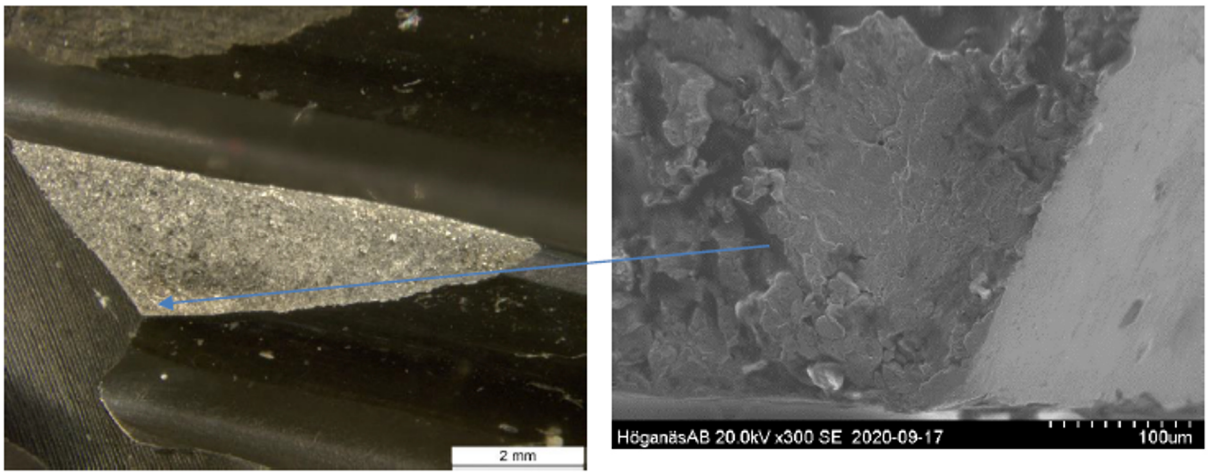

Figure 7-49: Fractured surface in the stereomicroscope (left). Fatigue fracture initiation was found in the corner (right)

Regarding the material structure of this gear, the densification was checked optically, Figure 7-50. In this figure it can be seen that the material porosity is very different around the gear's circumference. The crack was caused by the combination of local overloading and too high porosity.

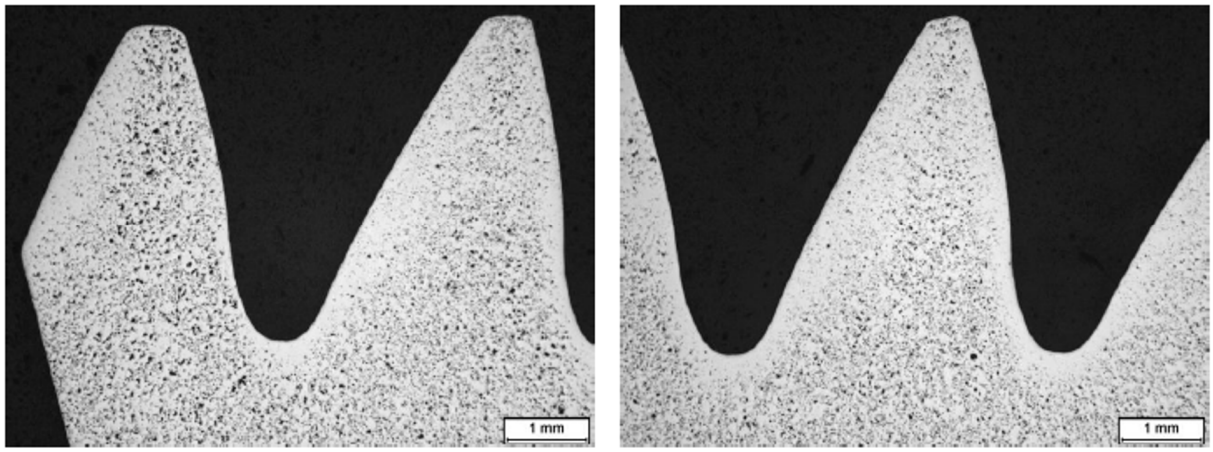

Figure 7-50: Material porosity in fractured gear is uneven for all teeth. In the left figure is the porosity higher than in another tooth in right figure.

Furthermore, cracks were also found on the small gear (z=31) at least on 6 teeth, Figure 7-51.

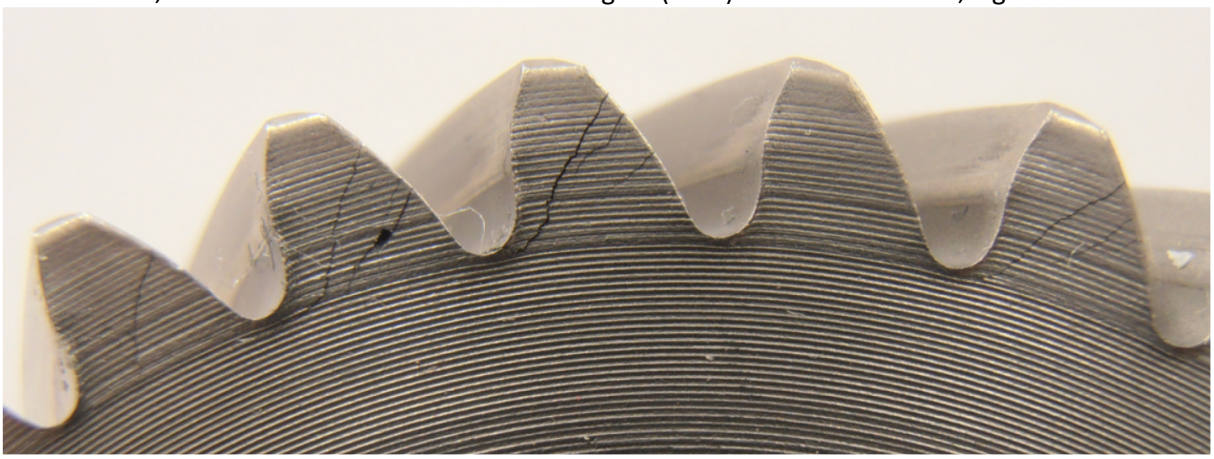

Figure 7-51: Found cracks on the small gear (z=31).

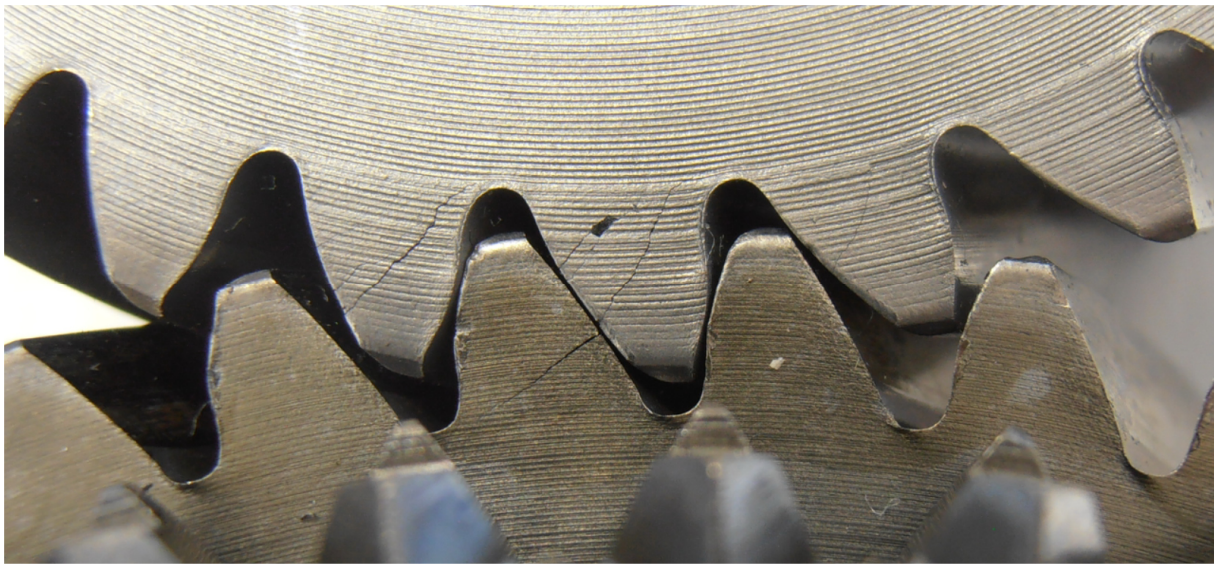

Figure 7-52: Meshing of PM rolled gears with asymmetric profile, both gears have already cracks.

All these tooth fractures, which occurred in less than two testing hours on both tested asymmetric gearsets are showing, that the surface geometry is crucial for the mesh quality and thus for the gear strength. Even with sufficient backlash. In Figure 7-53 is depicted a comparison between standardly produced gears finished with grinding (left) and rolled gears (right). The difference in the quality is obvious at the first glance.

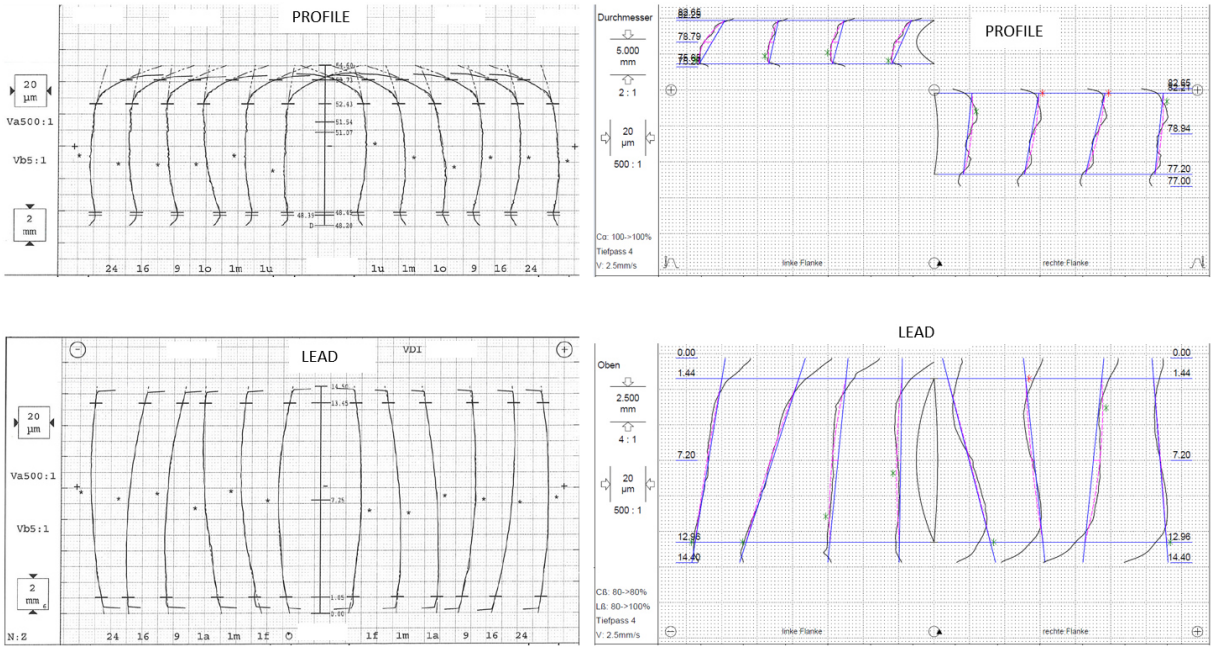

Figure 7-53: Comparison of the tooth flank quality between ground (left) and rolled (right) gears.

For this reason, it was necessary to grind our asymmetric gears to reach comparable tooth flank quality as HIP:ed gears. In the Czech Republic it was not possible, the only company which would be able to grind these asymmetric gears is the German company Kapp Niles. Unfortunately, due to COVID 19 crisis there were no financial resources to perform this grinding operation.

Until these asymmetric PM rolled gears will not be ground to have comparable mesh quality as serially produced gears, it would be meaningless to test (destroy) them, because the test result wouldn't describe the material and technology potential, which is the aim of this thesis.

For this reason, thesis target number 2 cannot be accomplished.

7.4 Tests Results Comparison of PM vs Serial Gears

In the laboratories of the CTU in Prague have been performed endurance tests of automotive gearboxes for many years. These tests were performed for gearing with either special heat or surface treatment. Within these tests were also tested serial gearsets, mostly in the technological gearbox. For all these tests, numbers of cycles until either pitting or tooth breakage were saved. These test results are depicted in Figure 7-55 for pitting and in Figure 7-56 for tooth breakage. Stresses within these tests and S-N curves were computed in the software KissSoft, according the standard DIN 3990. In the Figure 7-55 are depicted also results of tested HIP:ed gears, marked with black cross.

The tooth breakage wasn't reached for HIP:ed gears, therefore there are not included results of these gears in the graph of root bending stresses (Figure 7-56).

For all these tests the loading torque was always constant. The specific loading torque of the gearset depends on the gearbox type, according to the Formula (5-3) described in the Chapter 5.4.1. At the technological gearbox is the loading torque always lower than at the tested one. For this reason, all resulting stresses from technological gearbox are lower than at the tested one. Results acquired from tested gearbox are depicted with blue color, from technological gearbox with red color. Regarding HIP:ed gears, they were loaded with same torque but due to different geometry, also the stresses differ for 3rd and 6th speed.

To improve the gearing strength against the tooth breakage, additional shot peening in the root is standardly used in gears production. For this reason, the value of technology factor Y_T was set to 1,1 according to the guidelines in the KissSoft program, Figure 7-54.

Information

Technology factor Y_T according to ISO 6336-5	
Treatment of the tooth root area	**Technology factor Y_T** (only for case-hardened gears)
Shot-peening (Quality MQ)	1.10
Shot-peening (Quality ME)	1.05

Figure 7-54: Used value of technology factor Y_T in KissSoft for additional shot peening in the root.

Unfortunately, tooth fracture wasn't reached for HIP:ed gears, thus these results can not be included into these graphs. The same holds true also for asymmetric rolled gears, but for another reason – these tests weren't performed.

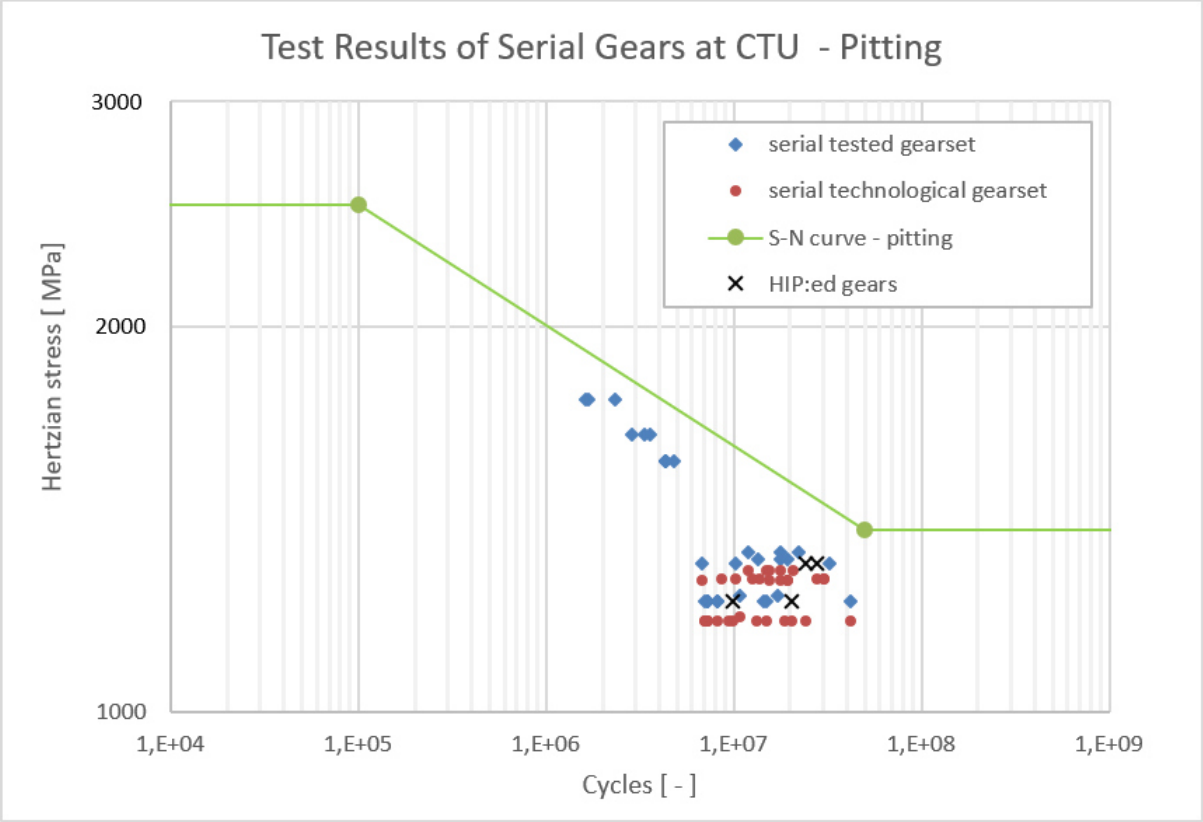

Figure 7-55: Results of performed tests of serial gears at CTU laboratories – pitting.

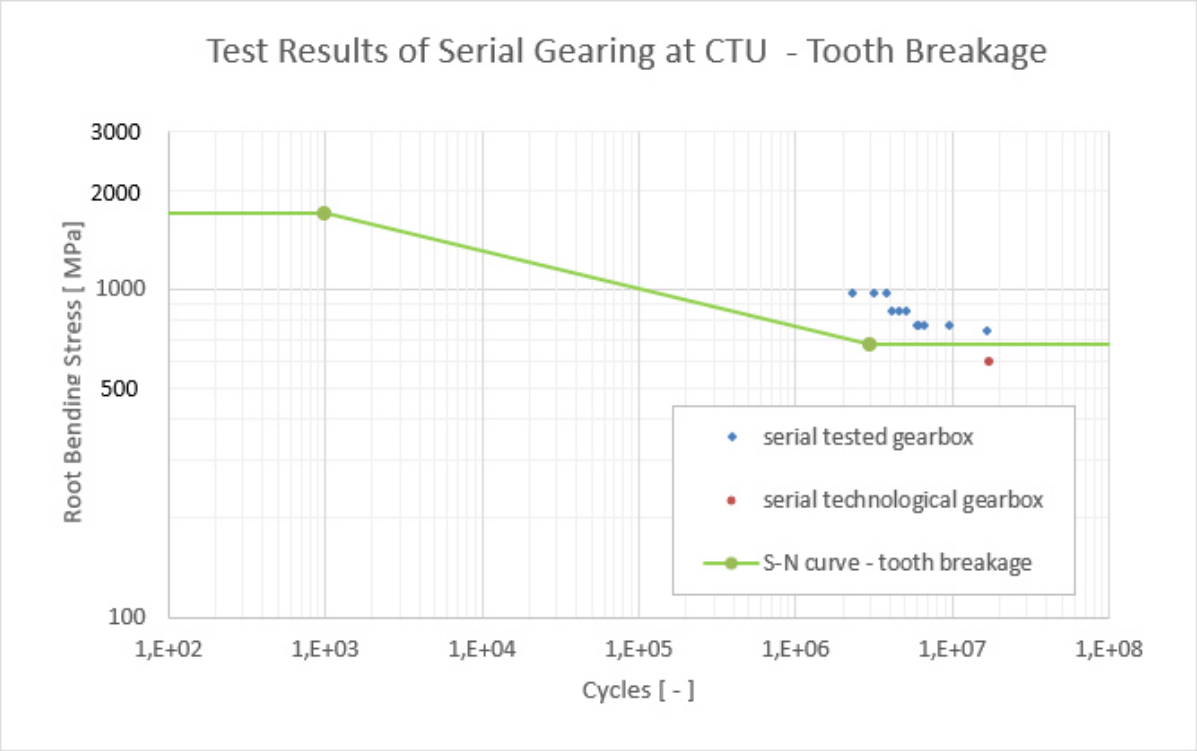

Figure 7-56: Results of performed tests of serial gears at CTU laboratories – tooth breakage.

	3rd speed		6th speed	
	serial gears	HIP:ed gears	serial gears	HIP:ed gears
Hours until pitting - mean value	68,7	107,5	56,6	63
ratio	**1,57**		**1,11**	

Table 7-4: Strength comparison between PM HIP:ed and serial gears of the 3rd and 6th speed.

In the Table 7-4 is shown a comparison between PM HIP:ed and serial gears with same loading conditions, which were performed in laboratories of CTU in Roztoky Science and Technology Park.

For the case of the 3rd speed, these results correspond exactly to the results described in the Chapter 7.1.4, because no other test of serial gears with same loading conditions were performed. For this reason, the strength increase of HIP:ed versus serial gears remains 57%.

For the case of the 6th speed, was for the comparison used some more serial tests with same loading conditions. This led to the reduction of the final test results ratio from the Chapter 7.1.5, namely to “only” 11 % strength increase.

8 Conclusion

In this thesis are presented new progressive possibilities in the field of gearing from the point of view of the material, geometry and technology. The PM technology seems to be very interesting from the point of view of the production, because it can replace expensive rough milling and turning operations. Only the final tooth flank grinding must be maintained.

For the case of the HIP:ed PM gears the tests were performed successfully. Unfortunately, for the case of rolled asymmetric PM gears could not be performed without final grinding.

To be able to design the gearing with asymmetric involute profile, the software for this purpose was developed.

Despite some natural disadvantages, PM material seems to be very perspective, especially for the mass production, which is for the automotive typical.

8.1 Thesis Targets Accomplishment

Beside standard thesis targets from the Chapter 3, which are described below, also the weight reduction should be mentioned in this chapter.

The weight reduction potential of asymmetric rolled PM gears due to natural porosity was described in the Chapter 7.2.3. Exact values of the weight reduction were 3 % for the pinion and 6,4 % for the gear.

The software for designing the involute gearing with an asymmetric profile was created using the programming language Python. It considers only the gearing's macrogeometry and is described in the Chapter 6.5.

The method of the strength calculation for gearing with an asymmetric profile was described in the Chapter 6.6. For this purpose, FEM calculation was used.

The description of thesis targets accomplishment follows.

1. ***Determine endurance potential (strength) of gears with original design made from PM material with special technology (HIP) based on test results performed directly in automotive gearbox.***

   These gears were produced and tested. Results of these tests are clearly depicted in the Figure 7-11 and Figure 7-19. The increase of the resistance against pitting of PM HIP:ed gears was for the 3rd speed by **56 %**, for the 6th speed by **57 %**.

   For the 6th speed can be the number of performed tests, used for the result comparison, increased by some other tests. The consequence of it is the reduction of the strength increase from previous 57% to "only" **11 %**, see Table 7-4.

2. ***Determine endurance potential (strength) based on test results of gears with asymmetric profile made from PM material with special surface treatment (rolling) based on test results performed directly in automotive gearbox***

   These gears were designed and produced too. Unfortunately, the surface microgeometry wasn't accurate enough to be comparable with symmetric serial geometry.

This issue could be fixed by additional grinding, but unfortunately, due to the COVID19 crisis, needed financial support wasn't found. For this reason, this target couldn't be fulfilled.

8.2 Future Steps

Within this thesis were designed and produced PM gears, which were also tested in the automotive gearbox. Test bench described in the Chapter 5 was used for these tests to simulate real conditions from the point of view of the gears placement (mesh conditions, lubrication). All these tests were performed with constant torque and speed (rpm), because they were considered as the initial ones, to determine the PM material potential.

In future steps, these gears should be tested also in dynamic mode, i.e. the load spectrum should be applied. This can be performed using an open test bench described in the Chapter 4.2.1.1 or a back-to-back test rig with the usage of the PTU, described in Chapter 5.3.2. The second possibility is not the best one, because there are still some issues with bearings, despite their previous improvement. My opinion is, that next supporting roller bearing should be used in the PTU to absorb radial forces of the input joint shaft of the technological gearbox.

In next step these PM gears should be loaded by an ICE for assuring correct input torque signal (course) and the final step should be the testing directly in the car on the testing circuit.

Next very interesting opportunity seems to be in the noise reduction potential of the PM material thanks to its natural porosity. But such tests cannot be performed directly in the automotive gearbox, because there are too many disturbing aspects (bearings, more gearsets, etc.), so the noise difference between standard and PM gearset is not measurable.

As an outlook to next work all these topics are summarized in next steps:

- finetune the design of the PTU to enable dynamic tests on the back-to-back test rig
- provide the grinding of **asymmetric rolled** gears and test them
- provide dynamic tests of the **symmetric HIP:ed** and **asymmetric rolled** gears on the open test stand
- provide dynamic tests of the **symmetric HIP:ed** and **asymmetric rolled** with the ICE
- provide dynamic tests of the **symmetric HIP:ed** and **asymmetric rolled** gears directly in the car on the testing circuit
- determine the noise reduction potential of PM gears

9 References

[1] EISENBEISS. *Winch Gears* [online] [cit. 13.07.2021]. Dostupné z: https://www.eisenbeiss.com/gear-system/winch-gears/

[2] Automotive transmission gearbox Gears inside on white background 3d render. In: *123RF* [online] [cit. 13.07.2021]. Dostupné z: https://www.123rf.com/photo_117314188_automotive-transmission-gearbox-gears-inside-on-white-background-3d-render.html

[3] Technologie | Frézování ozubení | Bondy s.r.o. In: [cit. 28.08.2021]. Dostupné z: http://www.bondy.cz/cs/technologie/frezovani-ozubeni

[4] Přizpůsobené přesné broušení ozubení díly platí pro automobilový průmysl. In: *Dongguan Lemo Precision Metal Products Co., Ltd* [online] [cit. 28.08.2021]. Dostupné z: http://cz.lemo-machining.de/cnc-machining-service/precision-grinding-service/customized-precision-grinding-gear-parts-apply.html

[5] Thread and Profile Rolling. In: *Profiroll Technologies* [online] [cit. 22.06.2021]. Dostupné z: https://www.profiroll.de/

[6] Kruhové válce. In: *Profiroll Technologies* [online] [cit. 22.06.2021]. Dostupné z: https://www.profiroll.de/

[7] *IWU-KB-Verzahnungswalzen.pdf* [online], s. 1, 2 [cit. 22.06.2021]. Dostupné z: https://www.iwu.fraunhofer.de/content/dam/iwu/de/documents/Broschueren/IWU-KB-Verzahnungswalzen.pdf

[8] BLACK, J T. a Ronald A. KOHSER. *DeGarmo's MATERIALS AND PROCESSES IN MANUFACTURING TENTH EDITION* [online]. USA: John Wiley & Sons, Inc., 2008, s. 460 [cit. 17.05.2021]. Dostupné z: https://anstudypedia.files.wordpress.com/2015/05/black-kohser-degarmos-materials-processes-manufacturing-10th.pdf

[9] BLACK, J T. a Ronald A. KOHSER. *DeGarmo's MATERIALS AND PROCESSES IN MANUFACTURING TENTH EDITION* [online]. USA: John Wiley & Sons, Inc., 2008, s. 465 [cit. 17.05.2021]. Dostupné z: https://anstudypedia.files.wordpress.com/2015/05/black-kohser-degarmos-materials-processes-manufacturing-10th.pdf

[10] RIAN GARCIA. *The Metal Injection Moulding Production Process* [online]. 2017 [cit. 12.05.2021]. Dostupné z: https://www.youtube.com/watch?v=mA_KCx_QxkQ

[11] STRUERS. *Metallographic preparation of powder metallurgy parts* [online]. 2019, s. 4 [cit. 17.05.2021]. Dostupné z: https://www.google.com/url?sa=i&url=https%3A%2F%2Fwww.struers.com%2F-%2Fmedia%2FLibrary%2FBrochures%2FEnglish%2FApplication-Note-Powder-Metallurgy.pdf%3Flm%3D20200211T153428Z&psig=AOvVaw2KTBTd3R7OA-5J1lkH5HY9&ust=1621327823296000&source=images&cd=vfe&ved=0CAIQjRxqFwoTCLCM6vyq0PACFQAAAAAdAAAAABAN

[12] ANDERSSON, Michael et al. Manufacturing full density powder metallurgy gears through HIP:ing. *Metal Powder Report*. 2019, roč. 74, č. 4. DOI: 10.1016/j.mprp.2018.12.076

[13] FUENTES, Alfonso et al. On the Behaviour of Asymmetric Cylindrical Gears in Gear Transmissions. In: SAE-CHINA a FISITA, eds. *Proceedings of the FISITA 2012 World Automotive Congress*. 193. Berlin, Heidelberg: Springer Berlin Heidelberg, 2013. DOI: 10.1007/978-3-642-33744-4_13

[14] *gear-innovations-brochure.pdf* [online], s. 5 [cit. 17.08.2021]. Dostupné z: https://www.gearinnovations.net/wp-content/uploads/2017/08/gear-innovations-brochure.pdf

[15] *ISO 6336-5:2003, Calculation of load capacity of spur and helical gears, Part 5: Strength and quality of materials*. 2003, s. 3.

[16] MORAVEC, Vladimír et al. Analysis of Power Flow in Closed Loop Stands for Endurance tests of Gears and Transmissions. roč. 2004.

[17] HÖHN, Bernd-Robert. Testmethods for Lubricant Related Influences on the Gear Load Capacity [online]. Dostupné z: https://www.oil-club.ru/forum/applications/core/interface/file/attachment.php?id=84765

[18] MORAVEC, Vladimír. Posouzení únosnosti ozubených kol pulzátorovými zkouškami. 2008.

[19] GE-STB-Cracked-Tooth_EDIT-Cropped-in-Paint. In: . Dostupné z: https://www.symbrium.com/symbrium-single-tooth-bending-gear-testing-systems/

[20] MORAVEC, Vladimír. *Konstrukce strojů a zařízení II.: čelní ozubená kola : teorie - výpočet - konstrukce - výroba - kontrola*. Ostrava: Montanex, 2001, s. 212, 213.

[21] Uzavřený zkušební stav pro MQ200 - TU of Ostrava. [online]. [cit. 2014]. Dostupné z: http://www.casopisstavebnictvi.cz/clanek.php?detail=534

[22] ETP Techno friction clutch. Dostupné z: http://www.etp.se/en/products/power-transmission/etp-techno

[23] MANSFELD, Jakub. *ÚPRAVY UZAVŘENÉHO ZKUŠEBNÍHO STAVU AUTOMOBILNÍCH PŘEVODOVEK*. 2019. Diploma thesis, CTU in Prague, s. 70.

[24] SVOBODA, Jiří, ČESKÉ VYSOKÉ UČENÍ TECHNICKÉ V PRAZE, a STROJNÍ FAKULTA. *Planetové převody*. Praha: Vydavatelství ČVUT, 2005. ISBN 978-80-01-03245-9

[25] KAPELEVICH, Alexander L. *Direct gear design*. Boca Raton: CRC Press, Taylor & Francis Group, 2013, kap. 5.1.2., ISBN 978-1439876183

[26] LANGHEINRICH, Andreas: Geometrie, Beanspruchung und Verformung asymetrischer Stirnradverzahnungen. TECHNISCHE UNIVERSITÄT MÜNCHEN. Dissertation. 2015. ISBN: 978-3-00-048243-4.

[27] FETVACI, Cuneyt; IMRAK, Erdem. Mathematical model of a spur gear with asymmetric involute teeth and its cutting simulation. *Mechanics based design of structures and machines*, 2008, 36. Jg., Nr. 1, S. 34-46., ISSN 1539-7742 (Online)

[28] ABDULLAH, Mohammad Qasim; JWEEG, Muhsin Jabir. Simulation of Generation Process for Asymmetric Involute Gear Tooth Shape with and without Profile Correction. *Simulation*, 2012, 3. Jg., Nr. 6., ISSN 2222- 2871 (Online)

[29] YANG, Shyue-Cheng. Study on an internal gear with asymmetric involute teeth. *Mechanism and Machine Theory*, 2007, 42. Jg., Nr. 8, S. 977-994.

[30] ZHAO, Xinran; VACCA, Andrea. Formulation and optimization of involute spur gear in external gear pump. *Mechanism and Machine Theory*, 2017, 117. Jg., S. 114-132.

[31] CAVDAR, Kadir; KARPAT, Fatih; BABALIK, Fatih C. Computer aided analysis of bending strength of involute spur gears with asymmetric profile. 2005.

[32] KALAY, Onur Can, et al. A comparative experimental study on the impact strength of standard and asymmetric involute spur gears. *Measurement*, 2021, 172. Jg., S. 108950.

[33] RAMESHKUMAR, M., et al. Load sharing analysis of high-contact-ratio spur gears in military tracked vehicle applications. *gear technology*, 2010, 1. Jg., Nr. 3, S. 43-50.

[34] SIGL, Lorenz S., et al. Evolution of gear quality in helical P/M gears during processing. In: *Proceedings of the P/M2004 World Congress & Exhibition Vienna*. European Powder Metallurgy Association Shrewsbury (UK), 2004. S. 649-656.

[35] FLODIN, Anders. Evaluation of Wear in an Automotive Transmission Using Powder Metal (PM) Gears. In: *CTI SYMPOSIUM 2018*. Springer Vieweg, Berlin, Heidelberg, 2020. S. 135-142.

10 Published Literature

[36] MILÁČEK, Ondřej: *Endurance testing of automotive gearbox.* Sborník Konference Studentské tvůrčí činnosti, České vysoké učení technické v Praze. Fakulta strojní. Praha, 2011. ISBN 978-80-01-04796-5. Available from: http://stc.fs.cvut.cz/history/2011/sbornik/papers/pdf/1100039-1.pdf

[37] MILÁČEK, Ondřej; ACHTENOVÁ, Gabriela: *Endurance tests of passenger car gearboxes*. VDI–Berichte 2199.2, International Conference on Gears. 2013. s.1523-1526, ISBN 978–3–18–092199–0

[38] MILÁČEK, Ondřej; ACHTENOVÁ, Gabriela: *Determination of power losses based on the measurement in closed loop test bench for automotive gearboxes.* 2014. Beroun. In 55th International Conference of Machine Design Departments, http://icmd2014.fs.cvut.cz/, ISBN 978-80-01-05542-7

[39] MILÁČEK, Ondřej; ACHTENOVÁ, Gabriela: *Innovative Configuration of the Closed-Loop Test Stand*. SAE 2015 World Congress & Exhibition. Detroit. DOI: 10.4271/2015-01-1092, https://www.sae.org/content/2015-01-1092/

[40] MILÁČEK, Ondřej; ACHTENOVÁ, Gabriela: *Endurance testing of (sintered powder metal) automotive gearboxes.* Powder_Science_Symposium, Höganäs AB, 2015, Sweden

[41] MILÁČEK, Ondřej: *Program pro návrh nesymetrického evolventního ozubení.* In Sborník přednášek 44. mezinárodní vědecké konference kateder dopravních, manipulačních, stavebních a zemědělských strojů. Kurdějov: Vysoké učení technické v Brně, Fakulta strojního inženýrství, 2018. ISBN: 978-80-214-5644-0.

[42] MILÁČEK, Ondřej: *Strength analysis of asymmetric involute gearing.* In *Sborník - 45. mezinárodní vědecká konference kateder dopravních, manipulačních, stavebních a zemědělských strojů.* Plzeň: Západočeská univerzita v Plzni, 2019. ISBN: 978-80-261-0884-9.

[43] MILÁČEK, Ondřej; ACHTENOVÁ, Gabriela; ANDERSSON, Michael: *Application of PM gearset in automotive gearbox*. In: FISITA Web Congress 2020 - Technical Papers. London: FISITA - International Federation of Automotive Engineering Societies, 2020. ISBN 978-1-9160259-1-2.

[44] MILÁČEK, Ondřej: Software for designing of gearing with asymmetric profile. In: Mecca online - Journal of Middle European Construction and Design of Cars [online]. 2020, vol. 17, no. 2, p. 9-20. MECCA, DOI: https://doi.org/10.14311/mecdc.2020.02.02, ISSN 1214-0821, ISSN 1804-9338 (Online)